ABSTRACT

Title of dissertation: THE ROLE OF ACTIN NETWORKS IN CELLULAR
                                  MECHANOSENSING

                                  Mikheil Azatov, Doctor of Philosophy, 2015

Dissertation directed by: Professor Arpita Upadhyaya
                                  Department of Physics
                                  Institute for Physical Sciences and Technology

        Physical processes play an important role in many biological phenomena, such as

wound healing, organ development, and tumor metastasis. During these processes, cells

constantly interact with and adapt to their environment by exerting forces to mechanically

probe the features of their surroundings and generating appropriate biochemical

responses. The mechanisms underlying how cells sense the physical properties of their

environment are not well understood. In this thesis, I present my studies to investigate

cellular responses to the stiffness and topography of the environment.

        In order to sense the physical properties of their environment, cells dynamically

reorganize the structure of their actin cytoskeleton, a dynamic network of biopolymers, altering the shape and spatial distribution of protein assemblies. Several observations suggest that proteins that crosslink actin filaments may play an important role in cellular mechanosensitivity. Palladin is an actin-crosslinking protein that is found in the lamellar actin network, stress fibers and focal adhesions, cellular structures that are critical for mechanosensing of the physical environment. By virtue of its close interactions with these structures in the cell, palladin may play an important role in cell mechanics. However, the role of actin crosslinkers in general, and palladin in particular, in cellular force generation and mechanosensing is not well known. I have investigated the role of palladin in regulating the plasticity of the actin cytoskeleton and cellular force generation in response to alterations in substrate stiffness. I have shown that the expression levels of palladin modulate the forces exerted by cells and their ability to sense substrate stiffness. Perturbation experiments also suggest that palladin levels in cells altered myosin motor activity. These results suggest that the actin crosslinkers, such as palladin, and myosin motors coordinate for optimal cell function and to prevent aberrant behavior as in cancer metastasis.

In addition to stiffness, the local geometry or topography of the surface has been shown to modulate the movement, morphology, and cytoskeletal organization of cells. However, the effect of topography on fluctuations of intracellular structures, which arise from motor driven activity on a viscoelastic actin network are not known. I have used nanofabricated substrates with parallel ridges to show that the cell shape, the actin cytoskeleton and focal adhesions all align along the direction of the ridges, exhibiting a

biphasic dependence on the spacing between ridges. I further demonstrated that palladin bands along actin stress fibers undergo a complex diffusive motion with velocities aligned along the direction of ridges. These results provide insight into the mechanisms of cellular mechanosensing of the environment, suggesting a complex interplay between the actin cytoskeleton and cellular adhesions in coordinating cellular response to surface topography.

Overall, this work has advanced our understanding of mechanisms that govern cellular responses to their physical environment.

THE ROLE OF THE ACTIN NETWORKS IN CELLULAR MECHANOSENSING

By

Mikheil Azatov

Thesis Submitted to the Faculty of the Graduate School of the
University of Maryland, College Park in partial fulfillment
Of the requirements for the degree of
Doctor of Philosophy
2015

Advisory Committee:

       Professor Arpita Upadhyaya, Chair
       Professor Wolfgang Losert
       Professor Helim Aranda-Espinoza
       Professor Garegin Papoian
       Professor Carol Keefer, Dean's Representative

Acknowledgements

First of all, I would like to thank my advisor, Dr. Arpita Upadhyaya. She gave me directions when I was lacking it, and she taught me to never give up in spite of past failures.

I would also like to thank the members of my committee who graciously volunteered their time to assist with my defense: Wolfgang Losert, Garegin Papoian, Helim Aranda-Espinoza, and Carol Keefer.

My fellow grad students, Christina Ketchum, King Lam Hui, Brian Grooman, and Ivan Rey, have been a tremendous source of encouragement and inspiration throughout the years, both within the lab and outside of it. I have enjoyed their friendship, and I hope that it will continue after I leave the lab.

I would like to show my gratitude to Kevin Belnap and Shirong Zhang, the best undergraduate researchers I ever had during my time in the lab, and I had a lot of them. I have no doubt that they will be successful in whatever field of science they choose to pursue.

Dr. Carol Otey and her team were an incredible help by supplying the lab the cell lines that we used in the experiments and collaborating over numerous projects. I cannot imagine how much longer this thesis would have taken without their help. I also thank Dr. John Fourkas and his students Xiaoyu Sun and Alexandra Suberi, who provided us with nanofabricated patterns which were essential for our experiments.

I would like to thank my lovely wife, Samantha Azatova, for all of her support, patience, and for keeping me sane for the past few years. I cannot imagine finishing grad school without her love and encouragement. Thank you for being my muse, editor, and my best friend. I look forward to all our next adventures.

Additionally, I am truly grateful for the encouragement and support of my in-laws, Kitrina Poe and Larry Poe. I feel blessed to have entered their family.

Thank you to my brother, Aleksandr Azatov, whose footsteps I followed to the University of Maryland, and whose mind for science has always been a great asset. He led by example, and I am proud to have him as a brother.

Finally, I would like to thank my mother, Violeta Zhamkochyan. She has been my inspiration in strength, perseverance, kindness, and love even from so far away. Thank you for never having anything but confidence in me.

Table of Contents

iv

List of Tables

List of Figures

and Palladin KD (grey) cells. Each data point is an average of forces from N=10 cells for each condition. The first data point represents the initial (pre-Blebbistatin) force. The graphs show the increase in cellular traction forces as the cell recovers from Blebbistatin washout, subsequent to 30 min incubation in Blebbistatin. **(H)** The percentage force (with respect to original forces before Blebbistatin addition) during recovery from Blebbistatin washout plotted as a function of time for EGFP-palladin cells (black) and KD cells (grey). **(I)** The percentage increase of stress after washout of Blebbistatin quantified as the difference between force recovered 1 hour after washout, F_{recov}, and the force after incubation in Blebbistatin for 30 minutes, F_{blebb} (percentages are with respect to the initial force prior to Blebbistatin addition). The data represents an average for 20-30 cells of each type. ($p<0.01$, t-test). **(J)** Percentage of EGFP-Palladin and Palladin KD cells that showed force recovery of less than 30% of the original force, one hour after drug washout ($p<0.01$,t-test)

1 Introduction and background

1.1 The discovery of cell and cell mechanics

In 1665, Robert Hooke, the man behind the famous Hooke's law of elastic spring, published Micrographia, the book describing his observations with telescopes and microscopes. When Hooke looked at a thin layer of a cork, he saw empty spaces separated by thin walls. He named them cells. This book ignited a spark among scientists and started the beginning of cell theory, which was eventually formulated in 1838. The theory stated that: (1) all living organisms are composed of one or more cells; (2) the cell is a basic unit of life; and (3) all cells come from preexisting living cells. Now, we know that cells multiply and interact with each other in many complex ways to build multi-cellular organisms, like animals or humans. By some estimates our bodies contain approximately 37 trillion cells. The proper function of these cells is vital for our health, which has motivated many scientists to study cell biology over the last several centuries.

For a long time, cell biology was a standalone field studied only by biologists; however, nowadays with more and more discoveries being made, the need for interdisciplinary fields is becoming more apparent. Currently, there are several approaches to studying cell biology. Biochemistry looks at the structure of proteins inside the cell to understand how they maintain cell architecture. The genetics approach looks at cells as tiny computers, decoding DNA and thus producing proteins accordingly, which work to maintain the cells' proper function. More recently, it is become apparent that mechanics plays an important role in cell biology. Cells push and pull on each other during embryonic development, they stretch and contract in heart and muscle cells, or

they crawl to the injury site during wound healing. By Newton's law, for all of these functions to take place, cells have to exert force on their surroundings and vice versa. Biophysics uses theories and methods of physics to study biological phenomena including cell biology[1].

While physics mostly deals with passive materials, biological systems are observed to actively react to their surroundings and maintain themselves out of equilibrium by the expenditure of energy. Cells can adapt to their environment by transforming mechanical cues from its surroundings into biochemical changes inside the cell, which make it possible for cells to provide an active response to the perturbation. In fact, many different proteins inside the cell have to work together to provide such a response. This phenomenon is called mechanotransduction, and it has made it necessary for physicists to come up with new models describing biological systems.

The complexity of mechanotransduction has encouraged many scientists nowadays to study different aspects of this phenomenon. In this thesis, we will look at cellular response to both elasticity and structure of its environment and hope to provide a small contribution to this emerging field of science.

1.2   Cytoskeleton

1.2.1 The components of cytoskeleton and their structure

The cell is the smallest unit of life made up of many complex, dynamic systems. The nucleus contains and organizes cellular DNA, the lipid bilayer membrane separates cellular contents from the extracellular environment and maintains an ionic gradient. The group of proteins that serves as a scaffold for a cell and thus of great importance to mechanotransduction is called the cytoskeleton. The cytoskeleton provides shape and structure not only to the cell, but its contents as well. The cytoskeleton is best described as a cohesive network of protein filaments that dynamically extends throughout the cell and is attached to plasma membrane and internal organelles. The filaments constantly assemble and disassemble to give them the ability to change their morphology. The cytoskeleton is necessary for cells to change shape, migrate, divide and to regulate their own mechanical properties. The cytoskeleton can reorganize itself dynamically over a range of different timescales. It is capable of changing its shape in seconds, allowing a cell to rapidly respond to stimuli, but it can also provide a stable structure for hours, allowing a cell to maintain its shape. The cytoskeleton has three main components: actin, microtubules and intermediate filaments (See Figure 1-1). The organization and dynamic remodeling of these components enable cellular mechanical responses.
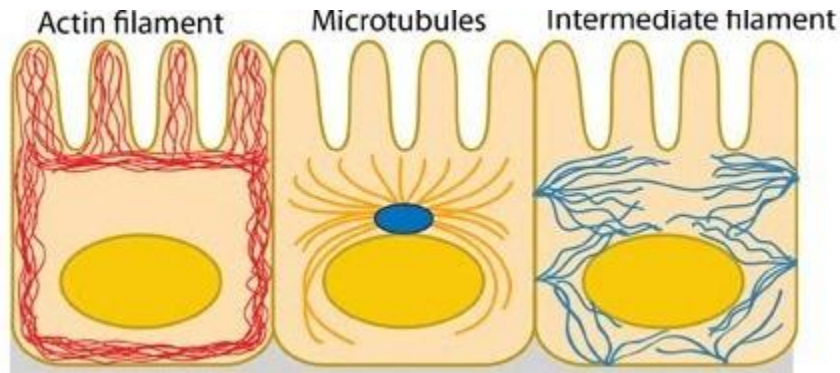
Figure 1-1 The components of the cytoskeleton. Each picture represents the localization of filament systems.
Figure used and adapted by permission from MBInfo: www.mechanobio.info; Mechanobiology Institute, National University of Singapore
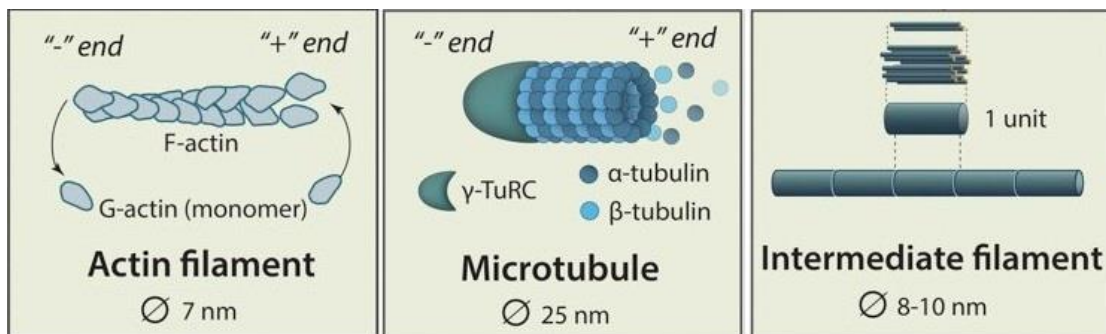
Figure 1-2 The components of the cytoskeleton. Each picture shows a schematic representation of each filament type as it is assembled from its subunits.
Figure used and adapted by permission from MBInfo: www.mechanobio.info; Mechanobiology Institute, National University of Singapore

Microtubules are the largest filaments, with a diameter of about 25 nm. They are long hollow tubes assembled from the protein tubulin, with the inner diameter of the tube being about 12nm [2]. They originate from a central structure called centrosome located close to the nucleus, are organized radially and point towards the edge of the cell (See

Figure 1-2). In comparison with the other two filament types, they are long and rigid. Microtubules can grow as long as 50μm. They determine the position of organelles of the cell, and participate in intracellular trafficking, as different vesicles and organelles can be transported along the filaments by specific motor proteins, such as kinesins and dyneins.

The next groups of polymers are called intermediate filaments (See Figure 1-2). They often have a spatial distribution similar to that of microtubules but have a smaller diameter of about 10 nm [3]. They are composed of different monomers that vary greatly from one cell type to another. Intermediate filaments have different functions like providing structural support to the nuclear membrane and structural integrity to cells in tissues [4]. They are more stable and do not reorganize constantly like actin and microtubules. There are not any known motors that can move along intermediate filaments.

Actin filaments are the third group of polymers composing cytoskeleton. They are thin, flexible filaments that combine into complicated three-dimensional structures. Actin filaments are essential for mechanotransduction of cells and will be discussed more thoroughly in the next section.

1.3   Actin cytoskeleton

1.3.1 Actin

The actin cytoskeleton allows the cell to maintain its basic structure, it integrates signaling pathways, and allows for cell motility. In fact, the actin cytoskeleton is involved in the movements of all known eukaryotic cells. It can assemble into different

higher order structures inside the cell with each of those structures responsible for particular cellular functions.

Actin can exist either as a globular protein, *G-actin,* or as polymer called *F-actin,* which is a linear chain of actin monomers. Actin has a variation of less than 5% among its 375 amino acids across all species of eukaryotic cells, making it one of the mostly highly conserved proteins. The molecular weight of each monomer is close to 42 kDa. The globular actin monomer generates a polymeric filament with a length of up to several micrometers by associating with other monomers through binding sites on its surface. The assembly of actin filaments can be divided into two parts. First, the monomers need to assemble into nucleating seeds. Second, actin monomers attach to either end of the filament to elongate (See Figure 1-3). Actin monomers are arranged in a double helical pattern, in which each monomer is in contact with four other monomers. Their distinct ends cause them to orient in the same direction within the filament, which creates a filament with naturally occurring "plus" and "minus" ends. The end products, actin filaments, have a diameter of approximately 8 nm. The polarity of actin filaments plays an important role in cell functions and will be discussed more in later chapters. The two ends of actin filaments grow at different rates. The rate of polymerization at the plus end of the filament, when the monomers have bound adenosine triphosphate (ATP), is nearly 10 times faster, than the polymerization rate at the minus end [2]. The ATP hydrolyzes soon after binding to the filament. At high concentrations actin monomers will nucleate on their own, but nucleating proteins such as Arp2/3 can begin the growth process, which allows the cell to control the nucleation and direction of new filaments. A concentration

of 1 µM (critical concentration) is necessary for spontaneous polymerization of filaments in an actin solution with ATP in the absence of nucleation factors.
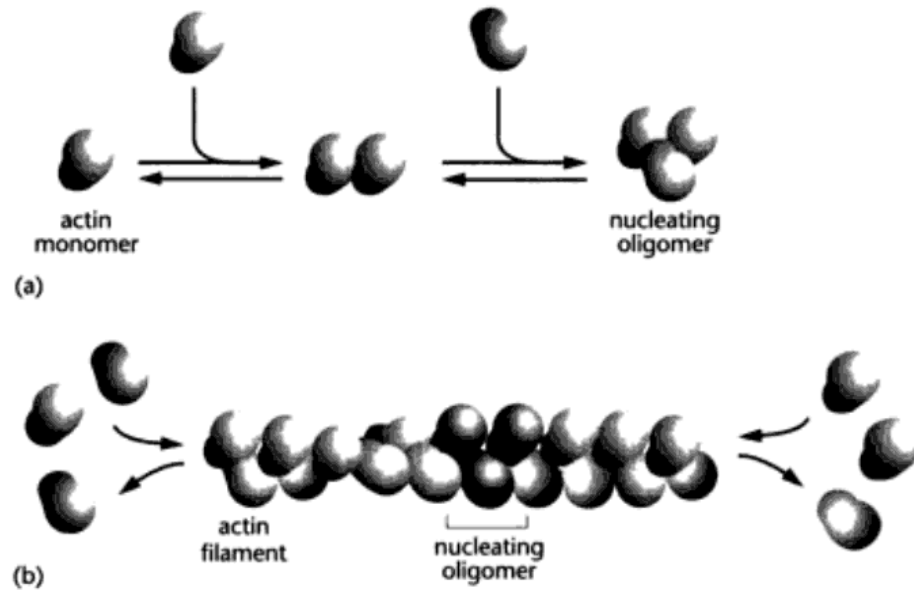
Figure 1-3 Two stages of actin polymerization. (a) Nucleation stage of actin assembly. This is the slower part of the assembly. (b) Addition of actin monomers to each end of the nucleating oligomer resulting in a long actin filament
Figure used by permission from Cell Movements: From Molecules to Motility.

A phenomenon known as actin treadmilling occurs because monomers bind and unbind at different rates at each end of the filament, thus enabling the filament to simultaneously lengthen at one end and shorten at the other [5] resulting in a seemingly "moving" filament. The total concentration of monomers directly affects the average length of the filaments. The amount of actin in excess of the critical concentration is found in filaments. The length of actin filaments is distributed exponentially within steady state in-vitro networks and normally distributed in the presence of stabilizing proteins [6].

1.3.2 Actin associated proteins

Actin filaments can assemble into an array of different structures (See Figure 1-4). Actin filaments can organize into a narrow parallel bundles present in filopodia, which protrude from the cell or microvilli, microscopic cellular protrusions that are commonly found on the surface of egg cells, epithelial cells, or white blood cells [7]. Filaments can assemble into a complex mesh at the leading edge of the cell, called a lamellipodium [7]. Another effective use of actin in the cell takes place during cell division, when actin forms a contractile ring at the interface where two new cells will be formed [7]. Filaments can assemble into contractile parallel bundles, called stress fibers, which span the entirety of the cell body. In muscle cells, actin assembles into sarcomeres, parallel structures of actin filaments and myosin that allow contraction of muscle cells.
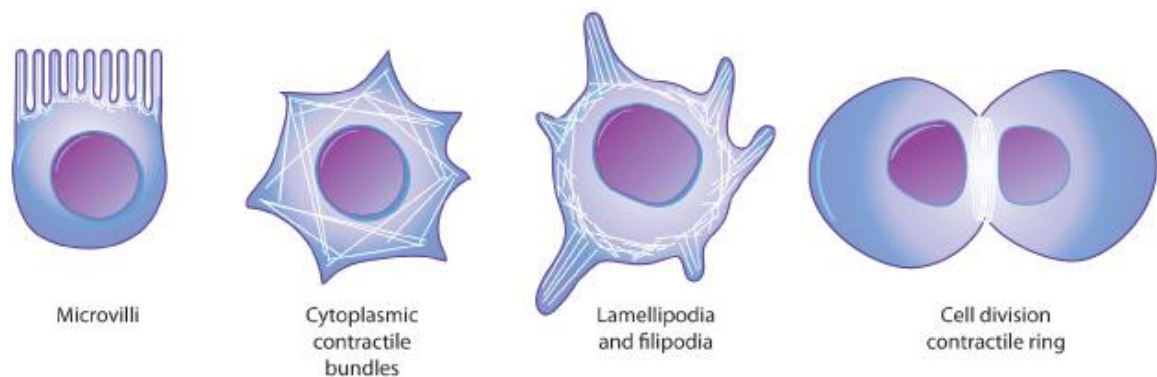
Figure 1-4 Examples of actin based structures. Actin filaments are shown in white, and nucleus is shown in purple in each picture.
Figure used by from Nature Education (2014)

These different types of actin networks are assembled using actin binding proteins (ABPs). There is a great diversity among ABPs. A review in 2003 counted 162 unique types of APBs[8]. These proteins direct the rate, location, and time of assembly and

disassembly of actin filaments. They can work as nucleation sites, or they may work to cap filaments, sever filaments, stabilize filaments, sequester g-actin to prevent polymerization, bundle or cross-link, bind to other objects in the cell, or use actin as a guide for transport as in the case of motor proteins. In the case of cross-linkers, ABPs can bind to two different actin filaments, thus bringing them into physical proximity. Cells can modulate the structure of actin networks by varying the concentration, composition and location of ABPs (See Figure 1-5). It is therefore of great interest to examine what each ABP is responsible for and how cells regulate them. Variations in the size and flexibility of ABPs will allow for the formation of different types of actin networks. Arp2/3 complex allows for nucleation and branching of actin filaments at a distinctive 70º angle from the mother filament. It is therefore enriched in the lamellipodia of cells facilitating the formation of branched actin meshworks. Short and rigid fimbrin and fascin allow actin to form parallel bundles, and therefore are enriched in filopodia, which are long and narrow protrusions [9]. α-actinin is involved in organizing actin filaments in contractile bundles called stress fibers. The ABP filamin is a large cytoplasmic protein that is involved in cross-linking cortical actin networks. Depending on the filamin to F-actin ratio, filamin can do one of two things: organize actin in bundles or organize it into a gel-like scaffold. . The difference in actin networks can be attributed to the shape and structure of the filamin protein. Since filamin is flexible and long, two filaments may bind at almost any orientation allowing for different actin structures to form [10]. Spectrin is an even longer protein with two actin-binding sites. It is often found in the actin networks near the plasma membrane. Dystrophin links membranes to muscle fibers. (See Figure 1-5)

9
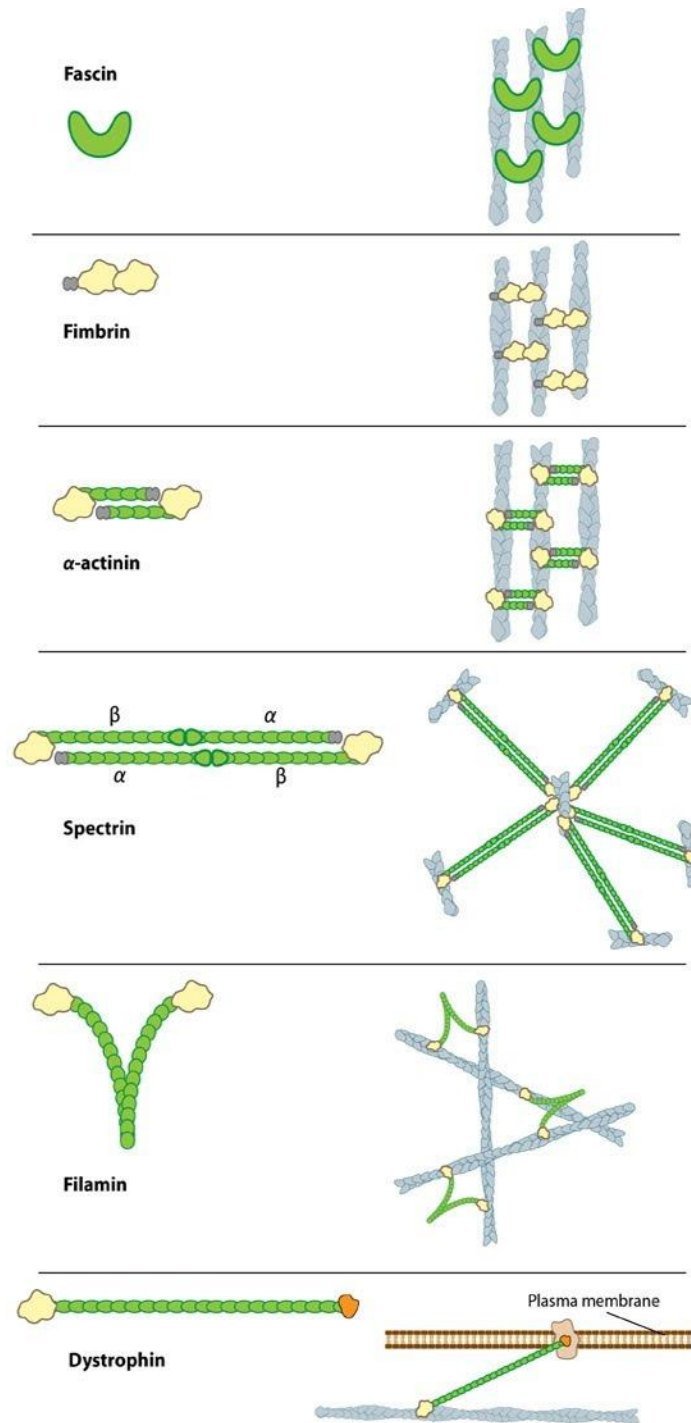
Figure 1-5 Actin binding proteins. Smaller, rigid, proteins assemble actin in tight bundles, while larger, flexible proteins create more space between filaments and to generate more flexible networks.

Figure used by permission from MBInfo: www.mechanobio.info; Mechanobiology Institute, National University of Singapore

Palladin is a recently discovered ABP, that was identified by two research groups - in 2000 in Carol Otey's lab [11] and in 2001 in Olli Carpen's lab [12]. Palladin is found in stress fibers, lamella and focal adhesions and therefore likely plays an important role in sensing the physical environment. It is implicated to play a key role in regulating cell morphology and movement during embryonic development and cancer and is therefore, of great interest. In fact, knocking out palladin in mice is embryonically lethal, underscoring its important function in cells. Besides actin, palladin can also bind to other ABPs. It can bind to α-actinin [13], an ABP that is involved in formation of stress fibers, to Vasodilator-Stimulated Phosphoprotein (VASP), a protein essential in focal adhesion formation and its linkage to actin stress fibers [11]. Among the other proteins that palladin can bind to are Eps8 [14], ezrin [12], Lasp-1 [15], and profilin [16].

Palladin is involved in many functions of the actin cytoskeleton. It is involved in the formation of stress fibers [17], focal adhesions [17], membrane ruffles and podosomes [14], which are thought to promote invasion of cancer cells. In fact, knockdown of palladin results in the loss of these structures, indicating that palladin is necessary for the organization of these organized actin structures in cells. Palladin is also found in growth cones [18], and at the leading edge of cells along a wound edge [19]. These results emphasize the role of palladin as a molecular scaffold for actin cytoskeleton. In particular, its presence in actin stress fibers and focal adhesions indicates that palladin may have a significant effect on the contractility of cells and overall mechanosensing of ECM. This is reiterated by the fact that palladin also binds to other ABP (such as alpha-actinin) which are actively involved in both stress fibers and focal

adhesions. Chapter 2 of my thesis will be focused on the role of palladin in cellular mechanosensing and include more details about the specifics of this protein.

1.3.3 Actin stress fibers

Many cells have contractile actin structures called stress fibers, which are bundles of actin filaments, myosin, and other actin binding proteins (ABPs). Stress fibers are usually composed of about 10-30 actin filaments [20], and are held together by different actin cross-linkers. The actin cross-linkers α-actinin and palladin are prevalent in stress fibers, although other cross-linkers like, fascin, and filamin have been seen in stress fibers as well [12], [13], [17], [22], [23]. Staining of α-actinin and palladin reveals that these two proteins are co-localized with each other and show a periodic pattern along actin stress fibers which alternates with periodic pattern of myosin (See Figure 1-6) [17], [23]. This result initially led to the belief that actin stress fibers in non-muscle cells were very similar to those in muscle cells [24], especially since both α-actinin and palladin are involved in Z-disk formation of muscle cells as well. Muscle cells consist of myofibrils where each myofibril consists of a specific, repeating actomyosin structure called a sarcomere. Each sarcomere consists of thin filaments containing actin and thick filaments containing myosin II, which are arranged into specific pattern that allows for this contraction (See Figure 1-7) [2]. This structure is maintained by a repeated arrangement of Z disks serving as borders for each sarcomere. Sarcomeres are about ~ 2μm long, but during muscle contraction, they can shorten by 70% of its length.
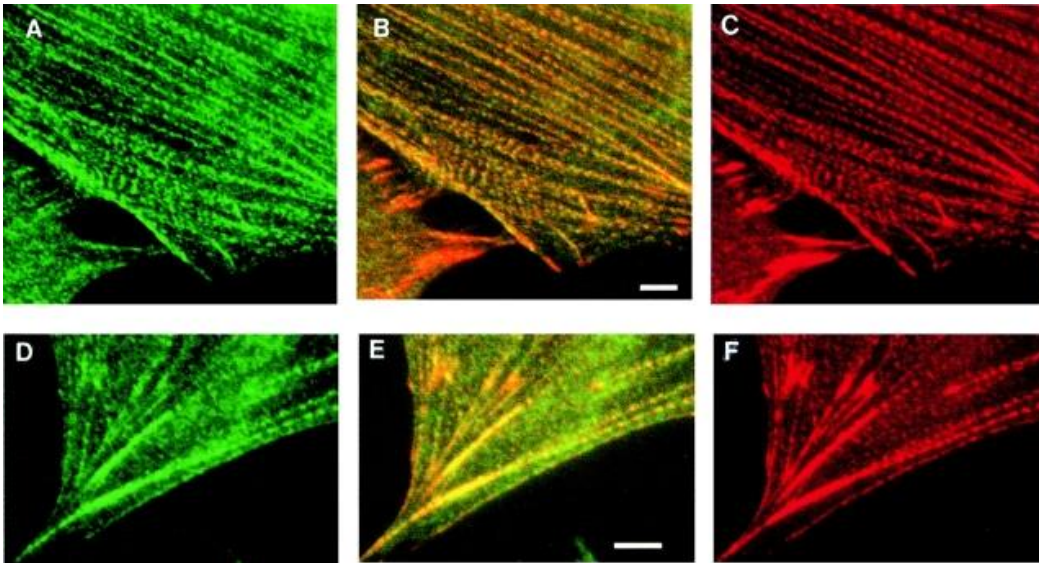
Figure 1-6 Colocolization of palladin and α-actinin in stress fibers. Green fluorescence (A and D) represent the images of palladin, red fluorescence (C and F) represent the images of α-actinin, while B and E show merged images.
Figure used by permission from Journal of Cell Biology 150 (2000)
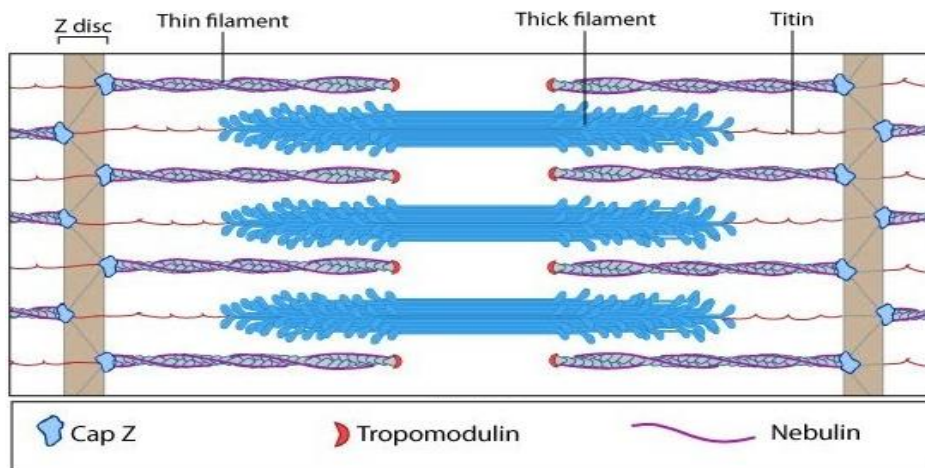
Figure 1-7 Schematic representation of sarcomere. Different accessory proteins help in insuring the proper function of sarcomere
Figure used and adapted by permission from MBInfo: www.mechanobio.info; Mechanobiology Institute, National University of Singapore

Although there are similarities between actin stress fibers and sarcomeres, now we have a better understanding of how stress fibers organize and the role of cross-linkers in it. Typically stress fibers are divided into three categories depending on their location and formation. These categories include ventral stress fibers, radial stress fibers (also called dorsal stress fibers), and transverse stress fibers [23], [25] (See Figure 1-8). As mentioned above, actin filaments have (+) and (-) ends which impart them with inherent orientation or polarity. Different stress fiber structures have different organization of filament polarity. Radial stress fibers (RSF) are attached at one end to the focal adhesion complex and have uniform polarity[20], [23]. They are enriched with α-actinin [26], [27], [28] and don't exhibit the periodic pattern, seen in myofibrils. Because of their polarity, myosin would not be able to contract RSF, as both ends of myosin would move in the same direction of the stress fiber. Therefore, in these structures, myosin is potentially involved in moving a cargo to focal adhesions. Transverse stress fibers usually show a sarcomeric-type structure - they are not attached to focal adhesions at both ends and exhibit retrograde flow, travelling from the leading edge of the cell towards the center. Similar to sarcomeres, they consist of periodic blocks, held together by α-actinin, each containing actin filaments of opposite polarity and non-muscle myosin (See Figure 1-8). Myosin is able to contract this structure by moving between two filaments. Transverse arcs can contract like sarcomeres, but because they are not attached to the membrane it is not clear whether they can transmit force to the surroundings [29], [23]. Ventral stress fibers span the entire cell body, and lie along the base of the cell (often under the nucleus) attached to the focal adhesions at each end [30]. These fibers show the most commonly observed graded polarity of actin filaments in cells [20], [23]. For fibers with graded

polarity to be able to contract, they should be able to displace α-actinin or other ABPs. In a model proposed by S. Pellegrin and H. Mellor, actin filaments are able to contract because of the rapid association/dissociation rate of α-actinin [23]. The filaments are thus allowed to move past each during the time when they are not kept together by α-actinin.
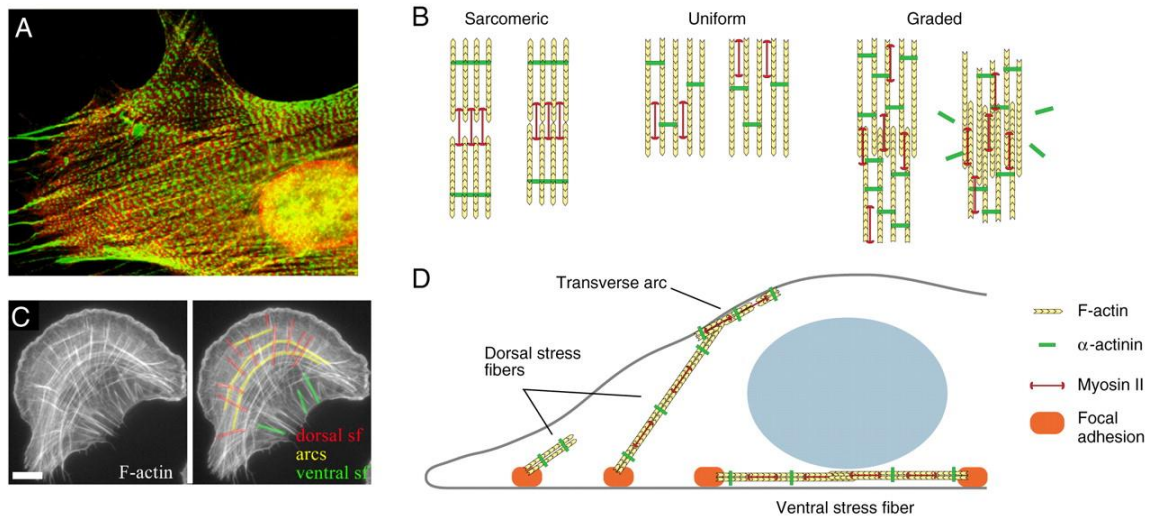
Figure 1-8 Actin stress fiber structure. (A) Gerbil fibroma cell stained for non-muscle myosin (red) and α-actinin (green) reveals the periodic banding of these components on actin stress fibers[31]. (B) Models of stress fiber structure and contractility. (C) U2OS osteosarcoma cells stained for F-actin, displaying the three categories of actin stress fibers(dorsal, red; transverse, yellow; ventral, green). (D)Model of stress fiber formation[29].
Figure used by permission from Journal of Cell Science 120 (2007)

1.3.4 Mechanical properties of actin filaments and actin stress fibers

Actin filaments *in vivo* are typically micrometers long and can deform over a similar length scale. Thermal fluctuations can bend the filament in a stochastic manner. The persistence length of a polymer is a measure of the length scale over which a polymer remains roughly straight in the presence of thermal fluctuations. Actin filaments are considered to be semi-flexible polymers because the length of a filament is on the

order of its persistence length, which is about ~15 μm. However, actin filaments can be assembled into very rigid structures. Actin binding proteins (ABPs), such as fascin for example, can assemble actin filaments into bundles that exceed the stiffness of individual filaments by orders of magnitude [9]. The organization of the individual filaments, and ABPs, can give rise to actin networks with different mechanical properties. On the scale of the whole cell actin networks are considered viscoelastic. Viscoelastic materials exhibit both elastic and viscous properties when under stress. Over short time scales actin networks behave elastically, meaning that their deformation is proportional to the applied stress, while over longer time scales they behave like a viscous material, meaning that their deformation continues to increase under constant stress.

Even though *in vitro* actin networks are viscoelastic, different types of actin networks within the cell exhibit different mechanical properties depending on organization of the individual filaments and actin binding proteins. As we have seen in the previous section, even within the stress fiber family there are different potential networks that can be assembled depending on just the orientation of the filaments. Recently it has been shown that individual stress fibers behave like viscoelastic rods [32]. By looking at retraction kinetics of actin stress fibers after cutting them with a laser nanoscissor, Kumar et. al showed that trajectories of the retracting actin stress fibers followed the prediction for a viscoelastic cable [32]. Furthermore, they showed that stress fibers are tensed almost entirely by myosin motors, as the retraction of stress fibers decreased for myosin inhibited cells [32]. This study highlights the importance of stress fibers in force generation within actin networks as stress fibers shortened by ~ 5 μm in length after the cut [32]. It is important to note that stress fibers only contribute to part of

16

the forces generated by cells as lamellar actin networks (which are less organized) can lead to significant force generation in the absence of stress fibers [26].

1.3.5 Focal adhesions

Cells make extracellular matrix (ECM), organize it, and degrade it. The matrix in its turn exerts powerful influences on the cells. These influences are exerted mainly through transmembrane cell adhesion proteins. These proteins act as matrix receptors and link the matrix outside the cell to the cytoskeleton located inside of it. However, the role of receptors is far greater than that of providing merely passive mechanical attachment. Components of the matrix can modulate cell behavior by binding to receptors. The main receptors for most extracellular matrix proteins on animal cells are integrins. There are several types of integrins, and a cell can have different integrins on its surface. The integrin family of proteins consists of at least 24 varieties in humans, but they all consist of two subunits, α and β heterodimers [33]. When tension is applied to an integrin, it can reinforce its binding to the cytoskeleton, by making conformational changes to proteins in the integrin pathway, while when the tension is lost, it can loosen its hold, releasing proteins on the inner side of the membrane [34]. Binding of integrins to the matrix can induce a biochemical signal in both directions - into the cell, as well as outward to control its binding to ECM [35], [36]. Integrins can attach to different extracellular matrix proteins, like fibronectin, collagen, or laminin, by binding their extracellular portion to specific amino acid sequences of ECM proteins. The intracellular portion is then linked to the actin cytoskeleton through a complex of proteins. The linkage consists of several proteins, such as talin, vinculin, paxillin, focal adhesion kinase (FAK), zyxin, etc., and is called focal adhesion [3]. On the other end the focal adhesion is connected to actin

17

filaments. The focal adhesion complex creates the connection between actin cytoskeleton and cell surroundings that is essential to control cell migration, wound healing, proliferation, morphogenesis, and differentiation [37], [26]. The exact structure and the role of each individual protein in this linkage is still a subject of a great debate. Beautiful work by Kanchanawong et al., shows the location of different focal adhesion proteins in the focal adhesion complex along the vertical axis using three-dimensional super-resolution fluorescence microscopy (PALM) (See Figure 1-9) [37]. The overall separation between integrins and actin was measured to be 40nm with all the focal adhesion proteins located in this region. The lowest level of focal adhesion complex consist of paxillin, focal adhesion kinase, and the head of talin, the next "intermediate force-transduction layer" contains talin and vinculin, and the top layer connecting to actin contains zyxin, VASP and α-actinin.
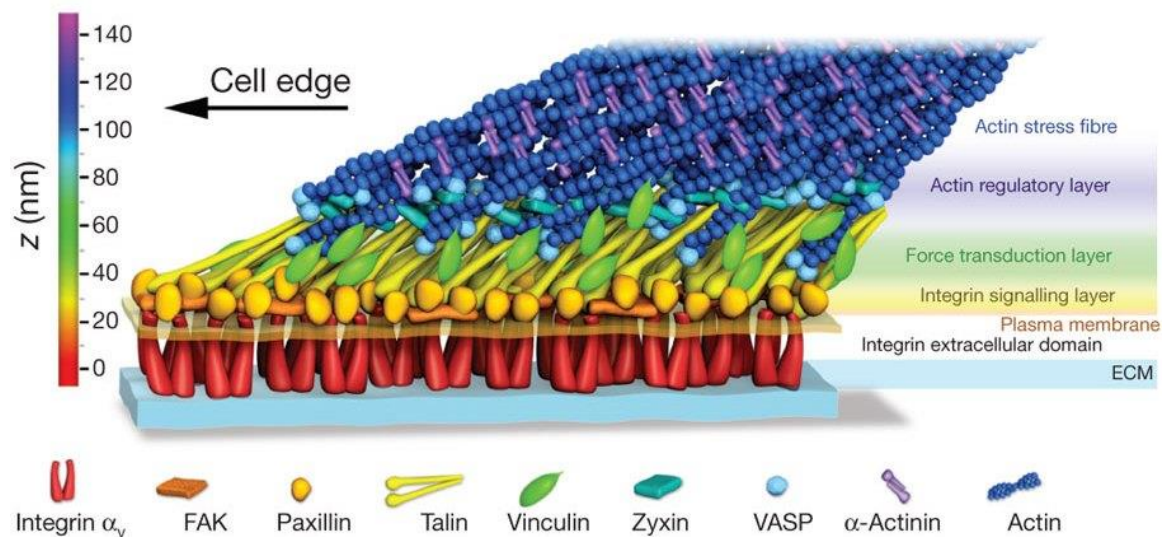
Figure 1-9 Schematic of focal adhesions
Figure used by permission from Nature 468 (2010)

During focal adhesion assembly, first small nascent adhesions are formed at the leading edge of the lamellipodium. As the lamellipodium advances, these nascent adhesions either disassemble or mature. During maturation, nascent adhesions elongate centripetally along actin stress fibers. There's evidence that α-actinin organizes radial stress fibers (RSF) emerging from focal adhesions as suppressing RSF impairs focal adhesion size [38], [39]. Maturation seems to be myosin II dependent as inhibition of myosin II with blebbistatin reduces the probability of focal adhesion maturation and enhances nascent adhesion turnover [39].

Because of their role in providing a mechanical linkage between cells and extra-cellular matrix, focal adhesions have been implicated as being critical for force transmission from the cytoskeletal network to ECM. A variety of studies have also shown that mechanosensing arises from the tension mediated maturation of focal adhesions [26], [40]. It was shown that 0.9 nN of traction force is required to stabilize and encourage focal adhesion growth [41]. Still, the exact mechanism of interplay between focal adhesions, actin stress fibers, and traction forces is a subject of great debate. While maturation occurs at the same time as radial stress fiber (RSF) growth, RSF are not required for force transmission. Still, RSF might be responsible for stabilization of focal adhesions as RSF depleted cells had focal adhesions of a shorter lifetime. It has been shown that focal adhesion assembly and maturation is dependent on presence of the forces generated in the actin cytoskeleton, as focal adhesion growth coincided with traction force increase, while the magnitude of the traction forces is not correlated with the size or composition of focal adhesions [26].

1.4   Mechanical response of cells

1.4.1   Cellular forces

The impact of cellular forces on all multicellular organisms is so great that their effect ranges from the length scale of individual cells up to the scale of an entire organism. The forces generated by cells and on the cells are experienced constantly, including simply when we lift weights in the gym. For example, in this scenario, muscle cells contract together to shorten muscle fibers. The heart also relies on cellular forces when it contracts periodically because of synchronized force generation of heart muscle cells, which then propels blood through arteries [3]. Cellular forces are important in other daily activities like walking or running. During these activities our ligaments and bones must constantly adjust to cycles of different mechanical loads. This occurs in order to ensure the health of bone cells, which have to react to these external stresses and remodel the structure of the bone accordingly [42].

Zooming in closer, we can see how mechanical forces affect behavior of a single cell. During cell division constriction forces separate the mother and the daughter cell apart [43]. Collective cell motion in wound healing is guided by organized pushing and pulling of neighbor cells on each other [44], [45]. Morphogenesis is another phenomenon that requires complex coordination of the forces involved in guiding and reshaping cells [46]. Mechanical forces play an important role in tumor metastasis [47]. Cancer cells from a primary tumor metastasize to other organs of the body by reaching the blood vessels and penetrating their walls both to enter and exit the blood stream and thereby experiencing different mechanical stimuli along the way. These cancer cells must be able to exert forces and sense the stiffness of their environment as they progress towards their

secondary site, as well as be able to move through different constraints of the environment as they go through complex structures of ECM, and go through our blood vessel walls [47].

From Newton's laws we know that for all of these processes to occur cells need to exert forces on its surroundings as well experience forces exerted upon them. Various mechanisms have been shown to provide cells the ability to exert forces. The most commonly mentioned mechanism involves motor proteins. Motor proteins are able to use chemical energy provided by hydrolysis of ATP and convert it into mechanical work [3]. There are several types of motor proteins: the kinesin, and dynein family of proteins move along microtubules, while the myosin family moves along actin filaments. Motor proteins are involved in many intracellular processes. Kinesin and dynein have been shown to play important role in intracellular transport of proteins and vesicles, motility of cilia and flagella, and cell division (mitosis and meiosis) [48], [49]. Many different types of myosins have been found in eukaryotic cells and are involved in various cellular processes such as vesicle transport, stress fiber contraction, filopodia motility, and cell migration [50]. Still they are best known for their involvement in muscle contraction. Using an optical trap researchers were able to directly measure the forces, displacement, and duration of the movement of actin filament generated by a single myosin molecule in one power stroke [2], [51]. During the contact between myosin II and F-actin, the molecule generates approximately 3-5 pN of force moving the filament by approximately 5-15 nm. Such a small step size would allow myosin II to bind to every actin subunit. In non-muscle cells, myosin II is localized along actin stress fibers which allows for generation of contractile forces through the actin cytoskeleton bundles similar to

sarcomeres. The coupling of the focal adhesions to the actin cytoskeleton allows for transmission of these forces to the substrate as traction allowing the cell to sample the mechanical properties of the substrate [52]–[54].

Motor proteins are not the only way cells can generate forces. Actin polymerization can drive the protrusion of the cells' leading edge which enables the cell to sense its surroundings. The motion of the bacteria *Listeria monocytogenes* is driven by polymerization generated forces alone [55]. These results were confirmed in vitro by observing actin filaments pushing on vesicles coated with ActA, a virulence factor promoting actin polymerization [56]. The Brownian-Ratchet model [57] explains force generation through actin polymerization. According to this theory, an actin filament grows, until there is no space between the filament and the load for additional actin monomers. However, thermal fluctuations can occasionally create a gap large enough for a new monomer to squeeze in and lengthen the filament, essentially pushing the load further (See Figure 1-10) [58]. The polymerization force of one actin filament has been directly measured to be about 1pN with optical tweezers [59].

a Brownian rachet
b Elastic Brownian rachet

Load

Brownian motion

ADP–actin   ATP–actin
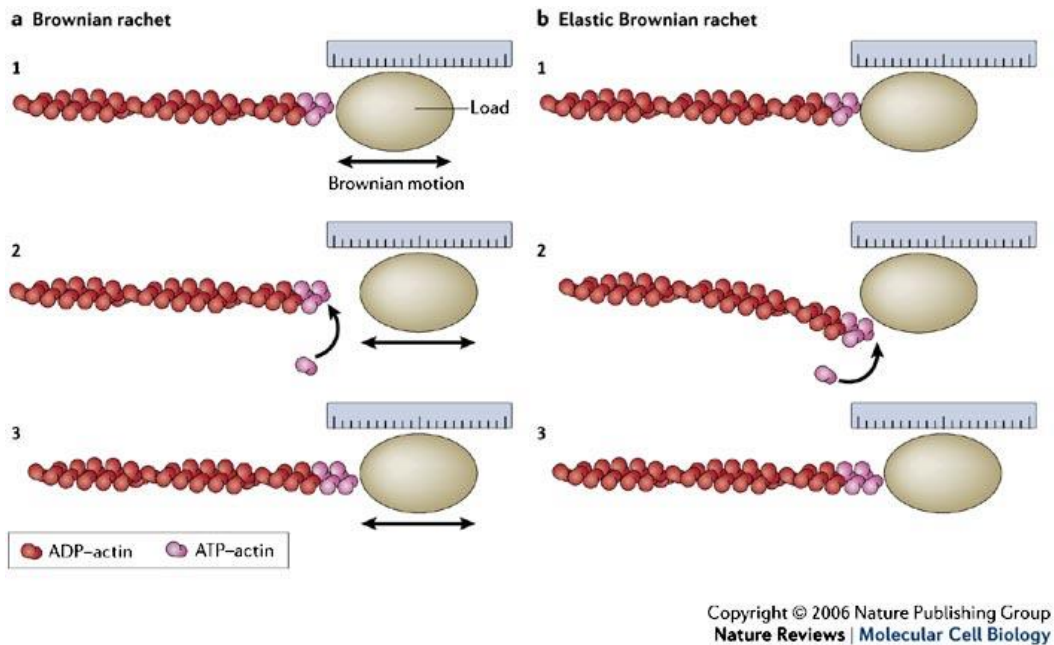
Figure 1-10 Schematic of Brownian-Ratchet Models. (a) Traditional Brownian ratchet model where the bead is being pushed by insertion of actin monomers between the bead and the actin filament. (b) Modification of the Brownian ratchet model in which the monomer is being inserted due to random bending of actin filament. The elastic energy of the filament than pushes the bead forward.
Figure used by permission from Nature Reviews Molecular Cell Biology (2006)

Cells use forces as a way to couple internal cellular signaling and biochemical responses with the external physical environment and physical stimuli. Cellular forces play an important role in many biological processes such as intracellular transport, cell division, cell-cell interaction, or migration around barriers. Together motor proteins and actin polymerization enable the cell to probe its environment by exerting forces on it. Through these forces cells are able to push, pull, tug, or squeeze their environment to determine the physical features of their surroundings, e.g. whether they are soft, stiff, or have certain barriers The ability of cells to actively respond to the properties of its environment gave rise to the area of cell biology called mechanotransduction.

1.4.2 Mechanotransduction

Mechanotransduction is the ability of the cell to respond to different mechanical stimuli. Cells can sense physical properties of their environment by converting physical stimuli into biochemical signals and reorganizing their cellular structure in response to those signals. As discussed above, there are different types of mechanical stimuli that a cell may encounter *in vivo*. There has been intense interest in the molecular mechanisms that allow cells to sense and respond to the mechanical properties of their environment [60]. The cytoskeleton and cell adhesions are key components of a cell that allow for cellular mechanosensing. There are numerous mechanisms over different time scales and length scales that enable cells to probe their environment.

At the level of the whole cell, acto-myosin networks could lead to mechanotransduction as these complex networks can act as global force sensors, by adapting their contractility to the resistance of their environment. Different actin structures have been observed on substrate of different stiffness even with similar focal adhesions suggesting a global response to the cellular environment [61]. Moreover, the experiments by Janmey and Miller suggest that the local stiffness of their substrates at adhesion sites was much higher than the global stiffness of the substrate suggesting that cells sense their surroundings over longer length scales [62]. Rigidity sensing through acto-myosin networks would lead to mechanosensing over tens of micrometers over the range of several minutes.

An extensive body of work has shown that focal adhesions act as mechanosensors [52], [63]–[66]. Cells can exert forces on their surroundings with the help of actin

dynamics and focal adhesions [52]–[54]. The tension within the actin cytoskeleton is usually generated by myosin II and is transmitted to the external substrate via focal adhesions [52]–[54]. Therefore, the proteins linking the actin cytoskeleton with focal adhesion and extracellular matrix are important for mechanotransduction [26], [39], [67], [68], [69]. One of the possible ways for focal adhesions to sense their environment involves conformation changes of focal adhesion proteins under stress. These changes can expose different binding sites of those proteins promoting stiffer or softer structure of focal adhesion [70]–[72]. Another possible way suggests, that focal adhesions could sense the surroundings through mechanosensitive channels near them [73], [74]. Both of these methods imply a local, short-time mechanism as the environment is probed by individual focal adhesions.

To study mechanotransduction, typically one perturbs the mechanical state of the cells. Usually this is done by examining cells on substrates of different stiffness, substrates with different mechanical constraints, applying a direct external force or stress, or a combination of these factors. In the next sections I will go over some of the aspects of these types of experiments.

1.4.3 Mechanotransduction on substrates of different elasticity

Cells live in environments of different elastic properties throughout our body. Each tissue type possesses a characteristic stiffness. Neurons compose one of the softest tissues in our body, while osteoblasts differentiate and live on much stiffer matrices, with properties similar to that of bone. Figure 1-11 shows the typical stiffness of different tissue types within our body.
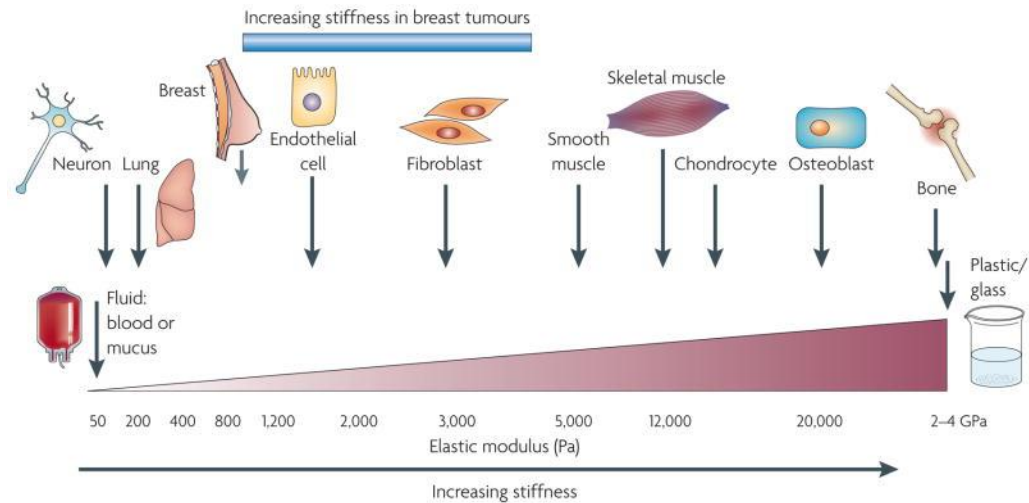
Figure 1-11 Characteristic stiffness of different cell types
Figure used by permission from Nature Reviews. Cancer 2 (2010)

One of the most impressive examples of cells responding to stiffness of the environment is during embryonic development. Stem cell differentiation is dependent on contractility which depends on the stiffness of the environment. Mesenchymal stem cell lineage specification can be guided by elasticity of the substrate. On soft gels, that mimic brain tissue stiffness (0.1-1kPa), the majority of the cells exhibit properties similar to neuron cells. On stiffer gels (10-40kPa), similar to muscle cells or bone, cells transform into myogenic and osteogenic lineages [75], [76]–[79]. Furthermore, there is evidence that substrate stiffness can affect lineage-specifying gene expression [80]. Another aspect of cell behavior, migration, is very susceptible to substrate elasticity, as cells tend to migrate from softer substrates towards stiffer ones [81]. Although it is increasingly clear that all of these different environments expose cells to varying mechanical stiffness, how cells sense and respond to these stiffnesses is an open question. Studying cells on substrates of different stiffness includes measuring overall morphology of the cell, migration, proliferation, or localization of different proteins inside the cell, like actin or

focal adhesion proteins, or measurements of traction forces exerted by cells. Currently the most widely used elastic substrates are made either from polyacrylamide gels or silicon elastomer, Polydimethylsiloxane (PDMS). The benefits of these gels are that the stiffness can be fine-tuned the stiffness of the end product in the wide range of relevant stiffnesses, and they are moderately easy to prepare in the lab. In our research we have been using polyacrylamide gels for several reasons. They are easy to use for fluorescent imaging since their optical properties are similar to that of glass, the gel thickness can be minimized to improve the quality of the image.

In addition to providing a means to modulate the elasticity of the cellular environment, polyacrylamide gels enable the measurement of traction forces exerted by cells. In 1980, Harris et. al. showed for the first time that cellular forces can be measured by observing the wrinkles generated on a silicon film [82], however a careful quantitative characterization of forces was not possible using that technique. In subsequent years, Traction Force Microscopy (TFM) has emerged as an effective technique to quantitatively measure the traction forces exerted by cells on flexible substrates [83], [84]–[87], [88]. This technique provides a method to measure forces at a reasonably high resolution (at the level of a single focal adhesion), is relatively easy to set up, and is suited for measuring forces over a large range. This technique has thus become widely popular in the last decade with researchers from different disciplines measuring forces of single cells as well as multicellular systems. In this method, fiduciary markers, such as beads, are embedded in an elastic gel in order to visualize deformations in the gel in response to cellular forces. These deformations can be quantified as a displacement field of beads with respect to their undeformed reference position. A number of computational

methods have been developed based on elasticity theory to obtain the traction forces from the displacement field of beads and the known stiffness of the gel [84], [87], [89]. This method will be described in more detail in the methods of the corresponding chapter. TFM is a continuously developing field and even recently, a new method was proposed to increase the resolution of TFM, by introducing fiduciary markers of different colors [90].

Different cell types show varied morphological behaviors on substrates of varying stiffness. Neuronal growth cones exert among the smallest traction stresses measured. Using TFM, Betz et. al. were able to find localization and magnitude of these forces [91]. T cells have been shown to be mechanosensitive as they exert higher forces on stiffer substrates [92]. Epithelial and fibroblast cell types are the most commonly studied cells in terms of response to substrate stiffness. These cells have been shown to have a marked dependence on the stiffness of the substrate wherein cells have a larger area on stiffer gels, exert higher forces, have increased stiffness, greater number of stress fibers and increased adhesions [93], [94], [95], [96]. Focal adhesions are thought to be the anchor through which forces are transmitted to ECM. Several focal adhesion proteins, such as zyxin, vinculin, and talin, have been identified as mechanosensitive, as their levels in the focal adhesion complex depends on the strength of the forces which are generated in stress fibers that couple to focal adhesions. Actin-binding proteins (ABP) help organize actin filaments into different types of networks that generate myosin II based contractile forces. The organization of the actin cytoskeleton defines the ability of a cell to exert forces and therefore, is essential in understanding mechanotransduction of the cell. Many ABPs have been already shown to affect traction forces. Inhibition of myosin II leads to a

diminished actin network and low traction forces [97], while inhibition of α-actinin leads to higher forces [26]. While the exact mechanism of force production is a subject of a debate, both motor proteins and actin binding proteins play an important role in force generation.

1.4.4 Mechanotransduction on substrates with different surface topography

Scientists have been actively studying the effect of surface topography on cell behavior for the last two decades. Tissues consist of a complex structure of different cell types and the extra-cellular matrix (ECM). ECM consists of different proteins and exhibits different structures ranging from nanometers to micrometers in size. Some of these structures, like collagen fibrils in the ECM can stretch for tenth of micrometers and can be as large 400 nm in diameter [98]. Besides the ECM, the basement of membranes also exhibit different nanostructures that influence cells around them [99], [100]. Therefore, the topography of the environment could be a critical regulator of cell shape and function and is important to study.

Advances in micro-fabrication and nano-fabrication have provided better tools to systematically explore the effects of surface topography on cell mechanics and cellular processes in general (including migration, polarization, differentiation, etc.) by mimicking naturally observed features in micro-fabricated or nano-fabricated substrates. These substrates include arrays of nanoposts [101], arrays of nanopits [102], as well as arrays of parallel nanoridges (nanogrooves). These nanoridges are of varying widths between two neighbor ridges and are among the most commonly studied substrates [103]–[106], because of their resemblance to commonly encountered by cells bundles of

collagen micro-fibrils in connective tissue, that run right beside each other in parallel, with many different types of cells attached to them [107].

Surface topography has been found to alter cellular functions on length scales spanning several orders of magnitude - from organization of proteins at the subcellular level to collective cell behavior. For instance, many cell types have been shown to decrease their proliferation rates when plated on non-flat surfaces [108]–[111]. By culturing cells on different topographical surfaces Lim et al., and Milner et.al found that cells had a significantly lower proliferation rate on substrates with larger nanoscale bumps [112], [113]. The sensitivity of cells to topographical cues is subtle as changing the surface topography by a few nanometers influenced cell proliferation. At the single cell level, it has been shown that nanotopographic features can alter differentiation of stem cells. Nanopits and nanotubes were shown to direct the differentiation of human mesenchymal stem cells into bone-like (osteogenetic) cells [114], [115]. However, introduction of osteogenetic media enhanced differentiation [116], suggesting that both geometrical and chemical cues can work together in guiding cell fate. Furthermore, cells were able to sense even subtle changes in surface topography as changes of tenths of nanometers in the height of nanopillars were shown to affect cell differentiation [117].

Zooming in closer on the cell, it has been shown that cells align along arrays of nanoridges, while elongating their shape, with the degree of this alignment depending on the geometrical parameters of the nanoridges. Observation of neurons from the peripheral nervous system polarizing along nanogrooves that were created specifically to mimic neurite bundles suggested that nanotopograpy could control the polarity of neuronal cells[118], [119]. At the subcellular level, lamellipodia, lamella, and filopodia usually

elongate along the direction of ridges [104]. Again, the degree of this alignment has been shown to depend on the widths of underlying structures [120], [121]. Along with the general orientation of the cell, different intracellular structures, like actin stress fibers or focal adhesions prefer to align along the direction of these topographical features [120], [121].

These studies show that small changes in surface topography can lead to drastic changes in cell morphology and behavior, reiterating the importance of topography sensing in cells. However, the mechanisms underlying sensing of surface topography and the details of the cellular machinery involved in this type of mechanosensing is not well understood. What makes a cell elongate in the presence of the ridges? How are cells able to differentiate between the tops and the bottoms of the ridges? How do local changes in surface topography affect global cytoskeletal properties of the cell, cell shape and cell behavior? These are just some of the questions that are topics of ongoing debate.

1.5 Summary and Motivation

As more and more evidence emerges about the importance of physical properties of biological systems and the role of physical stimuli in modulating biological processes, it is becoming more important to look at biological phenomena from a physical perspective. However, it is not enough to view these systems as simply biological or physical as the two fields are often intertwined in a complex way. Physical perturbations often lead to biological changes of the system and vice versa. Therefore it is important for both physicists and biologist to collaborate in order to obtain a deeper understanding of these questions. Cell biology is one of the areas of study where a combined effort of

both fields proves to be necessary. As previously discussed, environmental conditions can change cell behavior from reshaping focal adhesions and the cytoskeleton, to collective motion of cells in wound healing. Similarly, small changes in gene expression of cells can lead to drastic changes in structural organization and motility.

Contact of the cells with their surrounding tissue allows for adhesion complexes to form through which a cell can probe its environment by generating traction forces on its surroundings and adjust its intracellular structure to mechanical properties of the surroundings. At the same time cells can strengthen their adhesions under external pressure, such as the shearing of endothelial cells in the presence of blood flow. In both of these cases cells convert physical perturbations to biochemical signals that guide their fate, a phenomenon known as mechanotransduction. Understanding mechanotransduction of the cells is critical for many biological processes such as organ development, cancer, or wound healing. Reorganization of different cellular components leads to modulation of mechanical properties of the cell, but how mechanosensitivity arises from organization and dynamics of cellular components is not known. Forces generated by the actin cytoskeleton are transferred to the ECM through focal adhesions. There are two approaches currently in cell biology, one focusing on local mechanosensing through focal adhesion, and another focusing on global mechanosensing through acto-myosin networks.

Local mechanosensing can be quantified by looking at traction forces on level of single focal adhesion. Direction of traction forces exerted by cells have been shown to be correlated with orientation of focal adhesions [122]. On the other hand, the magnitude of traction forces does not always correlate with the size of focal adhesions. Balaban et al.

demonstrated that the magnitude of traction stresses increased linearly with the area of focal adhesions with the ratio of approximately 5.5nN/μm² [122]. At the same time a recent study by Stricker et al. demonstrated that adhesions of similar size did not exert the same stress suggesting that relationship between focal adhesion size and traction forces might exist only during initial focal adhesion formation [123]. Moreover, Beningo et. al. have shown that small nascent adhesions were able to transmit higher stresses in migrating cells [124]. [124]. These studies highlight the importance of focal adhesions on forces generated by the cell. However, it is still not clear how cells regulate these forces. Some current models explain local mechanosensing by conformational changes in various focal adhesion proteins under applied stress. Such conformational changes could potentially open up new binding sites for new proteins or increase the strength of the bond [125], [37], [71]. Similarly it has been shown that focal adhesions align with topographical features of its environment [121]. But, how molecular features at the nanometer scale impart the cell with global ability to respond to and sense it surroundings at the micrometer scale is not well understood.

One possibility comes from acto-myosin networks. Some of the models suggest that actin networks could potentially adjust their mechanical properties by adjusting their contractility to that of the environment. In these models focal adhesions serve merely as force transmitters, while actin cytoskeleton plays a main role. A simple model from active matter theory explains the dependence of traction forces on the rigidity of the substrate through the active component coming from contractility of the actin cytoskeleton [126], which does agree with experimental results [127]. In this model, both the cell and the extracellular matrix are represented by an elastic spring, while the

cytoskeleton has an active force component, F_A pushing on its environment (See Figure 1-12). Force balance on the cell reads,

$$k_{ext}(l_{ext}(t) - l_{ext}^0) = k_c(l_c(t) - l_c^0) + F_A, \qquad (1)$$

where k_c and k_{ext} are spring constants of the cell and the extra-cellular matrix, and l_c, l_{ext}, l_c^0, l_{ext}^0, and F_A are shown on Figure 1-12. The amplitude of the traction force F^{eq} then becomes

$$F^{eq} = F_{sat} \frac{k_{ext}}{k_{ext}+k_c}, \qquad (2)$$

where F_{sat} is the traction force when $k_{ext} \gg k_c$ .Moreover, Oakes et. al. have shown that the traction forces of cells are guided only by cell spread area [128]. They present a model that can predict traction stresses based only on the shape of the cell (area and curvature). While such phenomenological models are reasonable in predicting traction forces of cells, they do not take into account the local component of focal adhesion dynamics and therefore lack in understanding of physical processes that guide traction forces. Similarly, actin` cytoskeleton aligns with topographical features of the substrate [120], but how the degree of this alignment changes with the nanoscale changes in surface topography is not yet established.
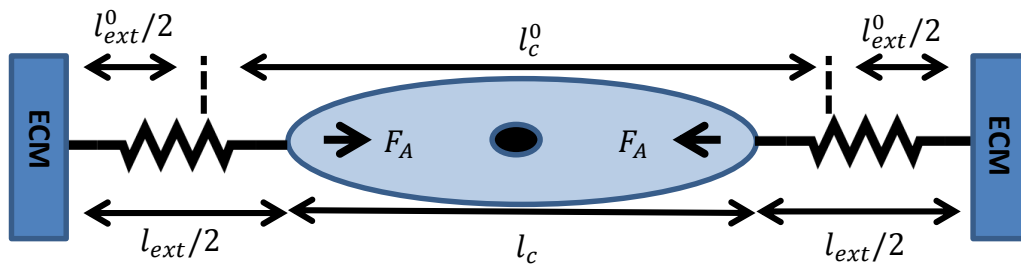
Figure 1-12 Schematic of the model proposed by Marcq et al. [126]

In this thesis, we have attempted to answer questions regarding the potential roles for actin crosslinkers in sensing substrate stiffness (especially the role of palladin, which affects both stress fiber formation and focal adhesion assembly), and regarding the role of surface topography on global and local actin organization and dynamics, by studying cellular mechanosensitivity to both substrate elasticity and topography.Chapter 1 has provided an introduction to various aspects of the field. Chapter 2 will give an overview of mechanosensing of substrate stiffness, and in particular we will describe our work to dissect the role of the actin binding protein palladin in cellular force generation and stiffness sensing. As described before, palladin is found in stress fibers, lamella and focal adhesions, and is therefore, a likely candidate responsible for mechanosensing of the physical environment. In our studies we wished to elucidate how palladin affects actin organization, traction force generation, and cell response to substrate stiffness. Chapter 3 will discuss our studies on the effects of surface topography on cells. Here, we look at tumor-associated fibroblasts, to understand how an array of parallel ridges can affect cell morphology, actin cytoskeletal organization, and the dynamics. Analyzing both static images of cells, as well as dynamics of actin cytoskeleton and focal adhesions, we have sought to provide some insights into mechanosensing of surface topography. Chapter 4 will provide a summary of the work and discuss possible implications and future work to be pursued.

2 The actin crosslinking protein palladin modulates force generation and mechanosensitivity of tumor associated fibroblasts

This chapter was adapted from M. Azatov, S. Goiccochea, C. Otey, A. Upadhyaya "The actin crosslinking protein palladin modulates force generation and mechanosensitivity of tumor associated fibroblasts", submitted to Biophysical Journal, 2015

2.1 Summary (Abstract)

Cells organize actin filaments into higher-order structures by regulating the composition, distribution and concentration of actin crosslinkers. Palladin is an actin-crosslinking protein that is found in the lamellar actin network and stress fibers, two actin structures critical for mechanosensing of the physical environment. Palladin also serves as a molecular scaffold for α-actinin, a key actin crosslinker. By virtue of its close interactions with actomyosin structures in the cell, palladin may play an important role in cell mechanics. However, the role of palladin in cellular force generation and mechanosensing has not been studied. In this study, we investigate the role of palladin in regulating the plasticity of the actin cytoskeleton and cellular force generation in response to alterations in substrate stiffness. Traction force microscopy revealed that tumor-associated fibroblasts are sensitive to substrate stiffness as they generate larger forces on substrates of increased stiffness. Contrary to expectations, knocking down palladin increased the forces generated by cells, and also inhibited the ability to sense substrate stiffness for very stiff gels. This was accompanied by significant differences in the actin

organization and adhesion dynamics of palladin knock down cells. Perturbation experiments also suggest altered myosin activity in palladin knock down cells. Our results suggest that the actin crosslinkers such as palladin and myosin motors coordinate for optimal cell function and to prevent aberrant behavior as in cancer metastasis.

2.2 Introduction

2.2.1 Motivation

In vivo, cells constantly interact with the surrounding microenvironment. It has been shown that a wide variety of physical and biological aspects of cell behavior are dependent on the physical properties of a cell's environment [129], [130]. Cell migration in particular is highly susceptible to the mechanical properties of the environment such as substrate elasticity [131]. Furthermore, stem cell differentiation into different cell types is modulated by the elasticity of the microenvironment [75]. Recently, it is becoming increasingly clear that the mechanical interactions of cancer cells with their environment are essential components in stages of tumor progression and metastasis [132], [133].

There has been intense interest in the molecular mechanisms that allow cells to sense and respond to the mechanical properties of their environment [60]. The cytoskeleton and cell adhesions are key components of a cell that enable it to sense the mechanical properties of its external environment. An extensive body of work has shown that focal adhesions act as mechanosensors [52], [63]–[66]. In accord with this, the size, morphology and dynamics of focal adhesions depend on the stiffness of the matrix [38], [122], [134]. The coupling of the focal adhesions to the actin cytoskeleton allows the contraction of myosin motors, exerting contractile forces on the substrate at focal

adhesions [52]–[54]. The contractile tension generated by myosin II is transmitted to the substrate as traction allowing the cell to sample the mechanical properties of the substrate. Proteins which link actin filaments with developing adhesions and the extracellular matrix, and which organize actin filaments into large-scale coherent structures are important for force generation [26], [39], [67], [68], [69]. However, their contribution to mechanotransduction is not well understood.

Most mammalian cells express a diverse array of actin cross-linking proteins. The contribution of cross-linkers in organizing the cellular actin networks has been examined in the context of actin crosslinking proteins such as α-actinin and zyxin [26], [39], [67], [135], [136]. It has recently been shown that α-actinin is involved in force transmission to the ECM via integrin binding [67], while zyxin is important in maintenance of stress fiber integrity under applied loads [136]. The actin binding protein, palladin, occupies a unique molecular niche, functioning as a molecular scaffold that directs the assembly and organization of actin networks [17]. Palladin directly binds actin filaments through its multiple Ig (Immunoglobulin-like) domains [137]. Palladin binds to the actin crosslinker, α-actinin, and colocalizes with α-actinin along stress fibers and also binds to the zyxin family member Lipoma Preferred Partner [11], [138], [139]. *In vitro* assays show that palladin cross-links actin into visco-elastic networks and synergistically combines with α-actinin [140]. There is evidence that palladin is up regulated in pancreatic tumor-associated fibroblasts which have been shown to promote the progression of pancreatic tumors, metastasis, and the resistance to therapy [141]–[143], [144]. Evidence suggests that the misregulation of actin reorganization resulting from altered palladin levels may contribute to aberrant cellular behavior. Given its localization in the cell, it is a likely

candidate for force transmission. However, the role of palladin in focal adhesion maturation and in organizing actin structures for appropriate force transmission and consequently cell response to ECM properties such as stiffness, is unclear.

Here, we use pancreatic tumor associated fibroblasts to examine the role of palladin in actin organization, force generation and mechanosensing. As a model to study mechanosensing, TAFs are of particular interest because of their complex role in the assembly and dynamic remodeling of the tumor stroma [145], [146]. In order to study mechanosensing of TAFs we used soft elastic substrates with varying rigidity. While a typical range of fibroblast tissues is ~ 3 kPa [147], we used a wide range of rigidities of 1-60 kPa to study the role of palladin in cellular mechanosensing. We found that palladin plays a role in adhesion maturation and stress fiber formation, and thus has a significant effect on cellular forces. We also found that palladin expression affects the morphology and dynamics of the cell membrane and actin flows. Our experiments further suggest that palladin may have an effect on myosin activity and organization in cells. Taken together, our results demonstrate an important role for palladin in regulating cellular forces and their mechanosensing function.

2.2.2 Tumor associated fibroblasts in cancer development

The pancreas is an organ that belongs to the digestive systems in vertebrates. In the human body it can be found in the abdominal cavity behind the stomach. The pancreas is a gland that produces many important hormones such as somatostatin, insulin, and glucagon. It also creates the pancreatic polypeptide that circulates in blood. In addition to its glandular function, it is also a digestive organ. It produces enzymes that work to assist digestion and absorption of nutrients in the small intestine. These digestive

enzymes all help to break down proteins, carbohydrates, and lipids. The pancreas can be functionally divided into two components: an exocrine component, which secretes pancreatic fluid that contains digestive enzymes, and an endocrine component composed of islets which secrete hormones (See Figure 2-1). Inside the exocrine component, there are ducts called acini that secrete digestive enzymes into the lumen of the acini. These acini use the pancreatic ducts to drain the digestive enzymes into the small intestine. Pancreatic stellate cells (PaSCs) are located in the exocrine pancreas along with many other types of cells. They are located in the periacinar space and make a ring around the base of the acinus. They help to maintain the extracellular matrix of the pancreas and assist in wound healing. They are also often found in periductal and perivascular regions of the pancreas [148]–[151].The pancreatic stellate cells are also incredibly important in the pathobiology of the major disorders involving the exocrine pancreas. These disorders include both pancreatic cancer and chronic pancreatitis. PaSCs are involved in the disease pathogenesis after converting from a quiescent state into an activated state. This activated state resembles a lot normal activated fibroblasts, called myofibroblasts[152], [153] . It is also important to note that pancreatic cancer is the fourth leading cause of cancer- related death. It is resistant to therapy and is usually only detected after metastasis. After diagnosis the majority will die within one year.
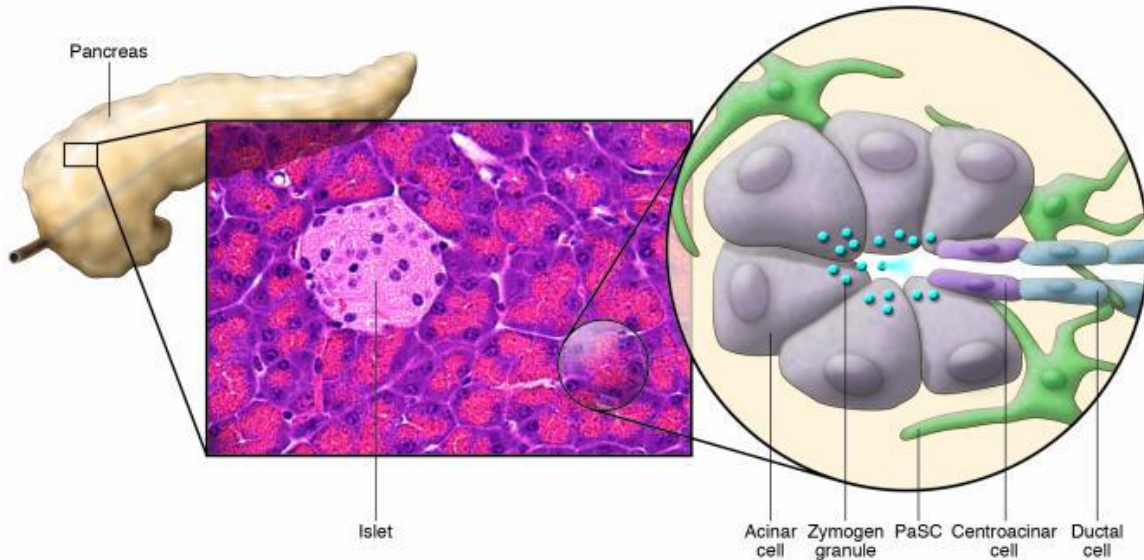
Figure 2-1 Schematic of the cellular components of the exocrine pancreas.
Figure used by permission from Journal of Clinical Investigation 117 (2007)

Evidence is emerging that there a symbiotic relationship between pancreatic cancer cells and PaSCs which helps the tumor to grow faster and more often. For example, research noted that when PaSCs were present, there was an increase in occurrences of tumor formation after only limited numbers of cancerous cells were injected. Due to the PaSCs presence tumors that, under normal conditions would be unable to form, were established [154]–[156]. The stroma diminishes tumor cells' ability to respond to radiation and chemotherapy. Conditioned medium from PaSCs sparked the proliferation, migration, and invasion of pancreatic tumor cells. This symbiotic relationship is enhanced further, as culture supernatants found in human pancreatic tumor cells lines increase the PaSC proliferation and production of ECM proteins [154]–[156]. Because of their relationship with tumor cells, these types of cells are often called tumor-associated fibroblasts (TAF), the notation that will be used throughout the thesis.

41

Interestingly, the palladin gene has been shown to be mutated in TAFs. Palladin is upregulated in both tumor cells and TAFs. There was excessive palladin in all of the precancerous and cancerous pancreatic tissues [157]. It was also overexpressed in the tissue adjacent to the tumor when compared to palladin levels in normal pancreas [157]. There was a significant difference in the levels of palladin expression between the normal pancreas and the following other three groups of tissues: pre-cancer, cancer, and normal adjacent. [157]. Since palladin is an actin binding protein (ABP), abnormal levels of palladin expression could lead to abnormal mechanical features of the cell. In fact, it has been shown that palladin can promote invasiveness of TAF by formation of invadopodia [158]. The details of palladin function and structure will now discussed in the next section.

2.2.3 Palladin structure and binding sites

As previously discussed, palladin is an ABP that was discovered in the last fifteen years, bundles actin in vitro and can cross-link actin into different types of networks [137]. There are several isoforms of palladin. The three most common have molecular weights of 200kD, 140kD, and 90kD. They are encoded from the same gene, and the differences arise from unique transcription start sites along the gene [15]. These three isoforms are found in most vertebrates, but the expression pattern depends on the cell type. For example, the 200 kD isoform is most commonly found in bone or heart [15]; the 140 kD isoform can be found in embryonic tissue, but in adults it seems to only be restricted to Z-discs of muscle cells. However, the 90 kDa isoform is the most common isoform of palladin. It is down regulated in adult organs, however universally present in

many developing organs [15]. In fact, knocking out palladin in mice is embryonically lethal, underscoring the importance of its function in cells.

Palladin is closely related to two other proteins called myotilin and myopalladin. Myopalladin and myotilin are mostly expressed in muscle cells. In muscle cells they localize to Z-discs[159]. All three proteins have several copies of immunoglobulin-like domains (IG-like) in common. These domains are found in all three isoforms of palladin. Palladin has three Ig domains (Ig3, Ig4,and Ig5) in its 90kDa isoform, four Ig domains (with additional Ig2 domain) in its 140kDa isoform, and five Ig domains in 200kDa isoform[137]. Ig domains are commonly found in proteins interacting with actin and myosin. They are also found in proteins involved in striated muscle, underlying their importance for actin organization [137] (See Figure 2-2). Among all Ig domains in different palladin isoforms, the third Ig domain Ig3, has been shown to be the minimum requirement for actin binding [137].
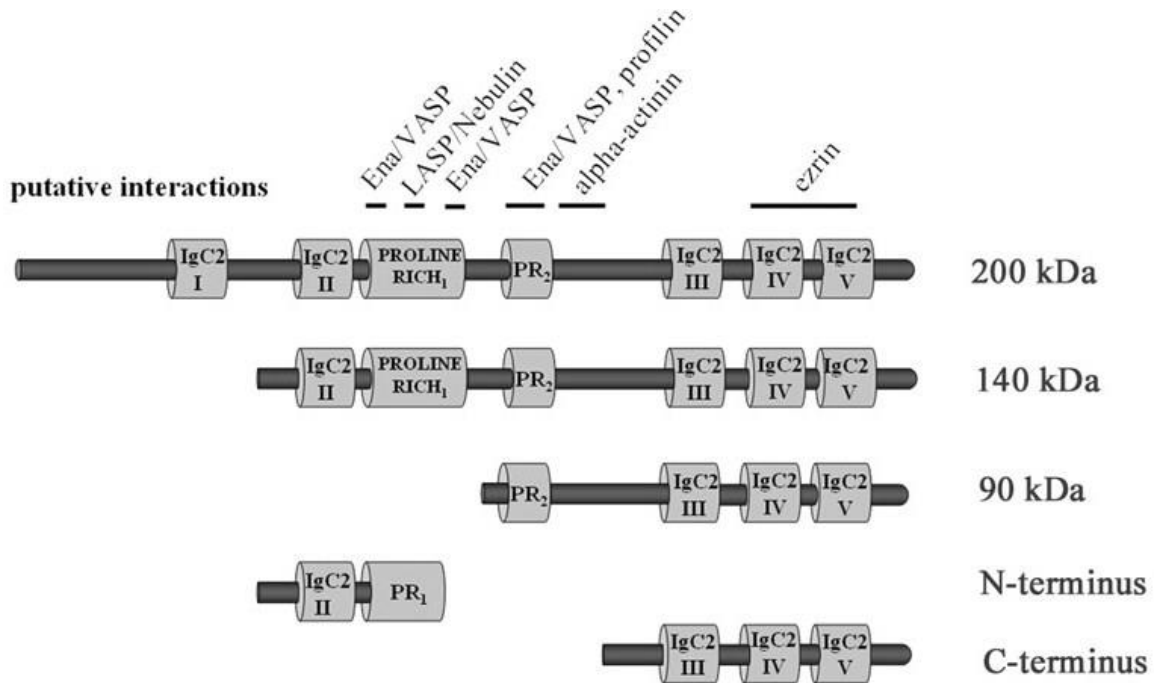
Figure 2-2 Schematic representation of thee palladin isoforms showing binding sequences for different ABP
Figure used by permission from Journal of Cell Science 119 (2006)

Besides Ig domains, there are two proline-rich domains, which bind several other cytoskeletal proteins (See Figure 2-2). VASP binds to palladin at its proline-rich domain. As mentioned earlier VASP is localized to stress fibers, is involved in focal adhesion formation, and is involved in cell migration, as it localizes at sites of actin polymerization at the leading edge of the cell. Among other proteins, palladin uses proline-rich domains to bind profilin [16], and Src [160]. Thus, both proline-rich domains and Ig domains play an important role in palladin's binding capabilities, and hence actin cytoskeleton organization.

2.3   Materials and Methods

2.3.1 Cell culture and transfection

. Wildtype cells, EGFP-palladin labeled cells and palladin KD cells (Palld4) were cultured in DMEM with 10% FBS, and 1% PS and sodium pyruvate at 37°C. For spreading experiments, cells were plated at 15% confluence on fibronectin (from bovine plasma, Sigma-Aldrich) coated glass coverslips. Fibronectin was coated on coverslips by incubating with 500µl of 10 µg/ml fibronectin solution for 2 hours at room temperature. Imaging media L-15 (Life technologies, Grand Island, NY) was used for microscopy. For area measurements cells were fixed using paraformaldehyde and stained with rhodamine-phalloidin. Transient transfections were done with m-Apple paxillin, mCherry-actin, mCherry-myosin using Fugene HD tranfection reagent (Promega, Madison WI) using standard manufacturer protocol.

2.3.2 Construction of cell lines

EGFP-palladin fragment was ligated into Z4-MSCV-mEos2-actin (a gift from Morgan Huse, Rockefeller University, New York, NY). Retroviruses were generated according to standard protocol [161], with Phoenix Amphotropic cells and transduced into TAFs. The cells were then selected in 100 µg/ml zeocin for 2 weeks and sorted with fluorescence-activated cell sorting to obtain bright fluorescent cells. I would like to thank King Lam Hui for making this cell line. The palladin knockdown cell line (Palld4), in

which palladin was silenced using shRNA sequence, was created as described previously [158].

2.3.3 Traction forces and preparation of PAA

For traction force experiments fibronectin-coated PAA gels containing 200-nm fluorescent beads on the top layer of the gels were prepared as before [162], [92]. The ratio of 40% acrylamide to 2% BIS (Bio-Rad, Hercules, CA) was varied (2:0.1, 3:0.1, 4:0.1, 5:0.1) to obtain gels of different stiffness ranging from 1kPa − 60kPA. Glass coverslips were coated with 3-aminopropyl-trimethocysilane and glutaraldehyde (Sigma-Aldrich, St. Louis, MO) to allow polyacrylamide gel to conjugate to the glass and the gel was allowed to polymerize on the glass coverslip. Later another thin (5μm) layer of 200 μm fluorescent beads was added to the top of the gel. 500 μl of sulfo-SANPAH (ProteoChem, Loves Park, IL) solution was added to the surface of the PAA gel and incubated in the dark for 30 minutes at room temperature. The sulfo-SANPAH solution was washed away with PBS and 500 μl of fibronectin solution (10μg/ml) was pippeted onto the PAA gel and placed two inches under an 8 W ultraviolet lamp for 8 minutes at room temperature.

After obtaining images of multiple cells and corresponding beads on a gel, cells were trypsinized to abolish adhesions and detach cells from the gel, and obtain a reference (or zero displacement) image for traction force analysis. Images were aligned to correct for drift. The displacement of fluorescent beads between the two images (corresponding to the deformed and undeformed gel) was calculated using particle image velocimetry (PIV) (using the freely available Matlab package MPIV,

46

http://folk.uio.no/jks/matpiv/index2.html) and these displacements were used to obtain the traction force maps using Fourier Transform Traction Cytometry (FTTC) [87]. Cells were treated with different concentrations of blebbistatin (Sigma-Aldrich Inc., St. Louis, MO) for 30 min and then allowed to recover for 1 hour. To remove blebbistatin the media containing it was washed away 3 times with 3ml normal imaging media.

2.3.4 Live cell microscopy

Fluorescence and Interference Reflection Microscopy images were collected at 37°C using an inverted microscope (TE2000 PFS, Nikon, Melville, NY) with a cooled CCD camera (Coolsnap HQ2, Photometrics, Tucson, AZ). TIRF imaging was done using a 60× 1.49 NA objective lens, a 491 nm laser (100mW, Andor, South Windsor, CT) for EGFP excitation and a 561 nm laser (75mW, Andor) for AF546 excitation.

2.4   Results

2.4.1 Shape and dynamics of spreading cells

We first examined the distribution and localization of palladin in TAFs. We expressed green fluorescent protein tagged palladin (EGFP-Palladin) in TAFs and visualized the morphology of the cell as it spread on fibronectin-coated glass coverslips. We obtained time-lapse images using total internal reflection fluorescence (TIRF), widefiled fluorescence, and interference reflection microscopy (IRM) (See Figure 2-3A-C). During early spreading, palladin appears diffusely throughout the cell or in small clusters with a modestly enhanced localization at the cell edge. Palladin forms highly mobile puncta that move on the cell surface contact zone as the cell spreads, forming nascent adhesions at the cell periphery. After about 30 min of spreading, when the area

47

of the spread cell is maximal, palladin puncta organize to form mature focal adhesions and palladin is recruited into assembling stress fibers. Upon completion of spreading, palladin undergoes a constant retrograde flow from the cell edge towards the interior along stress fiber templates. Rhodamine phalloidin staining to visualize filamentous actin simultaneously with EGFP-palladin showed that palladin strongly colocalized with actin and was observed as punctate spots along stress fibers (See Figure 2-3D), consistent with previous work [17], [139], [163], [12]. Figure 2-3F shows a line profile across the stress fiber in Figure 2-3E demonstrating the periodicity of palladin bands. From these line profiles we measured an average spacing between neighboring palladin bands to be 1.21 $\pm$ .05 μm which was similar to the band spacing found for alpha-actinin and myosin in various cell types [97].
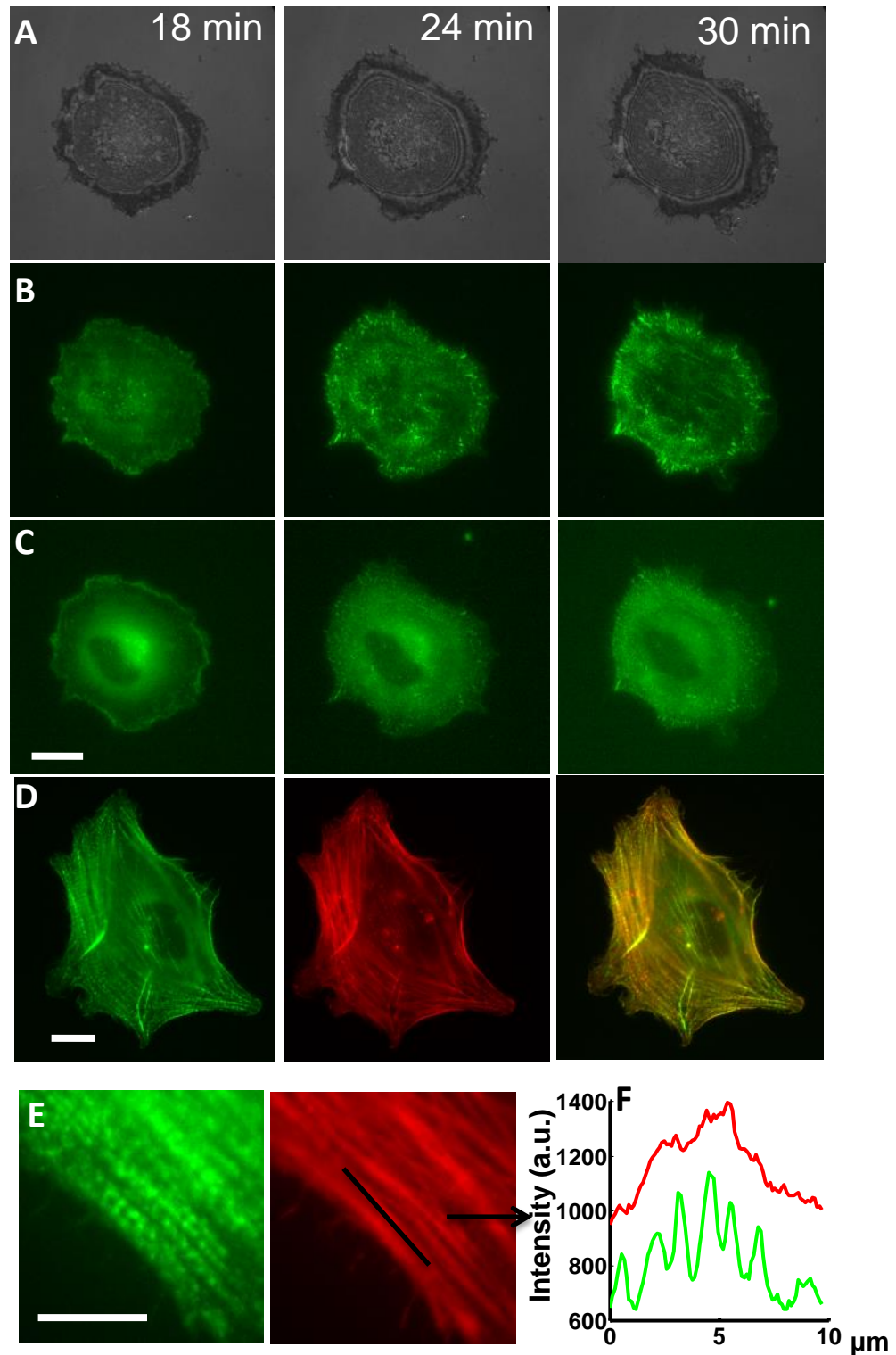
Figure 2-3 Palladin dynamics and organization in spreading TAF. (A) Time lapse IRM images of a representative TAF spreading on fibronectin coated glass coverslips. Cell spreading is completed at about 20 – 30 min after initiation of contact with the surface.

(B) Time lapse TIRF images of EGFP-Palladin for the same cell spreading on glass, showing the organization of palladin in a thin ventral section of the cell. **(C)** Time lapse widefiled fluorescence images of EGFP-Palladin for the same cell. Scale bar: 20 µm. **(D)** Snapshots of a fully spread cell at a later time point (60 min) showing that EGFP-Palladin (left panel) and actin (middle panel, as visualized by Rhodamine-phalloidine staining) are colocalized (right panel) in stress fibers. Scale bar: 20 µm. **(E)** Zoomed in image of an actin stress fiber in EGFP-Palladin cell showing the localization of palladin and actin across a stress fiber. Scale bar: 10 µm. **(F)** The intensity profile across the line shown in (D) proving the periodicity of palladin bands (green) and the smoother intensity profile of actin (red).

2.4.2 Palladin is important for focal adhesion maturation and radial stress fibers

A variety of studies have shown that mechanosensing arises from the tension-mediated maturation or dynamics of focal adhesions [38], [122], [134], [164]. The role of palladin in the formation and maturation of focal adhesions is not known. We therefore examined the kinetics of palladin during focal adhesion growth. In order to examine the effect of palladin expression on adhesions, we constructed a cell line knocked down in palladin (Palld4 or palladin KD) [163] (see Methods). We used paxillin, a key component of adhesion structures in cells, as a focal adhesion marker. We transfected EGFP-palladin and palladin KD cells with mApple-paxillin and used dual-wavelength TIRF imaging to visualize focal adhesion formation. Paxillin primarily localized to the tips of adhesions while palladin appeared in focal adhesions and stress fibers (See Figure 2-4B). During the early stages of focal adhesion formation, palladin was initially localized to a thin region at the cell periphery, while paxillin appeared next to palladin but towards the cell interior. Once formed, focal adhesions grew towards the interior as shown in the kymograph along a typical focal adhesion (See Figure 2-4B). As focal adhesions matured, the localization pattern of the two proteins switched – paxillin now appeared at the outer tip of the focal adhesion at the cell edge, while palladin was localized towards

the cell interior (See Figure 2-4C). This switch between palladin and paxillin localization is visible in a time-lapse of intensity profiles measured along the dotted line across a focal adhesion (See Figure 2-4D). Initially the peak corresponding to palladin (green) leads paxillin (red). As adhesions matured, both proteins were recruited into adhesions, but the peaks switched, with paxillin being closer to the outer edge of the cell membrane. Focal adhesions were often seen to merge and palladin puncta were rapidly incorporated into newly assembling stress fibers.

To examine if palladin expression affects focal adhesion maturation, we measured the lengths of focal adhesions and their timescale of formation for both EGFP-palladin and KD cells. A polygon was drawn around the maturing focal adhesions (See Figure 2-4E,F) and the focal adhesion length was defined as the diagonal of the rectangle around these polygons. To measure the maturation time of focal adhesions, we quantified the mean fluorescence intensity inside the defining polygons. The intensity rapidly increased when an adhesion formed and started growing (See Figure 2-4G, H). The time taken for the intensity to reach its maximum value from the onset of the rise was defined as the maturation time of the focal adhesion. We found that palladin knockdown resulted in focal adhesions which had a smaller maturation time (Figure 2-4I) and which were shorter in length (Figure 2-4J) compared with palladin expressing cells. This indicates a role for palladin in focal adhesion templating and growth.

We next examined whether palladin knockdown affected cell shape, and actin organization, specifically stress fiber formation. A wide variety of adhesive and contractile cells possess actin stress fibers, which have been postulated to play an important role in the transmission of actomyosin forces through the cell and the extra-

51

cellular matrix [32], [165]. Distinct populations of stress fibers have been observed including transverse arcs (which form parallel to the cell edge and are not associated with focal adhesions), ventral stress fibers (which span the entire cell body, and lie along the base of the cell, often under the nucleus, attached to the focal adhesions at each end), and radial stress fibers which are associated with focal adhesions and postulated to be important for force transmission [23]. Given our finding that palladin plays a role in focal adhesion maturation, and the fact that focal adhesions are known to serve as templates for stress fiber assembly, we hypothesized that palladin may be important for actin stress fiber formation in TAFs.
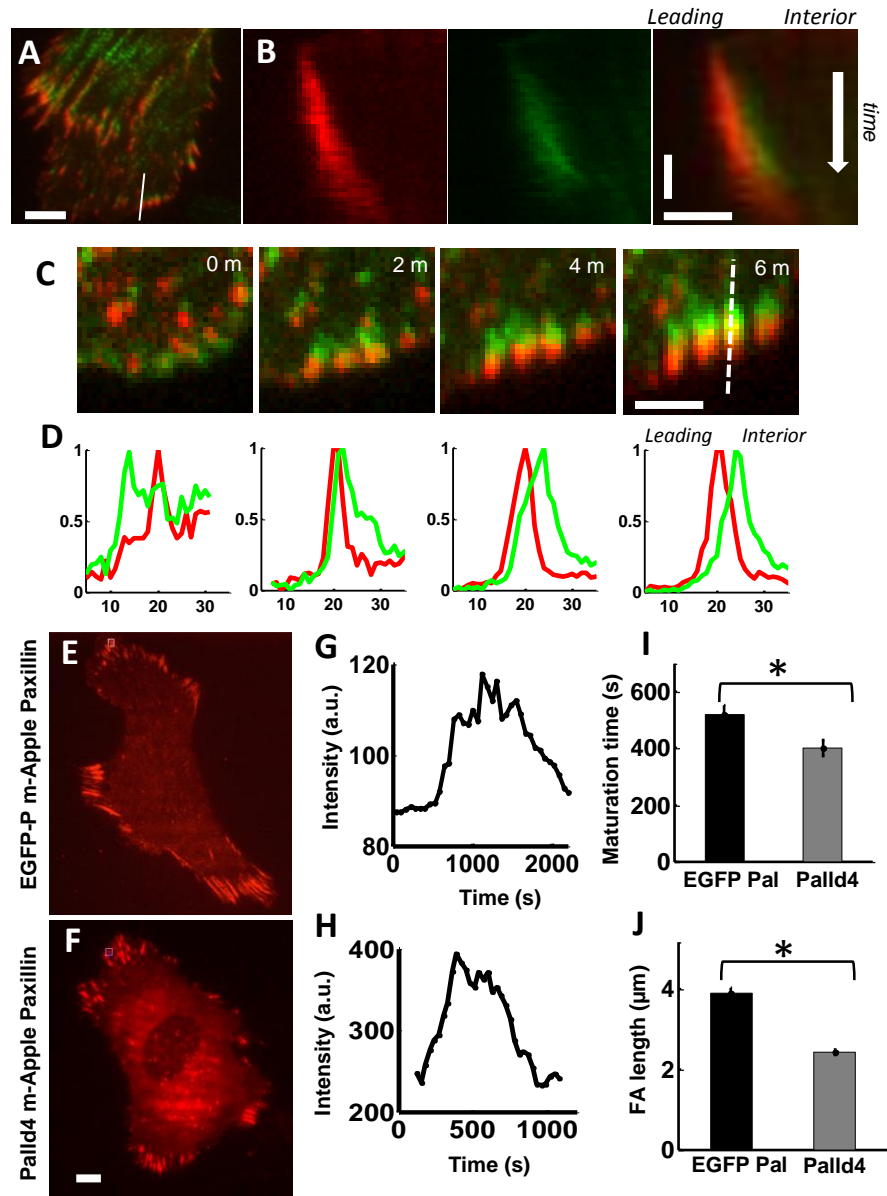
Figure 2-4 Palladin associates with focal adhesions and modulates focal adhesion maturation. (**A**) Dual color image of a cell expressing EGFP-Palladin (green) and mApple-Paxillin (red) showing focal adhesions and stress fibers. Scale bar: 5 μm. (**B**) Kymograph along the direction of growth of a focal adhesion (as indicated by white line in A), showing accumulation of paxillin (left) and palladin(middle) in a focal adhesion. Scale bars: 3 μm horizontal, 2 min vertical. (**C**) TIRF images of a region of the lamellipodia showing the temporal changes in the localization pattern of GFP-Palladin (green) and mApple-Paxillin (red) in growing adhesions. Scale bar: 3 μm (**D**) Graphs showing time course of intensity profiles of palladin (green) and paxillin (red) along the white line drawn in C. The palladin peak, which is initially closer to the cell periphery,

subsequently switches position with the paxillin peak, to localize at the cell interior. TIRF image of **(E)** EGFP-Palladin cell and **(F)** Palladin knockdown cell transfected with mApple-paxillin (red) showing multiple focal adhesions along the cell periphery. Scale bar: 15 μm**. (G)** Plot of the mean fluorescence intensity of a focal adhesion as a function of time during adhesion maturation in (G) an EGFP-Palladin cell and **(H) a** Palladin knockdown cell. **(I)** Bar graphs showing comparison of the maturation times of focal adhesions in EGFP-palladin and Palladin KD cells ($p<0.01$, t-test). **(J)** Comparison of focal adhesion length in EGFP-palladin and Palladin KD cells ($p<0.01$, t-test).

In order to examine the effect of palladin expression on cell shape, area, and spreading dynamics we allowed both types of cells (EGFP-Palladin and Palld4) to spread on FN coated coverslips and fixed cells at different time points after spreading initiation. We measured the contact areas for both cell types from IRM images at different time points as described before [166] (See Figure 2-5) Interestingly, we found that the spread areas and spreading kinetics were very similar for EGFP-Palladin and Palld4 cells. This suggests that palladin expression is not the rate-limiting step in these processes.
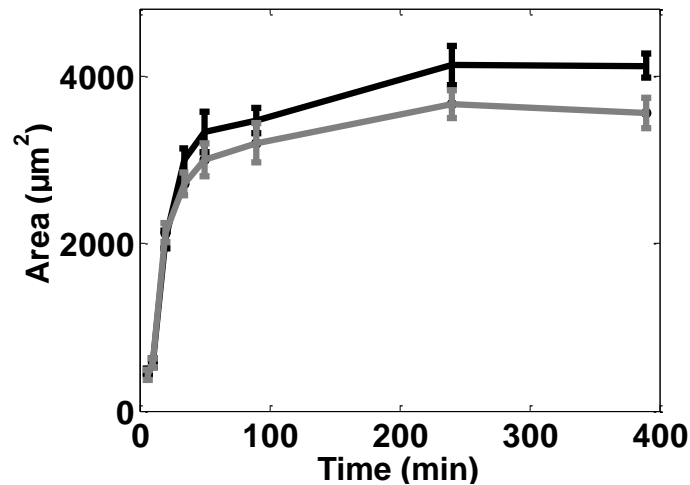
Figure 2-5 Spread area (as measured from IRM images) as a function of time for EGFP-palladin cells and Palladin knockdown (KD) cells. Areas were obtained by allowing cells to spread and fixing them at specific time points thereafter. Each data point represents an average of N > 30 cells (30<N<40). The rates as well as the final spread areas were similar in EGFP-Palladin(black) and knockdown cells(grey).

Previous work has shown that the actin crosslinker, α-actinin is involved in radial stress fiber (RSF) formation as knockdown of α-actinin decreased the number of RSF in cells [26], [28]. Since palladin accumulates at stress-fibers and co-localizes with α-actinin, palladin knockdown may have a similar effect on stress fibers. We allowed EGFP-palladin, palladin KD (Palld4) and cells with control sh-RNA (pGIPz) to spread on FN coated coverslips, fixed the cells after 4 hours of spreading, and stained with Rhodamine-phalloidin to visualize f-actin. EGFP-palladin cells displayed radial stress fibers enriched in both f-actin (See Figure 2-6A) and EGFP-palladin (See Figure 2-6B), visible as bright structures roughly oriented radially with respect to the cell edge, indicating that RSF are comprised of both palladin and actin. However, palladin KD cells showed significantly fewer radial stress fibers (Figure 2-6C). We confirmed that cells with control sh-RNA (PGIPZ) also displayed robust RSF formation (See Figure 2-6D). We quantified radial stress fiber formation by scoring cells to have RSF if they had more than five RSF. We found that a greater fraction of EGFP-Palladin cells have RSF as compared to palladin KD cells (See Figure 2-6E), consistent with previous results on α-actinin. Our results confirm similar findings that have been documented in osteosarcoma cells [27] and extend them to TAFs. We also observed qualitatively that RSF have enhanced levels of EGFP-palladin fluorescence, consistent with previous observations of increased F-actin in RSF [26]. These observations show that EGFP-palladin cells have a greater ability to form radial stress fibers confirming that palladin is involved in RSF formation. It's been previously shown that palladin KD cells have decreased Rac activity [14]. Conversely, increased Rac activity was shown to result in an increased number of

55

dorsal (radial) stress fibers [28], which correlates with our results of increased RSF in EGFP-palladin cells (cells with higher Rac activity as compared to KD cells).
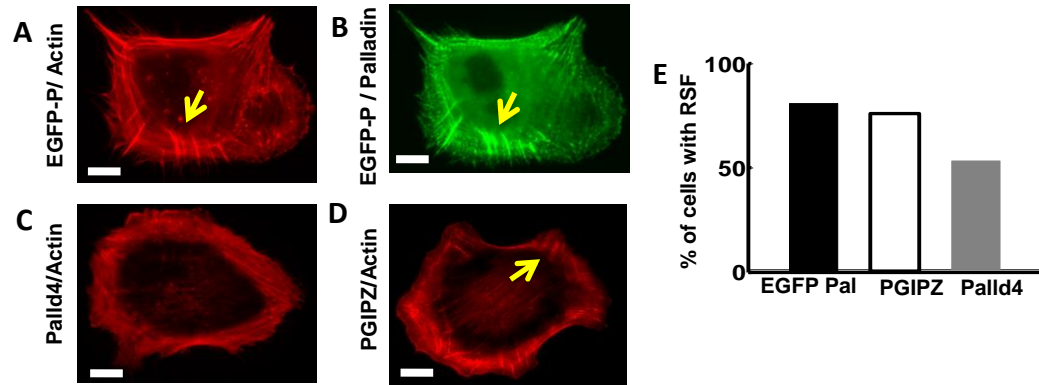
Figure 2-6 Palladin knockdown impairs radial stress fiber formation. **(A)** Snapshot of EGFP-Palladin cell labeled with Rhodamine-phalloidin for actin showing strong radial stress fibers (RSF). A typical RSF is indicated by the arrow. Scale bar: 15 µm. **(B)** Snapshot of EGFP-Palladin cell showing localization of Palladin in RSF. Scale bar: 15 µm. **(C)** Snapshot of Palladin KD cells labeled with Rhodamine-phalloidin showing a lack of radial stress fibers in the cell. Scale bar: 15 µm. **(D)** Snapshot of a control shRNA cell (PGIPZ) showing the presence of stress fibers as indicated by the arrow for an example. Scale bar: 15 µm for all panels. **(E)** Bar graph showing comparison of the percentage of cells (EGFP-palladin, control sh-RNA or PGIPZ, and Palladin KD or Palld4) which displayed radial stress fibers quantified at 4 hours after spreading initiation.

2.4.3 Tumor-associated fibroblasts are mechanosensitive

Our findings that palladin is an important regulator of focal adhesion maturation and radial stress fiber formation led us to surmise that palladin could be a critical candidate in cellular force generation and mechanotransduction. Further, because of the postulated role of radial stress fibers in force transmission from cells to ECM via focal adhesions, we wished to explore the role of palladin in cellular force generation and mechanosensing. While the role of α-actinin in force generation has been studied,

whether and how actin crosslinking proteins are important for mechanical sensing of the extracellular matrix is unknown. We first examined the response of TAF cells to varying stiffness of the matrix using traction force microscopy. Cells were allowed to spread on fibronectin-coated polyacrylamide gels for 3-4 h and then imaged with wide-field fluorescence microscopy. Fluorescence images of EGFP-palladin cells in the green channel, or bright-field images for wild type TAF cells were obtained simultaneously with images of beads in the red channel (See Figure 2-7A). Traction forces were obtained from the displacement of the elastic gel as they were deformed due to forces exerted by the cell as it moved or changed shape (see Methods for details). Figure 2-7B shows a representative traction stress map for stresses generated by the cell in Figure 2-7A. Typical peak tractions were measured to be on the order of a few hundred Pa, consistent with values observed in other cells [26], [41], [167]. Figure 2-7C shows a representative vector map of traction forces superimposed on the fluorescence image of the cell, showing centripetal or inward directed traction. We observed that the majority of the stress was exerted in the peripheral regions of the cell where strong cell-substrate attachments exerted an inward force.

In order to examine the effect of substrate stiffness on cellular force generation, we used elastic gels of varying stiffness. We modulated the gel stiffness by varying the ratio of acrylamide to the crosslinker, bis, during gel fabrication. Gels were coated with the same concentration of fibronectin. We measured the forces exerted by wild type TAF and EGFP-palladin cells on gels with stiffness ranging from 4-150 kPa. For each cell, we calculated the total force exerted by the cell as a scalar integral of all local forces exerted. To compare the traction stresses among cell populations, we calculated the mean total

force of all cells for a gel of a particular stiffness range. We found that wildtype TAF cells exert higher forces on gels of increasing stiffness, indicating mechanosensitivity over this range of stiffness (See Figure 2-7D). For large values of substrate stiffness, the total force exerted reached saturation and the cells thus appeared to lose this sensitivity. We verified that EGFP-palladin expression did not affect the overall mechanosensitivity of TAF cells. The traction forces exerted by EGFP-palladin cells were similar to those of WT cells and showed a similar increase as a function of gel stiffness (See Figure 2-7D). We next investigated the effect of gel stiffness on the structure of the actin cytoskeleton using Rhodamine-phalloidin staining of fixed cells to visualize f-actin. On the softest gels (stiffness range 2-4 kPa), the cell shape was more rounded and the cell area was smaller compared to cells on stiffer substrates. On these gels, fewer actin stress fibers were formed and the actin cytoskeleton assumed a more disorganized amorphous form. For stiffer gels, cells spread to a greater extent and formed robust stress fibers (See

Figure 2-7 E,F).
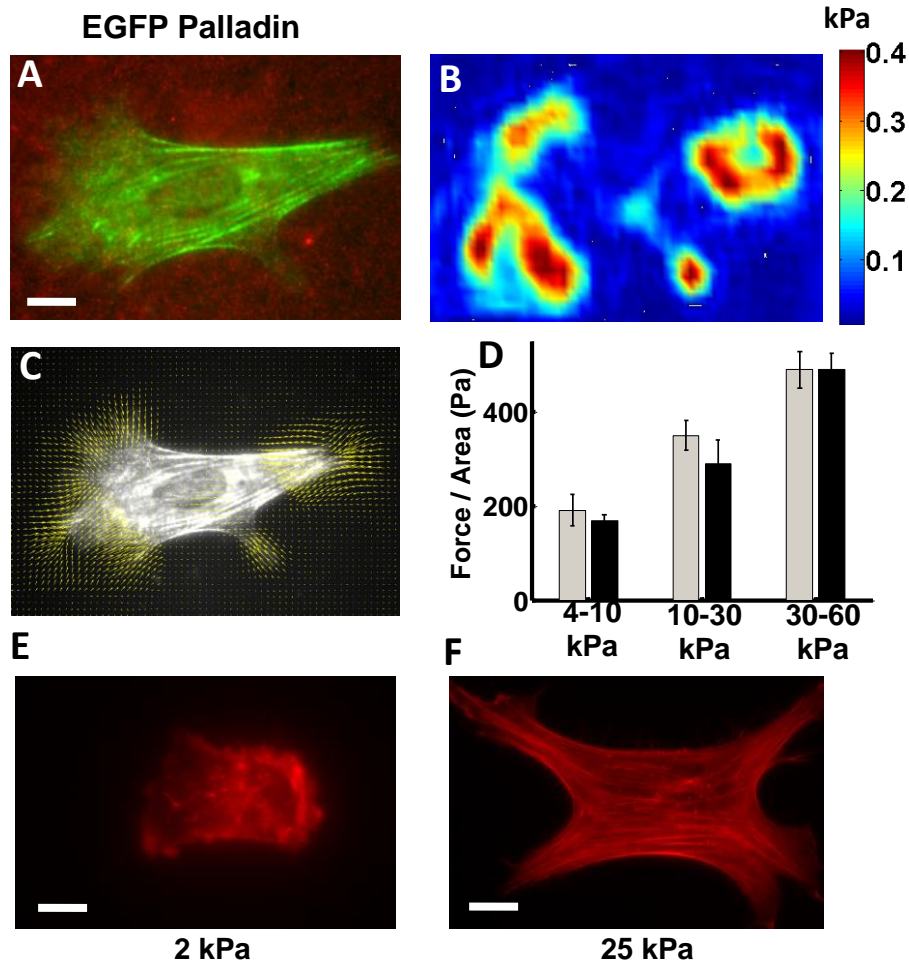
Figure 2-7 Tumor-associated fibroblasts are mechanosensitive. **(A)** Snapshot of an EGFP-Palladin cell (green) on an elastic gel (in the 10 – 20 kPa stiffness range) embedded with fluorescent beads (red). Scale bar: 10 μm. **(B)** Snapshot of the traction stress map for the stresses generated by the same cell. Colors correspond to the stress values as indicated by the color scale. **(C)** A map of the local traction force vectors superimposed on the cell contour. **(D)** Traction force per unit area for WT and EGFP-palladin cells on gels of different stiffness ranges. Rhodamine-phalloidin staining of a WT cell to visualize f-actin on **(E)** a soft (2kPa) gel and **(F)** a stiff (25 kPa) gel. Scale bars: 10 μm**.**

2.4.4 Palladin modulates cellular traction forces and mechanosensitivity

Actin crosslinking proteins have been implicated in the regulation of cellular mechanics and forces [26], [97]. In order to investigate the effect of palladin expression on cell mechanics, we quantified the dynamics of palladin KD TAF cells on elastic substrates and measured the traction forces exerted by these cells. Figure 2-8A shows a representative KD cell on an elastic substrate with embedded beads, with the corresponding traction stress map shown in Figure 2-8B. Note that these cells express cytoplasmic GFP as a marker of stable transfection, as described previously [158]. The traction stresses generated by the KD cell are higher than those exerted by EGFP-palladin cells, for a given stiffness range, as indicated by the higher stress values corresponding to the color scale. As before, we measured traction forces on gels of different stiffness ranging from 4 to 150 kPa. We found that palladin knockdown cells also exhibited sensitivity to substrate stiffness as they generated larger forces on stiffer surfaces. However, the nature of this mechanosensitivity was different from EGFP-palladin cells. For KD cells, the traction stress increased from soft to intermediate stiffness gels, but showed no further increase on the stiffest gels. The force per unit area, or the average stress exerted by KD cells was significantly higher (almost double) compared to those exerted by EGFP-palladin cells in the stiffness range 10-20 kPa (Figure 2-8C). We confirmed that the effect of palladin KD was specific as control shRNA cells (PGIPZ) showed similar results as WT cells with no significant difference in the forces exerted between PGIPZ, WT and EGFP-palladin cells (Figure 2-8D). We used Rhodamine-phalloidin staining of f-actin to examine the effect of gel stiffness on cell spread area and actin organization of KD cells. As in WT cells, we found that for the softest gels (2-4

kPa), cells spread less, lacked actin stress fibers and had reduced levels of f-actin staining

(Figure 2-8E), while stiffer gels (25kPa) cells had a larger area and numerous stress fibers

(Figure 2-8F). We found that the spread area of KD cells (grey bars) was smaller for the

softest gels (2-4kPa) compared to the stiffest gels (10-30kPa), similar to the results with

EGFP-palladin cells (black bars) (See Figure 2-8G). This indicates that the difference in

traction stress between EGFP-palladin and KD cells on soft and intermediate stiffness

gels is not merely due to a difference in spread area.
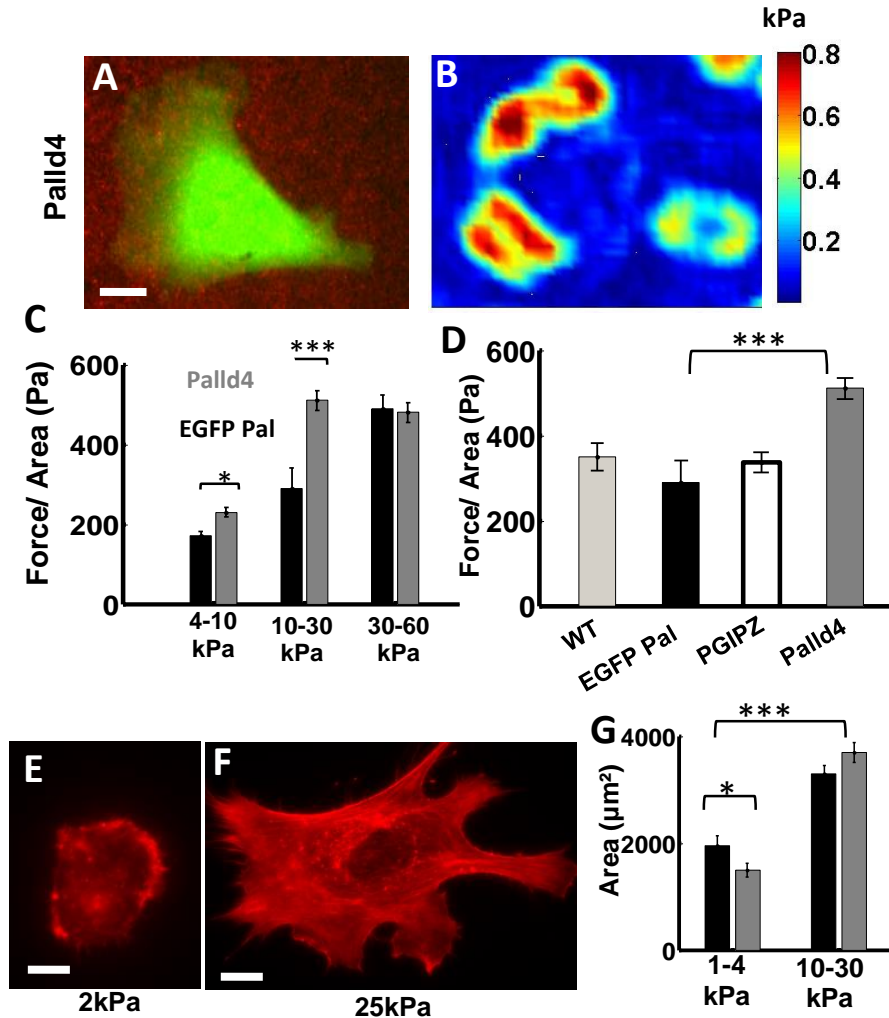
Figure 2-8 Palladin modulates cellular traction forces and mechanosensitivity. **(A)** A snapshot of a palladin KD cell on an elastic gel embedded with beads. Scale bar: 10 μm. **(B)** Snapshot of the traction stress map with color values corresponding to different stress values. **(C)** Total traction force per unit area of KD cells shown in the same plot with EGFP-Palladin cells for comparison. ($p < 0.001$, t-test). Each bar represents an average of data obtained from N = 30-40 cells. **(D)** Bar graph for comparison between traction stresses exerted by different cell types on intermediate stiffness (10-30 kPa) gels, showing that shRNA control cells exert similar stresses as WT and EGFP palladin cells. Rhodamine-phalloidin staining of a KD cell on **(E)** a soft (2kPa) gel and **(F)** a stiff (25 kPa) gel. Scale bar: 10 μm **(G)** Bar graphs comparing the spread areas of EGFP-Palladin (black) and KD (gray) cells as a function of gel stiffness.

2.4.5 Effect of palladin on myosin-based force generation

Actomyosin networks have been known to play an important role in cellular traction force generation [97]. Myosin is known to localize to stress fibers in a striated pattern resembling sarcomeres in striated muscle and suggests a role for myosin contractility in force transmission across the cell. In order to examine the relative localization of myosin and palladin in these cells, we transfected EGFP-palladin cells with mCherry-myosin. Fluorescence images of EGFP-palladin (green) and mCherry-myosin (red) were obtained to visualize the colocalization of the two proteins (See Figure 2-9A). We observed that palladin occurred in a striated pattern on stress fibers (See Figure 2-9B) similar to myosin. Intensity profiles along the stress fibers showed that myosin and palladin localized to alternate bands on stress fibers (See Figure 2-9). For selected regions of actin stress fibers, we calculated the correlation coefficient between the intensities of the two line profiles. While it varied throughout the cell, in regions with dense stress fibers the correlation coefficient was significantly negative (C = -0.39, p=0.02), indicating that palladin and myosin puncta were largely anti-correlated. For comparison, in areas away from stress fibers, C=0. The band spacing, as calculated from the distance between peaks in the intensity profiles was measured to be 1.1 ± 0.3 μm for myosin, which was very similar to the spacing $1.21 \pm .05$ μm measured for palladin bands (See Figure 2-9D). These observations are consistent with previous studies showing the localization of myosin and α-actinin in alternate bands across actin stress fibers [97], since α-actinin and palladin have been shown to co-localize. This periodic appearance and close physical proximity of myosin and palladin led us to hypothesize that palladin

expression may have an effect on myosin's ability to generate contractile stresses on actin

networks.
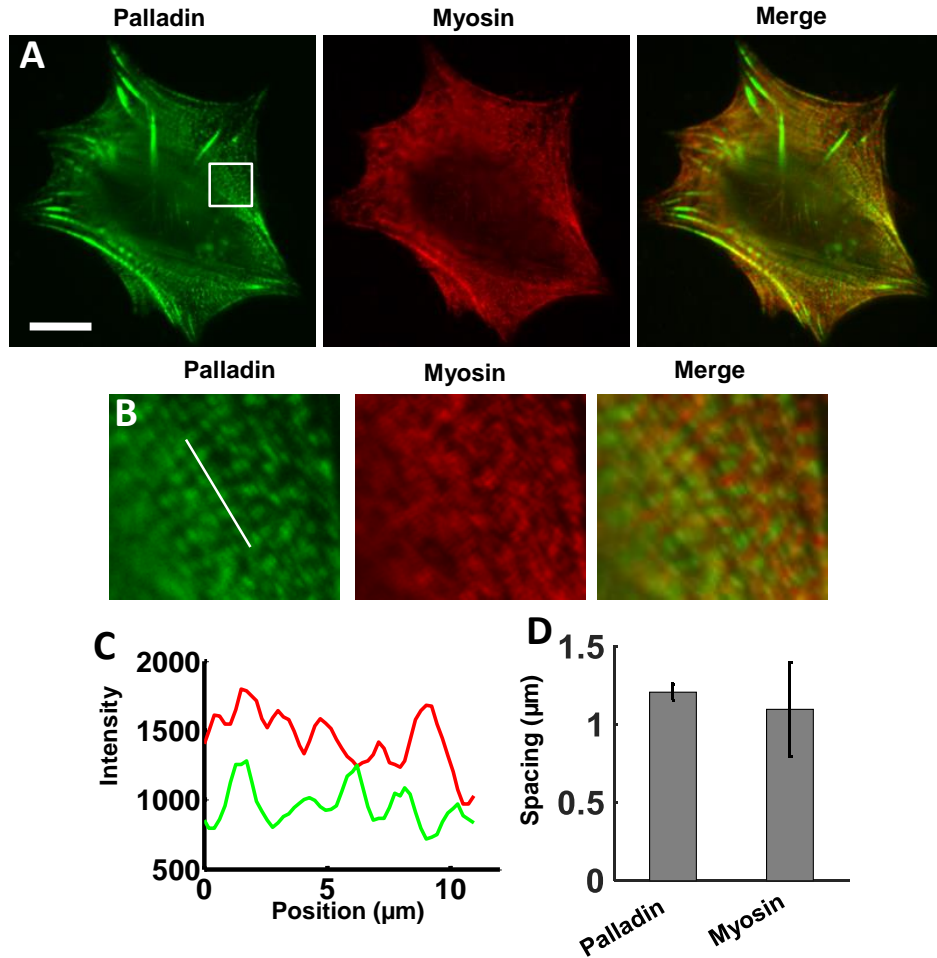
Figure 2-9 Palladin and myosin alternate bands across actin stress fibers. **(A)** Widefield fluorescence image of EGFP-Palladin cell labeled with mCherry-myosin showing localization of palladin (green) and myosin (red) in a spread cell. Scale bar: 15 μm **(B)** Zoomed in image of the square highlighted in (A) showing alternating bands of palladin (green) and myosin (red) along actin stress fibers. Scale bar: 5 μm **(C)** Intensity profile of the line highlighted in **(B)** showing alternating intensity peaks of palladin and myosin fluorescence. **(D)** Bar graph comparing the band spacing for palladin and myosin.

In order to examine the role of palladin in the generation of contractile stresses, we dynamically perturbed myosin contractility using blebbistatin, the small molecule inhibitor of myosin II. It is known that blebbistatin results in loss of stress fibers, focal adhesions and a large reduction in cellular force generation in a reversible manner [97]. Removal of blebbistatin leads to re-assembly of focal adhesions, actin networks and stress fibers thereby restoring cellular forces. However the contribution of actin crosslinkers to the development of forces is not well known. Here, we examined how the expression level of palladin modulated the development of myosin-dependent traction forces in TAF cells. We used blebbistatin to reversibly inhibit the activity of non-muscle myosin II (NMMII), and quantified the recovery of force upon removal of blebbistatin. For these experiments, we used gels of the intermediate stiffness range (10-30 kPa) as the greatest difference in forces between KD and EGFP-palladin cells were obtained for this condition. We plated cells on fibronectin-coated gels as before, allowed them to spread for 3 hours and imaged the cells and corresponding fluorescent beads. Blebbistatin (15 μM) was then added to the imaging chambers and incubated for 30 min to inhibit NMMII activity. After incubation was complete, blebbistatin was washed out and the imaging well was replaced with regular imaging medium while cell recovery was monitored. Time-lapse imaging of cells and corresponding beads throughout the washout and recovery process enabled the traction forces to be computed. Finally, cells were trypsinized to inhibit attachment to gels to obtain bead images for the reference position.

Upon treatment with blebbistatin, actin stress fibers disassembled as seen in EGFP-Palladin cells (See Figure 2-10). Cells drastically changed their shape, shrinking and leaving behind long retraction fibers (See Figure 2-10, Figure 2-11B). After

Blebbistatin was washed out, most of the cells recovered their shape and partially recovered their stress fibers (See Figure 2-10, Figure 2-11C).
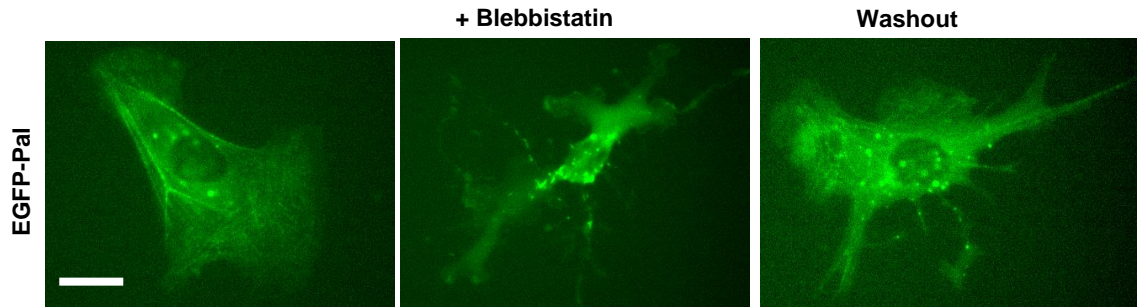
Figure 2-10 Effect of blebbistatin on actin stress fibers. Left: Widefield fluorescence image of EGFP-palladin on a gel of intermediate stiffness (10-30 kPa range). Scale bar: 15µm. Middle: Widefield fluorescence image of the same cell 30 minutes after incubation in 15 µM blebbistatin. Right: Widefield fluorescence image of the cell 1 hour after washout from blebbistatin, showing recovery of cell morphology.

Figure 2-11D shows the traction stresses exerted by the representative KD cell before myosin inhibition. Stresses dropped almost entirely upon incubation with blebbistatin for 30 min (See Figure 2-11E) and then largely recovered 60 min after washout (See Figure 2-11F). The changes in stresses upon perturbation were quite rapid. Traction forces usually dropped by greater than 90% of their original values within the first 15 minutes of myosin inhibition and recovered rapidly after washout. As seen from the plots of force recovery as a function of time, a large fraction of the force recovered during the first 20 minutes after washout of blebbistatin (See Figure 2-11G). After 20 min, the forces recovered by palladin KD cells continued to increase, while those of WT cells appeared to plateau. The absolute forces recovered by KD cells were larger than those by EGFP-palladin cells, which is to be expected since KD cells exerted higher

forces before inhibition. To quantify the relative values of forces recovered, we calculated the ratio of recovered force to the initial force (before blebbistatin treatment) for each cell to obtain the percentage recovery with respect to the initial force. We found that palladin KD cells showed a faster force recovery at early times (first 20 min during which time most of the force builds up) as compared to EGFP-palladin cells indicated by a larger slope (See Figure 2-11H). The reduction of force upon blebbistatin addition was greater for KD cells resulting in a lower starting point for the force recovery plots. Further, we quantified the increase in force after blebbistatin washout as the difference (D) between the force 60 min post-recovery and at the time of blebbistatin removal as a percentage of the original force. The extent of force recovery is higher for KD cells compared to EGFP-palladin cells, again indicating a more efficient recovery of forces in palladin KD cells (See Figure 2-11I). Occasionally some cells did not recover well from blebbistatin treatment, characterized by an inability to move, a continued shrinkage of cell shape and a very low value of stress after recovery (<30% of the initial value). We found that a larger fraction of EGFP-palladin cells were unable to recover after blebbistatin washout as compared to KD cells (See Figure 2-11J). These results indicate that the lack of palladin facilitates recovery from the effects of myosin inhibition and that lower levels of palladin are correlated with higher force generation.
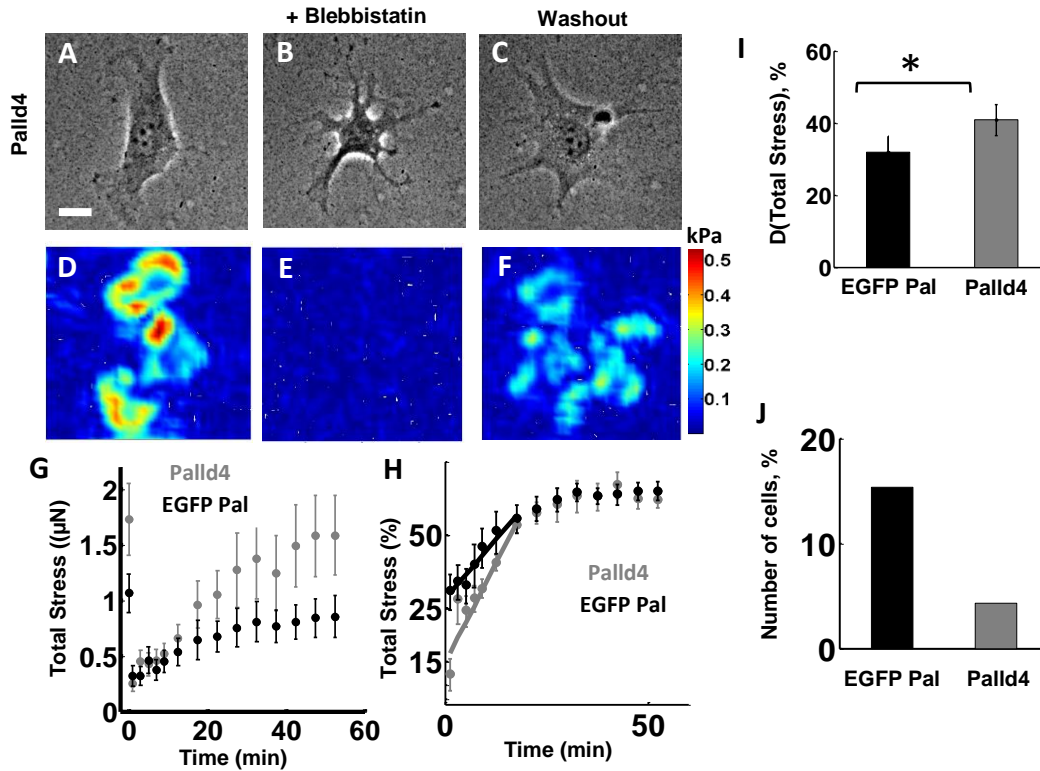
Figure 2-11 Palladin KD cells show more efficient recovery from blebbistatin treatment. (**A**) DIC image of a Palladin KD cell on a gel of intermediate stiffness (10-30 kPa range). Scale bar: 10 μm. (**B**) DIC image of the same cell as in A, 30 minutes after incubation in 15 μM Blebbistatin. (**C**) DIC image of the cell 1 hour after washout from Blebbistatin, showing recovery of cell morphology. (**D**) Traction force map of the cell in A showing robust generation of traction forces. (**E**) Traction force map of the cell in B, showing disappearance of traction forces upon addition of Blebbistatin. (**F**) Traction force map of the cell in C, showing recovery of traction forces 1 hour after Blebbistatin washout. (**G**) Total stress as a function of time after removal of Blebbistatin for GFP-Palladin (black) and Palladin KD (grey) cells. Each data point is an average of forces from N=10 cells for each condition. The first data point represents the initial (pre-Blebbistatin) force. The graphs show the increase in cellular traction forces as the cell recovers from Blebbistatin washout, subsequent to 30 min incubation in Blebbistatin. (**H**) The percentage force (with respect to original forces before Blebbistatin addition) during recovery from Blebbistatin washout plotted as a function of time for EGFP-palladin cells (black) and KD cells (grey). (**I**) The percentage increase of stress after washout of Blebbistatin quantified as the difference between force recovered 1 hour after washout, F_{recov}, and the force after incubation in Blebbistatin for 30 minutes, F_{blebb} (percentages are with respect to the initial force prior to Blebbistatin addition). The data represents an average for 20-30 cells of each type. ($p<0.01$, t-test). (**J**) Percentage of EGFP-Palladin and Palladin KD cells that

showed force recovery of less than 30% of the original force, one hour after drug washout (p<0.01,t-test).

2.4.6 Palladin modulates speed of retrograde flow

The coordination of actin dynamics and myosin II activity in lamellar and lamellipodial networks results in a continuous retrograde flow of actin, myosin, and other crosslinkers from the cell periphery towards the cell center [168] as also observed in TAF cells. Retrograde flow is determined both by actin assembly and disassembly kinetics as well as by myosin motor activity, and may be sensitively related to the forces generated at the cell periphery. Previous studies have shown that traction stresses are correlated with retrograde flow of actin in lamellipodia [167]. The role of actin crosslinkers in modulating retrograde flow is not well known. We examined the effect of palladin expression on the dynamics of retrograde flow by quantifying the flow speed for EGFP-palladin and KD cells spread gels of different stiffness. Cells were transfected with mCherry-myosin, plated for 3 hours on fibronectin coated gels, and imaged for 30 min to observe the centripetal flow of myosin and palladin (See Figure 2-12A). The retrograde flow speed was quantified by kymography analysis. Kymographs along radial lines parallel to the flow show fluorescent streaks corresponding to movement of myosin structures along the flow (See Figure 2-12B). The slopes of these streaks yield the local retrograde flow speed (See Figure 2-12C). We found that the retrograde flow rates varied with substrate stiffness. For EGFP-palladin cells, flow rates were found to be higher for intermediate stiffness gels, while the forces exerted on these gels were smaller. This suggests an inverse dependence between traction force and retrograde flow. The result is in agreement with the previously reported biphasic dependence [167] of retrograde flow

on traction forces since the velocities we observe (15-30 nm/s) are in the higher flow phase of the biphasic dependence curve. We also observed a similar trend of retrograde flow speeds on different substrates for KD cells. The decrease in retrograde flow speeds with respect to stiffness for EGFP-palladin cells was more dramatic compared to KD cells supporting the idea that KD cells are less mechanosensitive.
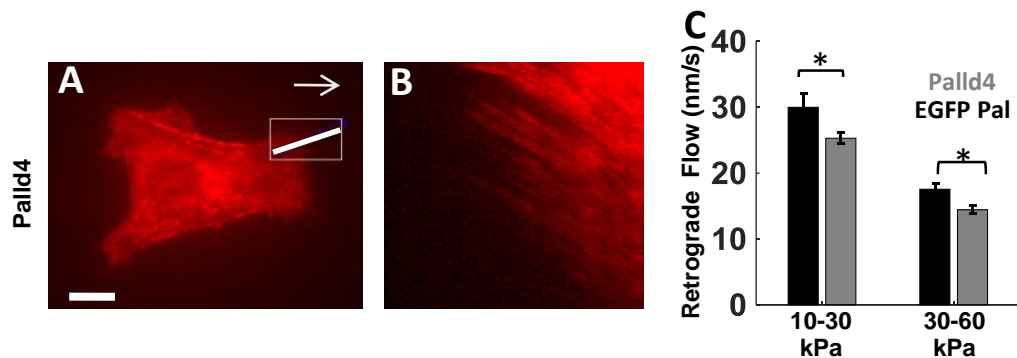
Figure 2-12 Palladin involvement in retrograde flow. **(A)** Image of Palladin KD cell expressing mCherry-myosin showing localization of myosin in the cell. Scale bar 10 µm. **(B)** Kymograph generated along the line drawn in A showing retrograde flow of myosin which appears as linear streaks of red. The slope of these streaks yields the flow speed. **(C)** Comparison of the retrograde flow speed for EGFP-palladin and KD cells for different conditions of stiffness. Each bar represents the average of about 100-200 tracked lines along the kymographs similar to the one in B ($p < 0.01$, t-test).

2.5   Discussion

In this study, we examined the role of the actin crosslinking protein palladin in cell mechanics. Our results show that palladin plays a critical role in cellular force generation and mechanosensing. Palladin is essential for the efficient formation of radial stress fibers consistent with previously published results in osteosarcoma cells [27]. Reduced expression of palladin affects focal adhesion maturation leading to smaller, more dynamic adhesions, which turnover rapidly. Importantly, we find that knocking

down palladin increases the force generating capacity of cells. Knockdown of palladin facilitates the rapid buildup of tension within the lamellar actin network but impairs the ability to sense substrate rigidity for stiff gels. We found that cells had a lower rate of retrograde flow on stiffer surfaces and consistently that palladin KD cells exhibit slower flows as compared to EGFP-palladin cells. These indicate that lower flows are associated with greater traction forces implying that palladin enhances myosin-mediated actin flows on soft substrates, which result in smaller traction forces. Overall, our findings indicate that the relationship between local changes in cell response e.g. actin flow, focal adhesion dynamics and actin organization can enable the cell to sense and adapt globally to the material parameters of the environment such as substrate stiffness.

Our finding that palladin knockdown cells exert forces that are almost twice as large as those exerted by wild type cells is consistent with previous studies showing that knockdown of the α-actinin also results in higher forces [26], [67]. We find that the loss of radial stress fibers, reduced retrograde flow and altered focal adhesion lifetimes that accompany the loss of palladin reduces the sensitivity of cells to sense substrate stiffness, suggesting that palladin may play a role in cellular mechanosensing. To obtain a deeper insight into the mechanisms involved, we dynamically inhibited myosin activity and examined the subsequent recovery of forces after removal of inhibitor in cells with normal and reduced levels of palladin. Palladin KD cells showed greater rate of force recovery, indicating that reduced expression of palladin facilitates more efficient force generation by myosin. The modulation of traction stresses and kinetics of force recovery suggest that palladin expression may modulate the behavior of the actomyosin network in cells. Experiments have shown that knockdown of palladin is correlated with higher

71

activation levels of Rho in cells (Goicoechea, unpublished). Since activated Rho is a positive regulator of myosin activity in cells, this may provide a potential link between palladin expression and myosin-based force generation.

Based on our observations and previous studies in the literature, we propose the following qualitative model of actin stress fiber contraction and force generation. As mentioned in Section 1.3.3, three types of stress fibers are observed in adherent cells including TAF – ventral stress fibers, which span the entire cell and lie along the base of the cell, radial stress fibers which are attached at one end to focal adhesions, and transverse fibers, with a sarcomeric structure, which are not attached to focal adhesions [23]. Of these, ventral stress fibers are attached to focal adhesions at each end and show a graded polarity of actin filaments, and hence are most likely associated with the generation of contractile force in cells [169]–[171]. For fibers with graded polarity to contract, they should be able to displace α-actinin and palladin relative to each other and along the filaments [172]. In a proposed model [23], actin filaments are able to contract because of the rapid association/dissociation rate of α-actinin. Palladin has been shown to have a higher association/dissociation dynamics than α-actinin [137]. We propose that the presence of two independent cross-linkers on stress fibers enables a cell to regulate the contractility of its stress fibers. In our representation of the proposed model [23] (See Figure 2-13A), the relative displacement of α-actinin and palladin is required for actin filaments to contract. Since the displacement of cross-linkers is modulated by association/dissociation, the probability of α-actinin and palladin being simultaneously detached would be lower than for a single type of crosslinker. Hence, a high concentration of crosslinkers would restrict filaments from sliding past each other and

stiffen the stress fiber, resulting in decreased contraction and force generation. On the other hand, lower expression level of cross-linkers (i.e. palladin KD cells) would lead to greater force generation as observed. Such a mechanism may enable the cell to regulate the generated forces by adjusting the relative concentrations of actin cross-linkers.

It is interesting to consider a case with a very low concentration of cross-linkers. Stress fiber can stretch for tens of micrometers but are composed of relatively short actin filaments with alternating polarity[20], [169]. The observed band spacing of palladin and myosin indicates a length scale of about 1 μm for actin filaments in the stress fiber. So a certain threshold of cross-linker concentration may be required to ensure integrity of stress fibers. Therefore, it may not be possible to examine the effect of extremely low concentrations on force generation by myosin motors. Furthermore, myosin itself can act as a cross-linker, so a high concentration of myosin itself could both provide structural integrity and lead to force generation of a stress fiber. Assuming a low concentration of myosin in cells, this model would therefore predict a decrease in forces for very low cross-linker concentration resulting from lack of stress fiber integrity, yielding an overall biphasic dependence of contractility on crosslinker density(See Figure 2-13B).
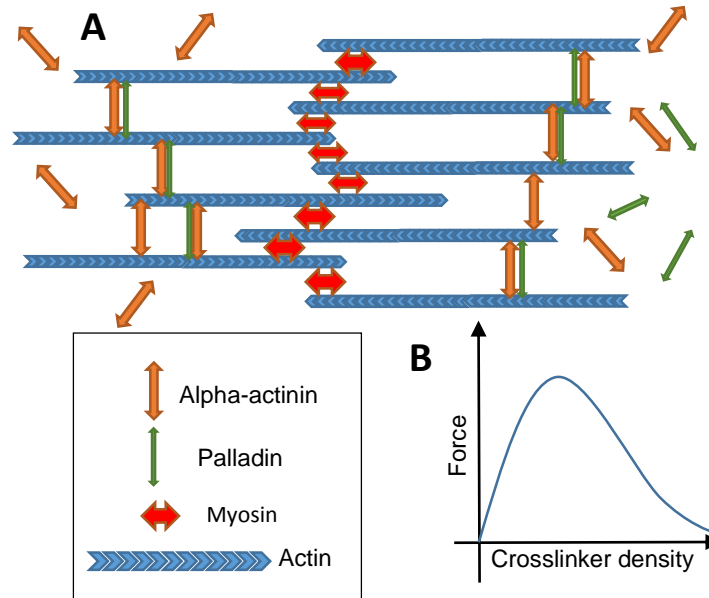
Figure 2-13 Model showing the role of palladin in stress fiber assembly and force generation. (A) Schematic representation of the proposed model. For actin filaments to move pass each other both alpha-actinin and palladin need to detach. Rapid association/dissociation of cross-linkers allows for that **(B)** Prediction for force dependence on cross-linker density.

Actin crosslinkers and myosin may be present in an optimum concentration for proper force generation and mechanical response. Exertion of forces that are too large may hinder the cells' ability to discriminate between different mechanical properties of substrates, as forces need to be tuned closely to match the cell surroundings. In summary, the differences in cellular contractility arising from palladin expression levels suggest that palladin is involved in many aspects of cell mechanics. Its interactions with myosin motors may serve as a foundation for traction force regulation. As previously mentioned in Section 1.5, there are conflicting studies regarding the dependence of focal adhesions size and the magnitude of traction forces [122]–[124]. Due to palladin's role in focal adhesions assembly and traction force generation, we, in particular, want to visualize

focal adhesions on elastic substrates and try to correlate traction forces with the size of focal adhesions. Understanding the molecular mechanisms underlying palladin's involvement in cellular forces and mechanical sensing will be a topic of our future studies.

3 The effect of surface topography on cell morphology and cytoskeletal dynamics

This chapter was adapted from the paper in preparation by M. Azatov, X.Sun, J. Fourkas, A. Upadhyaya, "The effect of surface topography on cell morphology and cytoskeletal dynamics".

3.1 Summary (Abstract)

Cells can sense and adapt to mechanical properties of their environment. The local geometry of the extracellular matrix can control the motility, shape, and cytoskeletal structure of cells. In particular, surface topography has been shown to modulate cell morphology, migration, and proliferation. However, the underlying mechanisms by which topography is sensed by cells remain unclear. Here we investigate the effect of surface topography on the morphology and cytoskeletal dynamics of human pancreatic tumor associated fibroblast cells (TAFs). TAFs have been shown to promote the progression of pancreatic tumors, metastasis, and resistance to therapy. Mechanisms by which these cells stimulate invasiveness and metastasis of cancer cells are not well understood. We have previously shown that these cells can mechanically sense the stiffness of their environment. In this study, we used an arrangement of parallel ridges (nanopatterns), with variable spacing between the ridges, to investigate the response of pancreatic TAFs to the topography of their environment.

We found that TAFs align along the direction of the ridges and modulate their shape depending on the parameters of the surface. Analysis of cell body and stress fiber alignment revealed a strong biphasic relationship between the degree of alignment and the pitch of the substrates. Furthermore analysis of focal adhesion localization and

orientation showed that focal adhesions were aligned with the substrates, preferentially formed on top of the ridges, and were longer once grown on tops of the ridges. In order to obtain a deeper understanding of the underlying mechanisms, we tracked the movement of palladin structures in cells as this enables the measurement of cytoskeletal dynamics as a function of surface topography. We observed that actin stress fibers underwent a complicated diffusive motion showing both subdiffusive and superdiffusive behavior. Through numerous analysis methods of the tracks we show that actin cytoskeleton prefers to move along the direction of the ridges and moves faster on the patterned surfaces with higher velocities along the direction of the patterns.

Our results provide insight into the mechanisms of how cells sense and respond to substrate topography suggesting a complex interplay between actin cytoskeleton and focal adhesions in coordinating cellular response on surface topography. Furthermore our results reveal a potentially promising method to study actin cytoskeleton dynamics and measure the amount of stress within actin networks.

3.2 Introduction

Tissues consist of a complex structure of different cell types and extra-cellular matrix (ECM). ECM consists of different proteins and exhibits different structures ranging from nanometers to micrometers in size. Some of these structures, like collagen fibrils in ECM can stretch for tenth of micrometers and can be as large 400 nm in diameter [98]. Besides ECM, the basement of membranes also exhibit different nanostructures that influence cells around them [99], [100]. The effect of surface

topography on the cell behavior has been in the center of attention of scientists for the last two decades. Surface topography has been found to alter proliferation, polarization, differentiation, and migration [170], [174]–[176]. Recently, advances in micro-fabrication allow scientists to mimic intricate topographical features of ECM. Some of the substrates that are being used by researchers, include, array of nonoposts [101], or array nanopits[102]. Still the most commonly studied substrate is an array of parallel nanoridges or nanogrooves with varying width between two neighbor ridges [103]–[106], [176].

In vitro studies have been consistent with some of the in vivo findings. Different cell types have been shown to migrate along nanoridges [177], showing increased motility on these structures [178]–[180], while in vivo, it has been shown that carcinoma cells migrated along ECM structures [181], [182]. These behaviors were observed in both single and collective cell experiments [104], suggesting the importance of surface topography in organized cell migration, which is essential for processes such as wound healing, tissue development, or metastasis.

It has been shown that array of nanoscale parallel ridges, called nanoridges, usually align cells along them, while elongating their shape [104]. The degree of this alignment has been shown to depend on spatial parameters of the nanoridges [104], such as pitch, width, and height. Many subcellular structures change their shape and orientation together with the cell. Actin networks, microtubules, and focal adhesions usually aligned themselves with the direction of the ridges tuning this alignment depending on the spatial characteristics of the underlying topography [120], [121]. These results suggest a complex interplay between nanoscale intracellular structures and overall

cell sensing of surface topography. Furthermore, previous studies have shown that mechanosensing of surface topography depends not only on spatial dimensions of the underlying structures, but also on culture media conditions, proposing that a combination of both geometrical and chemical cues affect cell mechanosensing [120], [121]. Yet, how these structures regulate cell morphology is not well understood.

Many of the previous studies focused on either migration of cells, or static analysis of the cell, looking at snapshots of fixed cells, thus lack in understanding of the exact intracellular machinery necessary for this type of mechanosensing. The structural basis for phenomena such as cell migration, polarization, or intracellular dynamics is the actin cytoskeleton. In mesenchymal cells such as fibroblasts, actin-binding proteins and motor proteins help the actin cytoskeleton to assemble into a complex network that serves as a scaffold for the cell. The network is very dynamic and is constantly rearranging itself to fit cell needs. Changes in cell morphology and dynamics imply significant changes in actin organization and motion, thus we believe that by analyzing the dynamics of such networks on different surface topographies, we can shed some light on the origins of topography sensing.

Here, we look at TAFs, with EGFP labeled palladin, to understand how an array of parallel ridges can affect cell morphology, actin cytoskeleton, and the dynamics of intracellular proteins. TAFs are a perfect candidate for this study because: (1) TAFs are mechanosensitive as they change their morphology depending on substrate stiffness (See Chapter 2.4.3), (2) TAFs play an important role in the assembly and dynamic remodeling of the tumor stroma, (3) TAFs have overexpressed levels of actin-binding protein, palladin, which has been shown to affect cellular mechanosensitivity (See Chapter 2.4.4).

As previously mentioned, palladin is a component of actin stress fibers and forms distinct bands or puncta along the length of the fibers (See Figure 2-3)**.** These puncta act as markers for the dynamics of the actin cytoskeleton and provide us with a unique tool to track and analyze the dynamics of actin in the cell. Analyzing both static images of cells, as well as dynamics of actin cytoskeleton and focal adhesions on a wide range of different surfaces, we hope to provide some insights, into mechanosensing of surface topography.

3.3   Materials and Methods

3.3.1 Cell culture

TAF cells were stably transfected with EGFP labeled palladin (See Section 2.3.2) EGFP-palladin labeled TAF cells were cultured at 37°C and 5% CO_2 Dulbecco's modified Eagle's Medium (DMEM) (Gibco) with 10% fetal bovine serum (FBS) (Invitrogen), 1%   Penicillin-Streptomycin (Invitrogen), and 1% sodium pyruvate (Invitrogen). For static measurements and stress fiber tracking experiments cells were plated on ridges 3 hours prior to the experiment. The glass coverslip, with nanofabricated ridges was glued to the bottom surface of Maktek dish. Ridges were coated with fibronectin (from bovine plasma, Sigma-Aldrich) by first coating them with Poly-L-Lysine and then incubating with 500µl 10 µg/ml fibronectin solution for 2 hours at room temperature. For microscopy we used CO2 independent imaging media L-15 (Life technologies).

3.3.2 Time-lapse experiments

Images were collected on Nikon TE2000 microscope, using Andor iQ acquisition software, coolsnap HQ2 cooled CCD camera (Photometrixs) and IXon X3 EMCCD camera (Andor Inc.), using a 60× 1.49 NA objective lens. A mercury lamp with appropriate filters was used to provide the blue light to excite the EGFP labelled palladin. A halogen lamp was used for bright field imaging in the phase contrast mode. Lasers of wavelength 491 nm and 561 nm were used to image cells in Total Internal Reflection Fluorescence (TIRF) mode. For stress fiber tracking cells were imaged every 20 seconds in widefield fluorescence mode. For spreading experiments cells were imaged every 20 seconds in TIRF channel.

3.3.3 Immunofluorescence staining

TAF cells were seeded on to substrates of interest, and allowed to spread for 3 hours. They were then fixed with 4% paraformaldehyde (PFA) solution for 7 minutes, washed with phosphate buffered saline (PBS) and permeabilized with 0.2% solution of Triton-X for 2 minutes. After that they were washed with PBS and incubated in blocking solution (2% BSA in PBS) for 1 hour. Next, cells were incubated with primary antibody (monoclonal mouse paxillin B-2, Santa Cruz Biotechnology) in blocking solution for 1 hour. Then, cells were washed in PBS and incubated in secondary antibody solution (Alexa Fluor 546 goat anti-mouse IgG2b, Invitrogen) for 1 hour in the dark. Cells were ready for imaging afterwards.

3.3.4 Pattern fabrication

Nanopatterns were fabricated using the Multiphoton absorption polymerization (MAP) technique by Xiaoyu Sun and Alexandra Suberi in Dr. John Fourkas' lab. This

technique which enabled creation of surfaces with adjustable height, width, and pitch. The patterns consisted of an array of evenly spaced parallel gratings, each 300 µm long (See Figure 3-1). The pitch of the patterns, defined as the spacing between two neighboring ridges, varied between 0.8 µm – 10 µm, while the height and the width were kept constant.
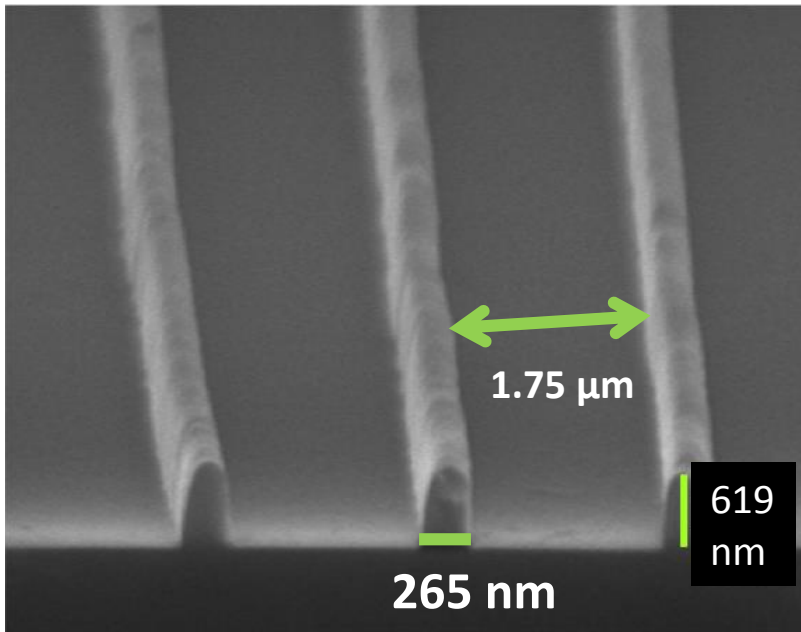
Figure 3-1 Scanning electron microscope (SEM) image of the ridges. Each ridge has a width of ~ 250 nm and height of ~ 600 nm, and a pitch of 1.75 um. (Personal communication from Xiaoyu Sun)

3.3.5 Analysis of cell shape and orientation

Automated Matlab software was written to analyze the shape and orientation of TAFs. First the built in edge detection tool from Matlab was applied to the cell fluorescence image. Detected edge pieces were connected by first dilating the image, second - filling in the holes in the cell boundary, and third - eroding the image back to its original edge since dilating the image advances the boundary of the cell. Using Matlab's

regionprops function the cell body was analyzed for area, orientation and eccentricity (See Figure 3-2). Orientation and elongation were obtained from fitting an ellipse around the cell, where orientation is defined as an orientation of the ellipse' major axis, and elongation is defined as the ratio of major and minor axes.

Figure 3-2 Analysis of cell shape and orientation (A) IRM image of a cell on 10 µm pitch substrate after spreading for ~ 3 hours. The black diagonal lines correspond to tops of the ridges. Scale bar: 20 µm (B) Output of Matlab program after running the analysis of this cell. The white is the detected outline of the cell. In red we have an ellipse fit around the cell with its major and minor axis (C) Epi-fluorescence image of EGFP-palladin for the same cell.

3.3.6 Analysis of stress fiber orientation and order parameter

Stress fiber detection software was adapted from a previous version of automated Matlab software written by Brian Grooman [183]. To identify stress fibers, the images are first run through a band pass filter to minimize the interference of noise and low-frequency background fluorescence, and then converted to a binary image. Using Matlab's regionprops function, segments of stress fibers are identified along with their approximate direction. A direction specific closing algorithm is applied in order to better connect the identified stress fibers without the merging of parallel stress fibers while

83

connecting segments from the same fiber (See Figure 3-3). Stress fiber orientation and order parameter were quantified as below. Stress fiber orientation (SFO) was measured as a weighted average of cosines of the angles of each individual stress fiber, with respect to the angle between individual stress fibers and the ridges (α). The average is weighted by stress fiber length.

$$\text{SFO} = \frac{\sum Length(SF) * \cos(\alpha)}{\sum Length(SF)} \tag{3}$$

where *Length (SF)* is length of that stress fiber. For large number of randomly distributed stress fibers, $SFO_r = \frac{\int_0^{\pi/2} \cos x \, dx}{\pi/2} = \frac{2}{\pi} \approx 0.64$. Similarly, stress fiber order parameter (SFOP) was measured as a weighted average of cosines of the angles of each individual stress fiber (γ) with respect to the average direction of stress fibers (β). The average angle, β is found as, the weighted average direction of stress fibers.

$$\text{SFOP} = \frac{\sum Length(SF) * \cos(\beta - \gamma)}{\sum Length(SF)} \tag{4}$$

For large number of randomly distributed stress fibers, $SFOP_r = \frac{\int_0^{\pi/4} \cos x \, dx}{\pi/4} = \frac{2\sqrt{2}}{\pi} \approx$ 0.90, while the minimum value of SFOP would be for the cells with only two perpendicularly oriented stress fibers which would results in $SFOP_m = \cos\frac{\pi}{4} \approx 0.71$.
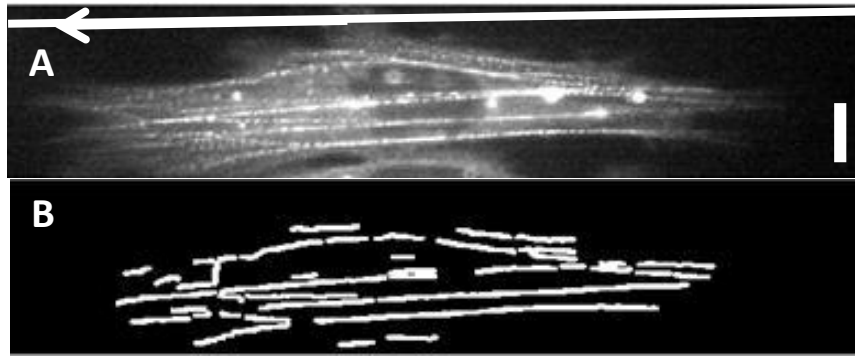
Figure 3-3 Analysis of stress fiber orientation and alignment. (A) Epi-Fluorescence image of EGFP-palladin labeled cell on a 3µm substrate. Stress fibers exhibit a very strong alignment with ridges. The white line with an arrow on top of the image show the direction of the ridges under the cell. Scale bar: 10µm. **(B)** Processed image of the cell after applying the analysis program. White lines show the detected stress fibers in the image above. From the length and direction of each individual stress fiber we find overall stress fiber orientation and order parameter.

3.3.7 Analysis of focal adhesion length and orientation

We used ImageJ software to analyze focal adhesions in TAFs . We drew a polygon around each focal adhesion that could be visually identified. Using ImageJ we fit an ellipse around each highlighted polygon and found the length and orientation of focal adhesion as a length and orientation of ellipse's major axis similarly to length and orientation of entire cell body. By comparing the fluorescent image with IRM and Brightfield images we were able to tell whether each individual focal adhesion was located on or off the ridge.

3.3.8 Tracking of palladin bands

The tracking algorithm consists of two main parts. Spot identification for every frame and combining spots in tracks. The final version of the software was created combining the spot detection code provided by Francois Aguet [184], a tracking algorithm provided by Don Blair, and stress fiber tracking GUI provided by Brian Grooman. The spot identification algorithm allows us to vary minimum spot brightness of detected spots to control the quality of located spots. After the spot locations are determined, the algorithm uses center of mass calculation in the pixels around the maximum to measure sub-pixel coordinates of the spot. The tracking algorithm allows control of minimum number of points per track and maximum distance between two frames in a track. These parameters are unchanged for all cells analyzed to minimize potential human bias. The direction and location of ridges can be found by applying a band-pass filter to a brightfield image, similar to the one used for stress fiber detection. Once the angle, pitch, and location of at least one spot on the ridges is determined, the positions of all ridges throughout the image can be recreated. Figure 3-4 shows an example of the analysis output of the algorithm applied to a cell imaged on a substrate with 3 µm ridge spacing.
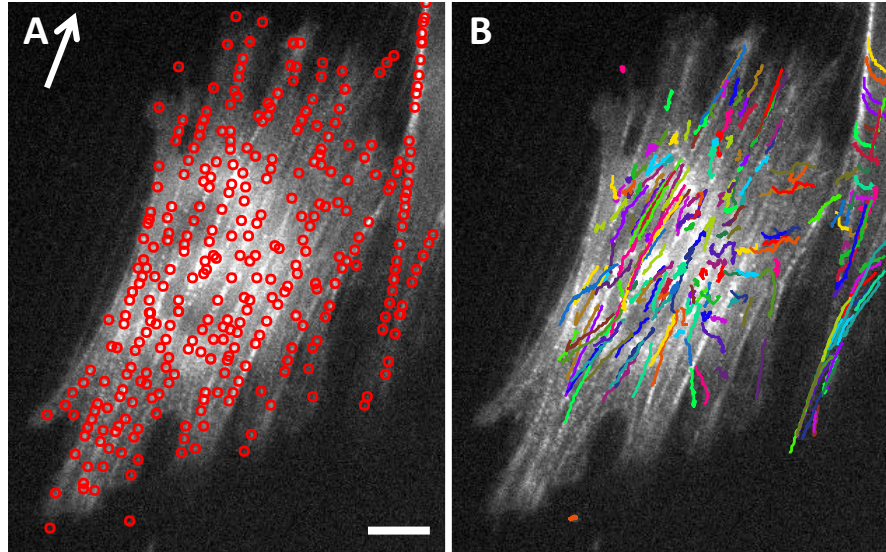
Figure 3-4 Tracking of palladin bands. **(A)** Example of a cell spread on 3 µm pitch substrate after application of a spot detection software by Francois Aguet. The red circles indicate the positions of every band. The white line with an arrow in the upper left corner shows the direction of the ridges. Scale bar: 10 µm. **(B)** An image of the cell after application of a spot tracking algorithm by Don Blair. Different tracks are shown with a different color.

3.4   Results

3.4.1 TAF elongation depends on the size of the ridges

First we wished to quantify how TAF cells respond to patterns of different sizes by analyzing the alignment of cell body for a wide range of pitches (0.8µm − 10 µm) . EGFP-palladin cells were allowed to fully spread on patterns of different pitch for ~3 hours. As a control we used a flat surface. We analyzed cell area, elongation and orientation of the cell body (defined in Methods 3.3.5) depending on the size of the patterns we were using. We used IRM imaging to find the direction of the ridges and

Epit-fluorescence imaging to outline of the edge of the cell. This outline of the cell was fit to an ellipse, which helped us to quantify both alignment of the cell with the ridges and elongation of the cells. To measure elongation, we used the ratio of two axes of the ellipse, while to quantify alignment we measured the angle between ellipse's major axis and orientation of the patterns. All calculations were automated in Matlab to remove human bias from the analysis (see Methods 3.3.5).

Cells on all patterned surfaces exhibited a very strong alignment with the direction of the ridges, as they elongated their shape in that direction (See Figure 3-5). The cell-substrate contact area decreased for all patterns compared to a flat surface. For the patterned surfaces, the area was largest for surfaces with 10 µm spacing, which we expected, since larger gaps should approach the case of a simple flat surface (See Figure 3-6A). Interestingly, both alignment and elongation were very sensitive to the size of the patterns used (See Figure 3-6B-C). For all of the patterns the median of the angle was within 10º of the direction of the ridges. The median of elongation was above 2 for most of the substrates peaking with a median of 4 for 3 µm pitch substrate. This indicates that cells on a 3 µm pitch surface are elongated almost in 4 times compared to a flat surface. Both orientation and elongation exhibited biphasic dependence on the pitch of the patterns peaking at about 3 µm ridge spacing.
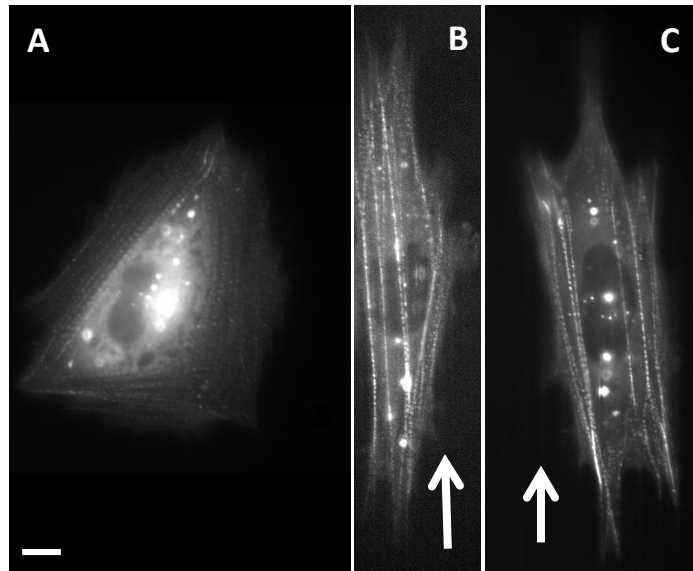
Figure 3-5 Cell alignment on nanopatterns. Widefield fluorescence image of EGFP-Palladin cell spead on (A) a flat surface, (B) 3µm susbtrate, and (C) 5µm substrate. Scale bar: 10 µm. Arrows point in the direction of the ridges.

While most of previous studies have shown that cells align with patterns, the degree of this alignment appears to differ between different cell types and different pattern heights [103], [104], [105], [106]. It is expected that cells may lose their substrate sensitivity for patterns with large pitch as they approach the topography of a flat surface, however the loss of sensitivity on patterns with smaller pitch is still somewhat puzzling. Previous studies [104], [106] have shown the loss of alignment of cells on both ends of the pattern pitch spectrum. However, due to fabrication limitations ridges with small pitch size would usually also have smaller heights, implying that the loss of substrate sensitivity on patterns of smaller pitch could potentially come from the lower height of the ridges. Since for our studies, the ridge height did not vary with pitch size, our results

indicate that cells can lose their sensitivity on smaller pitch patterns independent of ridge height.
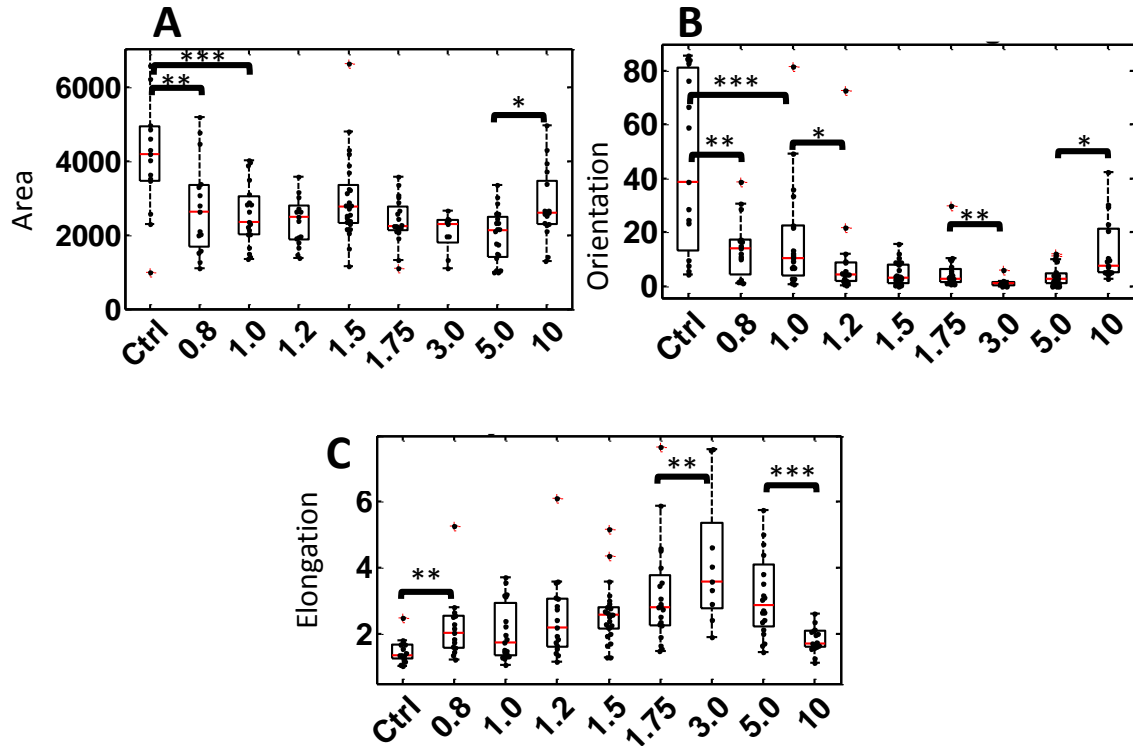
Figure 3-6 Cell shape and orientation. **(A)** Comparison of area of cells spread on patterns with different pitch ranging from 0.8 µm to 10 µm (as indicated on the x-axi . The control is represented by a flat surface and is labeled as 'Ctrl'. All surfaces show a decrease in overall cell area. **(B)** Comparison of the angle of the cell body with respect to direction of the ridges. **(C)** Ratio of the length of two axes of the fit ellipse showing the relative elongation of the cell with respect to the pitch of the surface. All surfaces were statistically different from control (p<0.5). Statistical significance tests were performed using Wilcoxon test. 15-20 cells were analyzed for each topographical surface used.

3.4.2 Stress fiber orientation depends on the size and direction of ridges

Stress fibers span the entire cell, running along the edges of the cell, often determining cell's shape and orientation. Our results showing alignment of overall cell

90

shape with the surface topography led us to expect that stress fibers may also sense surface topography. We therefore quantified how stress fiber orientation and order parameter (See Methods 3.3.6) depend on surface topography. We expressed green fluorescent protein tagged palladin (EGFP-Palladin) in TAFs to visualize stress fibers. As before, cells were allowed to fully spread on patterns of different pitch for ~3 hours. Using automated Matlab software, we quantified stress fiber orientation and order parameter (See Methods 3.3.6).

As expected stress fibers showed a strong alignment with surface topography as indicated by widefield fluorescence of EGFP-Palladin (See Figure 3-5). Both stress fiber orientation and order parameter exhibited a biphasic behavior as a function of the pattern pitch (See Figure 3-7). Stress fibers were aligned with patterns for all pitches, as seen from significant differences in stress fiber orientation (SFO) between all patterned and a flat surface. The degree of their alignment peaked at 3 µm, as both SFO and SFOP were largest for that value. The control case was not significantly different from SFO_r, the value of SFO for randomly distributed stress fibers (See Methods 3.3.6). SFOP for flat surface was between $SFOP_r$, and $SFOP_m$, the value of SFOP for large number of randomly distributed stress fibers and the minimum possible value of SFOP (See Methods 3.3.6). These results correlate with cell shape alignment results. We found that stress fibers at the cell edges as well as in the interior of the cell aligned with the patterns, indicating that intracellular structures also align with surface topography, further suggesting that understanding stress fiber alignment is important in understanding overall cell-topography mechanosensing. We wished to further investigate this dependence in order to obtain a better understanding of the underlying mechanisms of topography

91

sensing and the preferential alignment along 3 um pitch ridges. Analysis of the dynamics of stress fibers should provide important insight into the processes that lead to stress fiber alignment and topography mechanosensing.
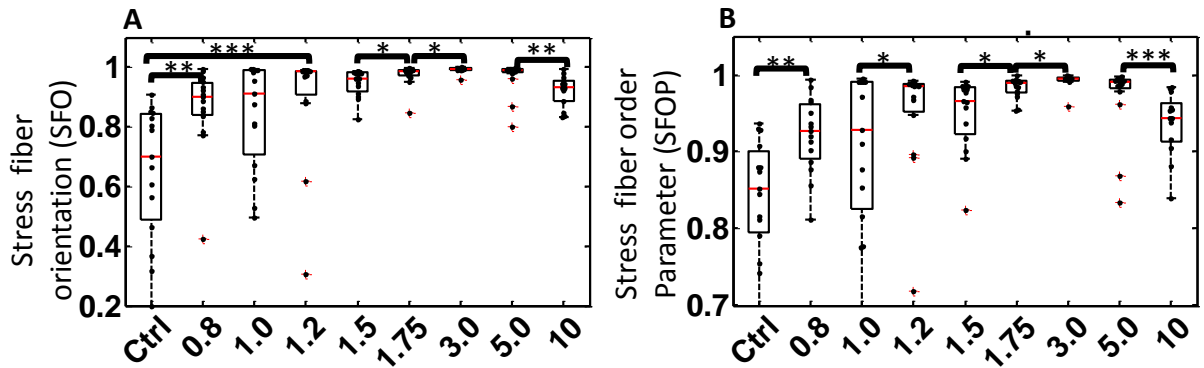
Figure 3-7 Stress fiber orientation and order parameter depend on substrate topography. **(A)** Comparison of stress fiber order parameter on patterns of different pitch ranging from 0.8 μm to 10 μm (as indicated on the x-axis). Stress fibers are more aligned with each other for patterned surfaces. The alignment peaks at 3 μm as the value of SFO was the largest for that pitch size. **(B)** Stress fiber orientation with respect to the pitch of the patterns. Stress fibers are aligned with ridges for all patterns with the alignment peaking for 3 μm substrate. All patterned surfaces were statistically different from control (p<0.05). Statistical significance tests were performed using Wilcoxon test. 15-20 cells were analyzed for each topographical surface used.

3.4.3 Analysis of actin cytoskeleton dynamics

The actin cytoskeleton is a highly dynamic network of cross-linked semiflexible filaments. The dynamics of actin networks and intracellular dynamics in general is complex and time-scale dependent. Tracking and analyzing the motion of intracellular objects can provide an insight into the forces that dominate at different scales. At short timescales, such as milliseconds, thermal fluctuations dominate the motion. At longer times scales, from milliseconds to seconds, thermally driven motion can be relevant, but

motion of intracellular objects have been shown to couple with myosin-based stress fluctuations of the cellular cytoskeleton [185], [186]. At even longer timescales on the order of minutes to hours, the motion of intracellular components is dominated by directed transport or collective movements of particles, as significant remodeling of the cytoskeleton can place. Previous work has studied movements of external particles and beads embedded in the cell, over short timescales in the range of milliseconds to seconds [187],[188], [189]. However, cytoskeletal dynamics occur over longer time scales e.g. actin bundles in the cell reorganize over time scales of minutes to hours. In order to study these dynamics, we used EGFP-palladin cells in which the labeled palladin localizes as punctate bands on stress fibers and thus provides us with a unique opportunity to measure the dynamics of the actin cytoskeleton in cells. Most previous studies have used cytoskeletal bound beads to measure the dynamics of actin networks. To the best of our knowledge, this is the first time that intrinsic features of the cytoskeleton have been tracked to characterize intracellular dynamics. By quantifying the motion of palladin bands, we wished to obtain a better understanding of the dynamics of actin stress fibers as a function of different surface topographies.

3.4.3.1   Analysis of tracks of moving palladin bands

. Depending on the cell we could get approximately 100-500 tracks of palladin bands throughout the cell. The tracks resembled superdiffusive motion showing directionality in their movement predominantly moving along the ridges (See

Figure 3-8), while still looking like diffusion on short time scales (See Figure 3-9). Cells were imaged every 20 seconds for one hour. Each track needed to have minimum of 30 frames (15 min.) to be accepted. Positions of palladin spots were corrected for drift, by tracking position of immobile structures in IRM image, and computing the mean displacement of those structures for every frame. For each track we computed mean-squared displacement (MSD) defined as,

$$\langle \Delta r^2(\Delta t) \rangle = \langle (\vec{r}(t + \Delta t) - \vec{r}(t))^2 \rangle \tag{5}$$

where, $\vec{r}$ is the current position of the spot and Δt is the time gap. The brackets indicate the time average for each particular track. Each MSD was fit to the following equation,

$$\langle \Delta r^2(\Delta t) \rangle = c + D \left(\frac{\Delta t}{t_0} \right)^{\beta} \tag{6}$$

where $t_0 = 20 \ sec.$, and c, D, and, β, are fit parameters. Equation (6) is an empirical equation used in [187] to fit the data. As seen from Equation (6), as $\Delta t \to 0$, $\langle \Delta r^2(\Delta t) \rangle \to c$, while for large as$\Delta t$, $\langle \Delta r^2(\Delta t) \rangle \to D \left(\frac{\Delta t}{t_0} \right)^{\beta}$. The power-law exponent β shows the type of diffusive motion exhibited by the particle. $\beta < 1$ indicates subdiffusive motion, $\beta = 1$ denotes Brownian diffusion, while $\beta > 1$ indicates superdiffusive motion. It is not a prediction of the theory, but rather a phenomenological equation that we found best describes our data. The best fit line was found by minimizing the residuals on the log-log plot for the first 30 time points (15 min.) of a track, as it was the minimum

number of frames required for the track. From the best fit line we obtained parameters, c, D, and β.

Figure 3-4 shows an example of a measured track of a palladin spot on a stress fiber. In order to quantify the directionality of the track. To do that we defined two angles, θ and φ.

$$\theta(t, \Delta t) = \angle\left([\vec{r}(t + \Delta t) - \vec{r}(t)], \vec{d}\right),$$

(7)

where $\vec{d}$ is the direction of the ridges, and

$$\varphi(t, \Delta t) = \angle(\vec{r_1}, \vec{r_2}), \text{where}$$

(8)

$$\vec{r_1} = \vec{r}(t) - \vec{r}(t - \Delta t), \quad \vec{r_2} = \vec{r}(t + \Delta t) - \vec{r}(t)$$

(9)

Both angles help us understand the directionality of the track. While distribution of θ shows us how aligned the track is with respect to the ridges, distribution of φ gives us overall directional persistence of the track with respect to itself.
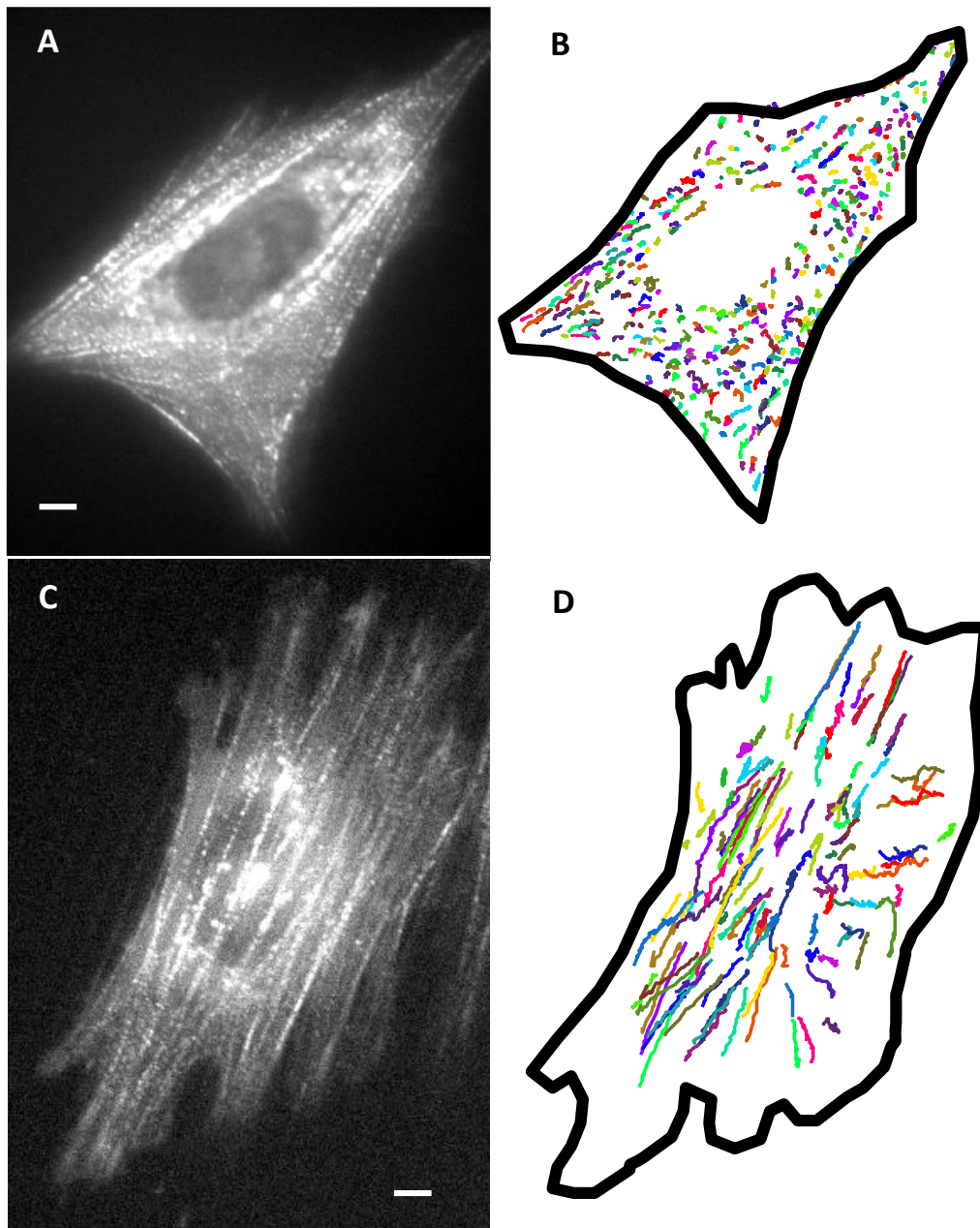
Figure 3-8 Actin cytoskeletal dynamics depends on topography of the surface. **(A)** Widefield fluorescence image of EGFP-Palladin cell on a flat surface. Scale bar: 5 µm. (B) Examples of palladin tracks superimposed on the outline of the cell in (A). Each track is represented by a different color. (C) Widefiled fluorescence image of EGFP-Palladin cell on 3 µm susbtrate. Scale bar: 5 µm. (D Examples of palladin tracks superimposed on the outline of the cell in (D).Longer tracks in (D) show a faster dynamics of actin cytoskeleton on patterned surfaces.
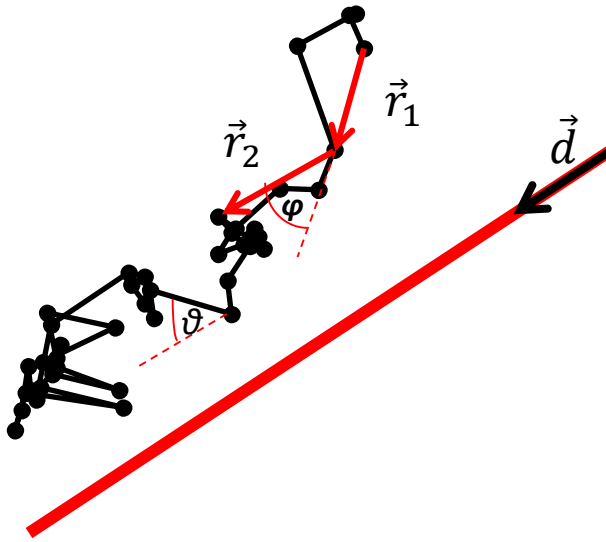
Figure 3-9 Analysis of the tracks of palladin bands. An example of the trajectory of one of the palladin bands obtained from a cell on 5 μm substrate. This example illustrates the definitions of $\theta(t, \Delta t)$, $\varphi(t, \Delta t)$, $\vec{d}$, $\vec{r_1}$, and $\vec{r_2}$.

3.4.3.2   Palladin bands prefer to move along the direction of the ridges

Our first goal was to quantify the overall directionality of stress fiber motion and its dependence on surface topography. EGFP-palladin labeling allowed us to track and analyze the dynamics of the actin cytoskeleton. We allowed cells to spread on the surfaces for ~3 hours and then imaged cells for 1 hour every 20 s. We chose the time interval of 20 s to allow for imaging cells without photobleaching during the duration of the movie. We used automated custom Matlab software to detect and track the movement of individual palladin bands (See Methods 3.3.8).

First we wanted to see if the directionality of palladin tracks depends on the surface topography. We measured the angle $\theta(t, \Delta t)$, between the instantaneous velocity of the track and the direction of the patterns. For each patterned surface we combined all angles for all cells to obtain the distribution of angles. For all patterned surfaces the distributions highly resembled a Gaussian function, while the distribution on a flat surface was uniform for all angles (See Figure 3-10A-B). We fit the angle distributions on patterned surfaces to Gaussian functions and found that the distributions peaked at ~ 0 degrees, indicating that palladin bands were more likely to move parallel to the ridges. The direction of the instantaneous velocities and hence the distribution will depend on the time step Δt. We compared the standard deviation of the Gaussian fits for different patterned surfaces and different lag times Δt, as shown in Figure 3-10C. The width of the Gaussian functions, or standard deviation, indicates overall preference to go in the direction of the ridges. Interestingly, the standard deviations decreased for larger time steps implying that we are more likely to see motion along the ridges on longer time scales. Standard deviation also varied as a function of ridge spacing. Substrates with 1 μm and 10 μm spacing had the largest standard deviation, while the smallest standard deviation corresponded to 3 μm spacing. The differences in standard deviations indicate that palladin tracks on 3 μm patterns have a higher probability to move along the ridges compared to other patterns. Since we observed the directional bias on both shorter and longer time scales, these results hint that nanoscale features of surface topography potentially directly modulate the direction of movement of the actin cytoskeleton, by

decreasing the probability of individual palladin bands moving orthogonal to the ridges.
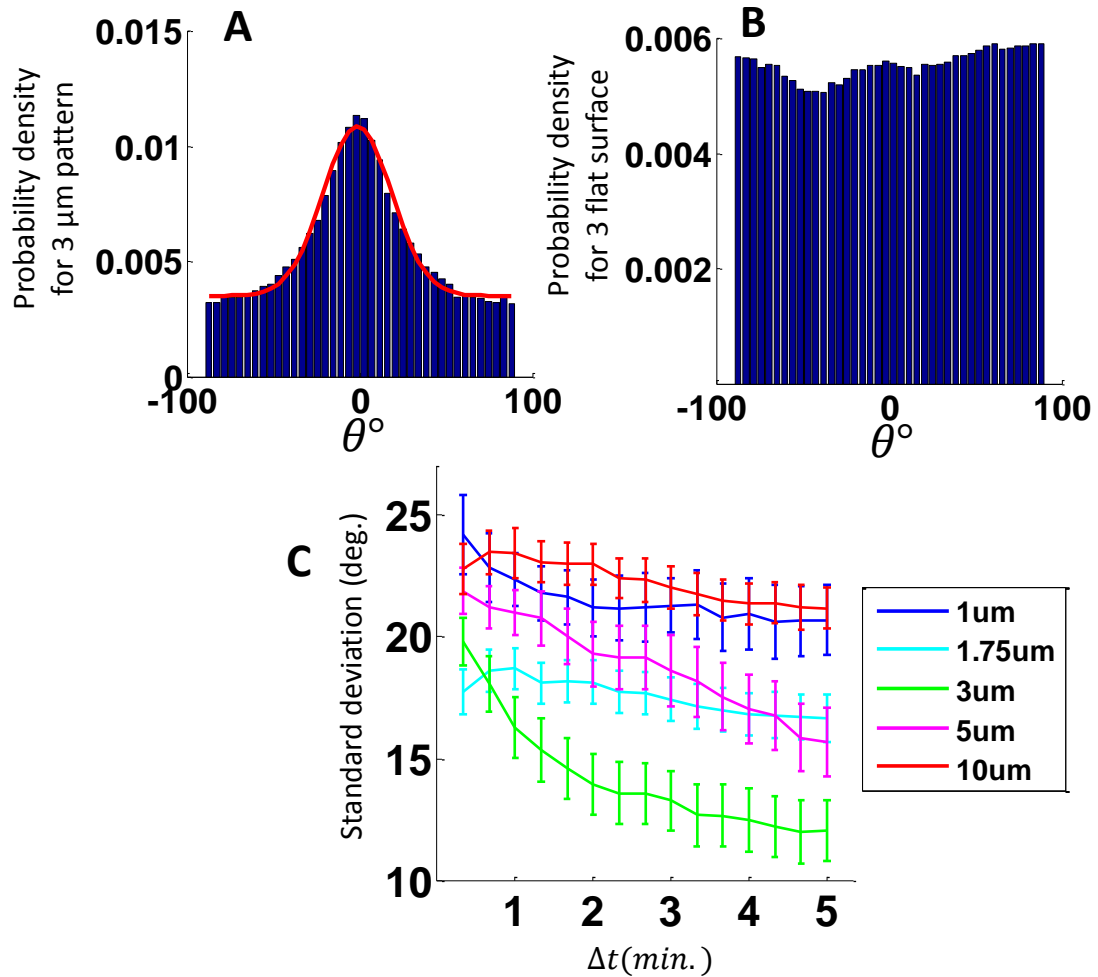
Figure 3-10 Distribution of angles of the track with respect to ridges.**(A)** Distribution of all angles $\theta(t, \Delta t)$, for Δt = 20 sec., and 3 μm substrate. Distribution of $\theta(t, \Delta t)$, for all cells and all Δt fit closely to a Gaussian distribution with y-offset, and average around 0. Red line illustrates the fit of a Gaussian function to the angle distribution. **(B)** Distribution of angles for flat surface. As expected tracks do not have a preferred direction of motion on flat surfaces. **(C)** Standard deviation of Gaussian fit in degrees as a function of both pattern pitch and Δt. Each color represents different pitch size while x-axis represents time lag Δt.

3.4.3.3 TAF are more active on intermediate size ridges

We next examined how the velocities of palladin bands were modulated by the topography of the surface. We obtained the probability distribution of instantaneous velocities for each surface from all the analyzed tracks for all cells. Figure 3-11 shows a typical distribution of velocities. As you can see from Figure 3-11, the velocity distribution of palladin bands is not Maxwellian, since it has a long tail not accounted by Maxwell distribution. Figure 3-12A shows a velocity distribution for both flat and ridged surfaces. Both distributions peak at ~ 3 nm/sec and have a very heavy tail, which is typical for superdiffusive motion. The velocity corresponding to the peak of probability distribution on patterned surfaces was at a slightly higher value compared to the flat surface. The velocity distributions on ridged surfaces also had a heavier tail, as seen in the comparison between flat surface and 3 μm pattern (See Figure 3-12A). A cumulative velocity distribution shows the comparison between distributions on substrates with different pattern sizes (See Figure 3-12B). As seen from this distribution, the velocities have a biphasic dependence on pattern size, with the largest magnitude being for 3 μm pitch patterns, similar to other parameters such as cell elongation, orientation, or stress fiber orientation.
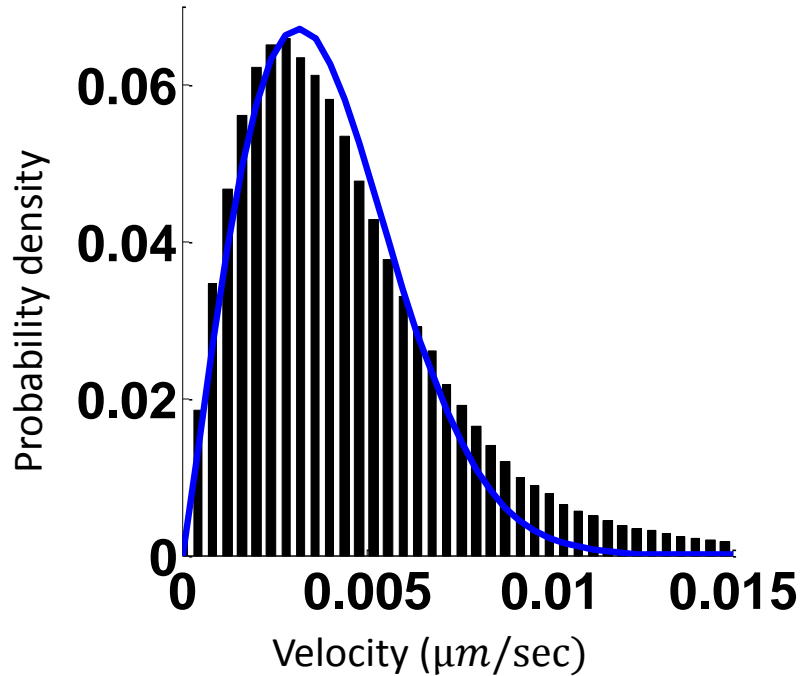
Figure 3-11 Velocity distribution of palladin bands for a flat surface. Blue line shows the attempted best fit line of 2D Maxwell distribution.

We next examined whether there was a dependence of velocities on the direction of motion. We divided the range of all possible directions (from -90º to 90º) into 5º bins. We averaged all velocities in a given bin and plotted the resulting distribution (See Figure 3-12C). The distribution is not uniform, but appears to be Gaussian, peaking at ~ 0º. This indicates that each track is more likely to make larger steps in the direction of the ridges and smaller steps perpendicular to them. Thus, particles are not just more likely to move in the direction of the ridges, but they do so with a higher velocity than in orthogonal directions. We found that particle velocities on all pattern sizes showed a similar behavior. We fit the distributions to the Gaussian functions and found the height and the width of the distributions. As seen in Figure 3-12D, the height of the distributions is the largest for 3 μm pitch, showing a familiar biphasic relationship. This indicates that

particles on 3 μm substrates have larger velocities due to increased step size along the direction of the ridges.

These results indicate that, in addition to cell shapes being aligned with topographical features of the surface, the movement of intracellular cytoskeletal components is also strongly modulated with surface topography. Further, we see that alignment of palladin tracks is guided by not just geometrical constraints, but by the overall preference to go faster in the direction of the ridges. This may allow for faster transport along the direction of ridges creating intracellular "highways" in that direction, and thus further facilitating alignment and elongation of the cell.
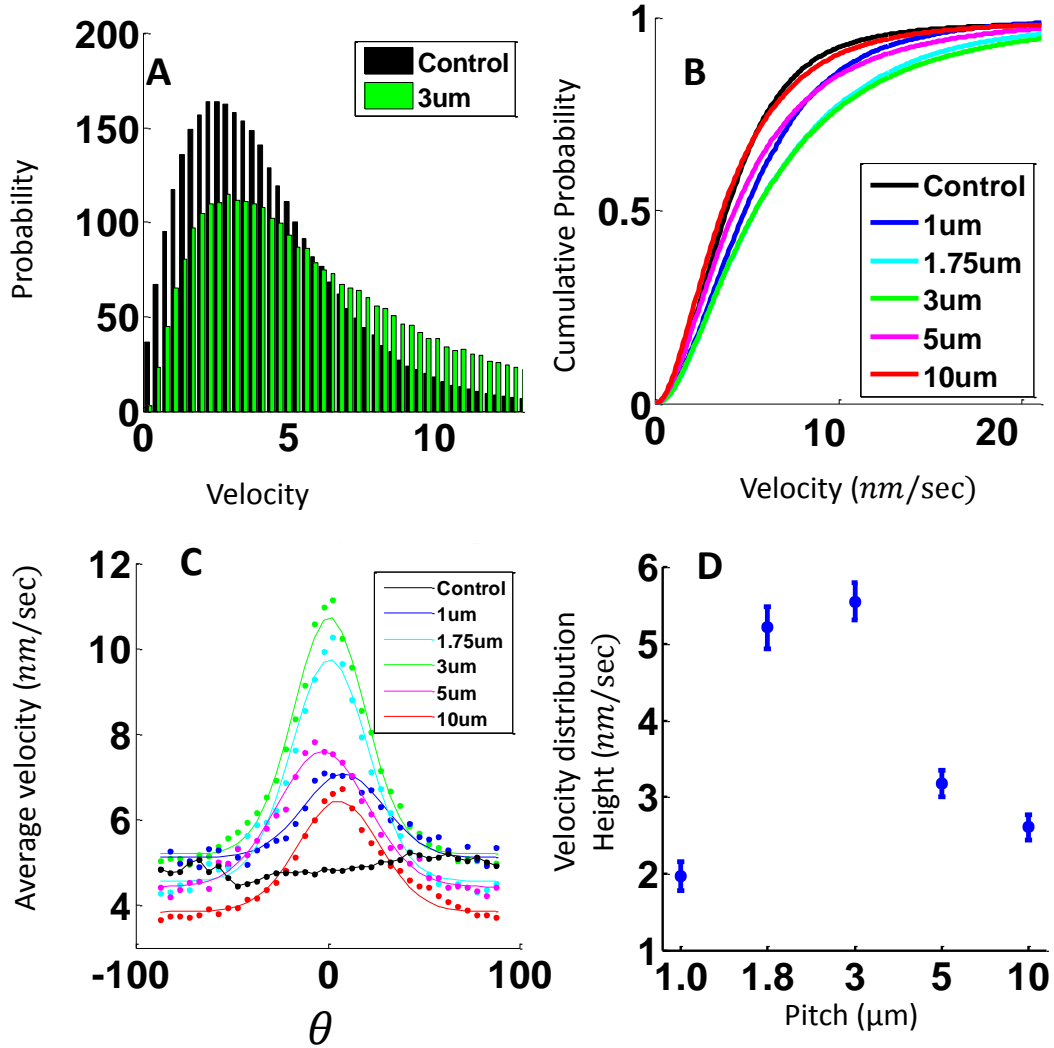
Figure 3-12 Distribution of velocities of the tracks with respect to ridges. (**A**) Probability distribution of velocities for control (flat surface, black) and 3 µm pitch surface (green). Distributions show a non-Maxwellian behavior with a long tail. (**B**) Cumulative distribution of velocities for all patterns. 3 µm and 1.8 µm patterns show the highest velocities among all substrates. (**C**) Distribution of velocity with respect to its angle to the ridges for all surfaces. Each point represents an average of all velocities within that range of angles. Binning was done every 5 degrees . Velocities exhibit Gaussian distribution centered around 0. All distributions besides the control case were fitted with Gaussian distribution with y-offset. (**D**) The height of the velocity distribution obtained from the Gaussian fits. 3 µm and 1.8 µm surfaces show the largest peak of velocity distributions.

3.4.3.4   Mean-Square Displacement of palladin bands

One way to characterize such complex motion is using Mean-Squared Displacement (MSD) (See Equation (5)). MSD, calculated as a function of lag time, provides a tool to measure the extent of random motion in a system on different time scales. MSD quantifies the observed displacement of a particle over time lag chosen, and is typically fit to the power-law function (See Equation (6)). One can divide different types of motion into subdiffusive, diffusive, and superdiffusive. The power-law exponent of the fit function provides and important characteristic of the regime of the motion and can separate between subdiffusive, diffusive, and superdiffusive motions (See Section 3.4.3.1).

As expected from the velocity distribution results, the MSD exhibited superdiffusive motion on long time scales. It followed closely the power law function introduced in Equation (6). Figure 3-13A shows an ensemble average MSD for all cells for each surface, and Figure 3-13B shows the numerical values for the power-law exponent, β, the parameter D, and the constant c. The power-law exponent, β, was high for all surfaces,   indicating a strong superdiffusive motion, and peaked for the 3µm pattern. The fit parameter, D, which is an effective diffusion coefficient, was larger for all patterned surfaces (except 10 µm) as compared to the flat surface, with the 3 µm surface exhibiting the largest D. The constant c, varied between the different surfaces and coupled with D, and β describes MSD for small Δt as both terms in Equation (6) become of the same magnitude. It will be more methodically analyzed in the next section.
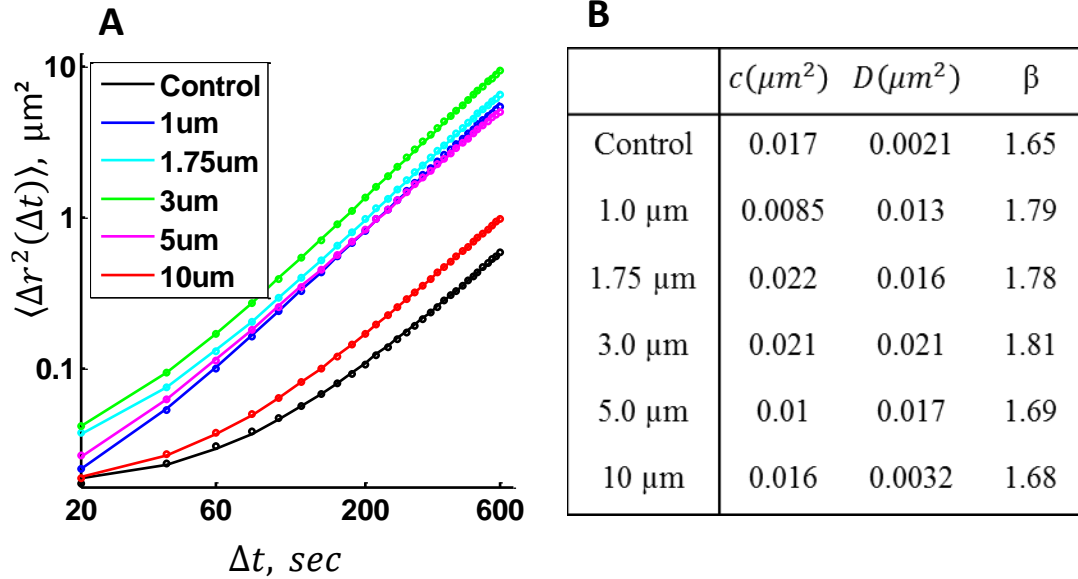
Figure 3-13 Ensemble MSD of palladin tracks. (A) Ensemble MSD for all cells on different patterns as a function of time lag Δt. MSD followed a power-law function described in Equation (6). All best fit lines had r² > 0.99. **(B)** Table of parameters c, D, and β from best fit lines of the graphs to the left. For all tracking experiment we analyzed ~ 10 cells per topographical surface used, which corresponded to ~ 1000-3000 individual tracks per condition

We investigated the tracks of palladin bands more thoroughly by fitting each individual track with Equation (6), and comparing distributions of the different fit coefficients. Individual tracks fit Equation (4) well, with over 94% of all tracks having r^2 value bigger than 90%. We selected the tracks that had $r^2 > 90\%$ and calculated the probability distributions of each fit parameter. The distribution of β showed a rightward skew that peaked around 1.8 and declined fast at 2 with less than 0.5% of all tracks exhibiting β >2.1 (See Figure 3-14A) Parameter D, varied over a large range of values spanning several orders of magnitude and following a roughly log-normal distribution (See Figure 3-14B). Cumulative probability distribution of the fit values across all

substrates showed that the parameter D showed the largest difference (See Figure 3-14). Similar to ensemble average distributions, D was much larger for patterned surfaces. The median of D for 3μm was around 0.26 μm^2, while for flat surface it was around 0.038 μm^2, almost 7 times smaller. Probability distributions of power-law exponent β looked very similar for most of the substrates. While there were significant differences between some individual pairs of substrates (like 5 μm and 1 μm, p<0.05), they were not significant for majority of the pairs (two-sample Kolmogorov-Smirnov test).

Together these results indicate an overall more dynamic behavior of the cells on ridges and confirm our previous results on biphasic dependence of different parameters on the pitch of the ridges.
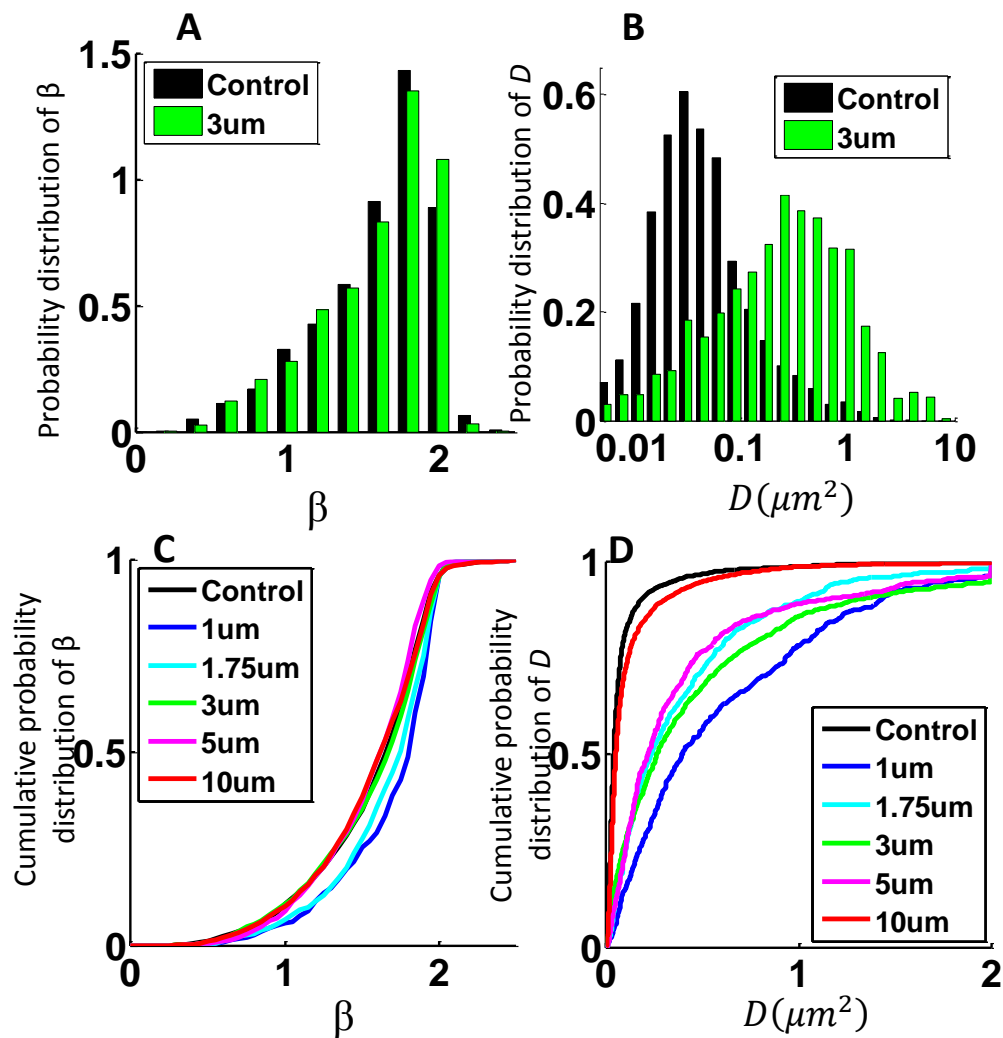
Figure 3-14 Distribution of MSD fit coefficients. **(A)** Probability distribution of power-law exponent β showing two histograms for control/flat and 3 μm surface. **(B)** Probability distribution of effective diffusion coefficient D, showing two histograms for control/flat and 3 μm surface. **(C)** Cumulative probability distribution of power-law exponent β. **(D)** Cumulative probability distribution of effective diffusion coefficient D.

3.4.3.5 Superdiffusive and subdiffusive motion of palladin bands

As mentioned previously, the constant *c,* also differed between different surfaces.

Constant *c,* represents the amount of noise and fluctuations in the track as $\langle \Delta r^2(\Delta t) \rangle \rightarrow$

c, when $\Delta t \to 0$. Looking at the first few points on the MSD plot in Figure 3-13, one can see that most of the MSD plots had a smaller slope (less than 1) for small Δt. This change of slope indicates that for smaller time scales the motion is subdiffusive, while for larger time scales, it is superdiffusive, switching approximately in the first minute of Δt. As $\Delta t \to 0$, $\langle \Delta r^2(\Delta t) \rangle \to c$ and the slope approaches 0, while for large Δt, $\langle \Delta r^2(\Delta t) \rangle \to D \left(\frac{\Delta t}{t_0} \right)^\beta$, and the slope approaches β. The time Δt_1, for which the slope is equal to one, is the point where the MSD switches from subdiffisive to superdiffusive behavior. From Equation (6), one can derive the time $\Delta t_1 = \left(\frac{c}{D(\beta-1)} \right)^{\frac{1}{\beta}}$ of this switch. Since Δt_1 exists only for superdiffusive motion, we calculated Δt_1 for all tracks with $\beta > 1.2$ (~84% of all tracks). The cumulative distribution of Δt_1 shows that both flat and 10 µm surfaces have the largest Δt_1 which implies that the switch between subdiffusive to superdiffusive motion occurs much later for those conditions.
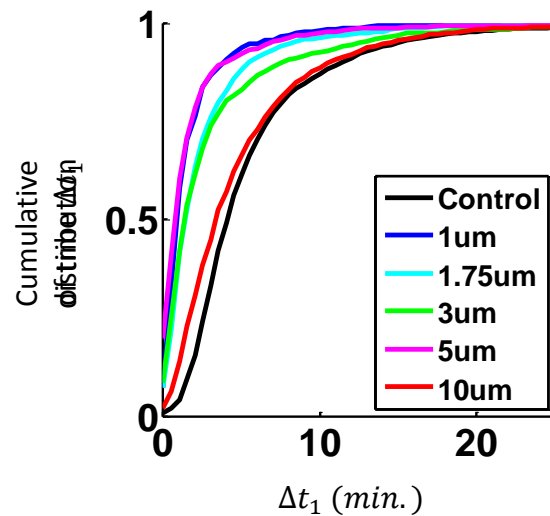
Figure 3-15 Cumulative distribution of time Δt_1 when the track switches from subdiffusive to superdiffusive motion for all tracks with $\beta > 1.2$

To further investigate the sub-diffusive behavior of palladin tracks we examined the directionality of the motion of palladin structures, which can be quantified by probability distributions of turning angles $\varphi(t, \Delta t)$ as a function of time lag Δt (See Section 3.4.3.1)[187][190]. If the motion is persistent, then the distribution will have more turning angles around 0º, while for anti-correlated motion, the majority of the angles should be around 180º. A pure random walk will have a flat distribution of turning angles. Plotting how the velocity distributions depend on this turning angle, should allow us to determine whether some directions were more or less favored.

We observed different regimes of turning angle distribution in our system depending on the time lag chosen. Figure 3-16A-C shows the turning angle probability distributions for different surfaces and different time lags. Interestingly all surfaces exhibited partially restricted motion for smaller time lags. All distributions had 2 peaks, one around 0º, and another around 180º. For larger time lags, the 180º peak slowly dissipated as the 0º peak increased. 0º peak corresponds to persistent part of the motion as it indicates the particle continuing the next step in the same direction, while 180º peak corresponds to restricted part of the motion, as it indicates the particle going backwards on its next step. We next examined whether there was a dependence of velocities on the turning angle. We divided the range of all possible directions (from -90º to 90º) into 5º bins. We averaged all velocities in a given bin and plotted the resulting distribution (See Figure 3-16D-F) for different surfaces and different time lags. Distributions had 2 peaks, one around 0º, and another around 180º. For larger time lags, the 180º peak slowly dissipated as the 0º peak increased indicating that palladin tracks underwent a much larger step size when it is in the same direction as the previous step. We found that

particle velocities on all pattern sizes showed a similar behavior. Velocity distributions exhibited biphasic dependence on substrate pitch with highest average velocities for 3 µm for all time lags Δt, confirming our previous results on biphasic dependence of different parameters on the pitch of the ridges.

Subdiffusive motion may arise from different uncertainties in experimental procedure like stage vibrations, temperature fluctuations or photon count noise. To test whether observed subdiffusive motion is a product of experimental error, we performed a control experiment to quantify the amount of noise in our apparatus and analysis. We plated immobile beads on the same substrates, imaged them under similar conditions, and performed the same analysis. Even though the beads are immobile, the tracking algorithm finds different coordinates for each frame, leading to different velocities and turning angles. Comparing results of different substrates with the results for noise (See Figure 3-16), we find that 1) noise turning angle distribution has only one peak around 180 ° as expected for constrained particle and 2) noise velocities are lower than velocities of palladin bands within cells, indicating that our tracking precision is indeed below measured values.
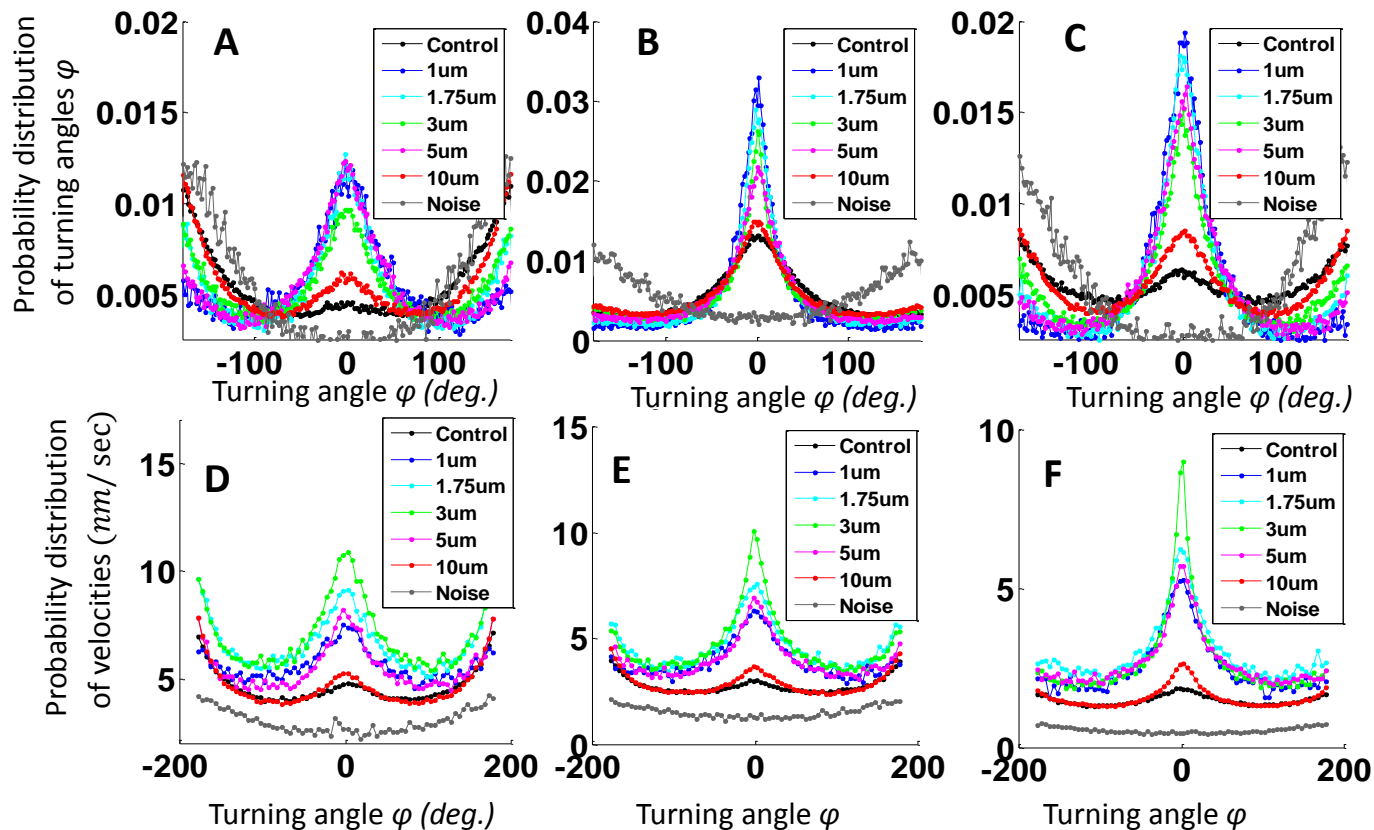
Figure 3-16 Distribution of turning angles $\varphi(t, \Delta t)$ and corresponding velocities for 3 time lags Δt. **(A-C)** Probability distribution for $\Delta t = 20, 40, 120 \, sec$ showing two peaks around 180 ° and 0 °. **(D-F)** Average velocity as function of a turning angle for $\Delta t = 20, 40, 120 \, sec$ showing two peaks around 180 ° and 0 °. Each point represents an average of all velocities within that range of angles. Binning was done every 5 degrees . The distribution shows a clear biphasic relationship of velocities peaking at 3 μm. The different colors correspond to different patterns, the grey line corresponds to noise.

For all substrates, the 180º peak in turning angle distribution disappears for $\Delta t >$ 2 $min.$, indicating two regimes of motion, anti-persistent on smaller time scales and persistent for larger time scales switching approximately in the first minute of Δt resembling the switch from subdiffusive to superdiffusive motion we found in MSD.

3.4.4 Role of focal adhesions in guiding cell alignment

Focal adhesions have been proposed to play an important role in topography sensing since focal adhesions align themselves along the direction of the ridges [120][104] and could potentially align stress fibers which originate from focal adhesions. While the basic idea of mechanosensing of surface topography through focal adhesions has been discussed previously, it is still not clear how focal adhesions align along the ridges and how they may induce the biphasic dependence of alignment as seen in our experiments. We wished to understand the role of focal adhesions in topography sensing by analyzing the distributions of focal adhesion locations, directions, and lengths.

To characterize the properties of focal adhesions as a function of surface topography we fixed cells on substrates of different pitch size and stained them for paxillin, a protein known to localize in focal adhesions [37]. Cells were allowed to fully spread for 3 hours prior to fixing and staining. Upon first observation we noticed that focal adhesions were strikingly aligned with the ridges on all substrates (See Figure 3-17). In fact, we found that focal adhesions are most likely to form on top of the ridges, as opposed to the space between ridges. While we cannot confirm these results from fluorescent images due to the small height of the ridges, comparison of fluorescent images of paxillin and IRM image of the ridges strongly suggest this, as indicated by the line profiles in Figure 3-17C-E. Furthermore comparing different patterned substrates, we find that the percentage of focal adhesions on top of the ridges changes drastically with the pitch size. While most focal adhesions grow on top of the ridges for smaller pitch substrates, the percentage of focal adhesions growing on top declines quickly for 3μm and 5 μm substrates with almost none growing on top for 10 μm substrate (See Figure

3-19A). Furthermore, as seen from Figure 3-19B, for most surfaces, focal adhesions did

not cross the ridges adjacent to them, except for the smallest tested ridge spacing of 0.8

µm, where we saw a noticeable amount of focal adhesions that crossed ridges. Figure

3-18 shows an example of a cell spread on 1.5 µm substrate with a few focal adhesions

that do cross the ridges. This is quantified in Figure 3-19B and confirms the results in

[191] that focal adhesions can indeed bend around large boundaries, but it also indicates

that it is not favorable.
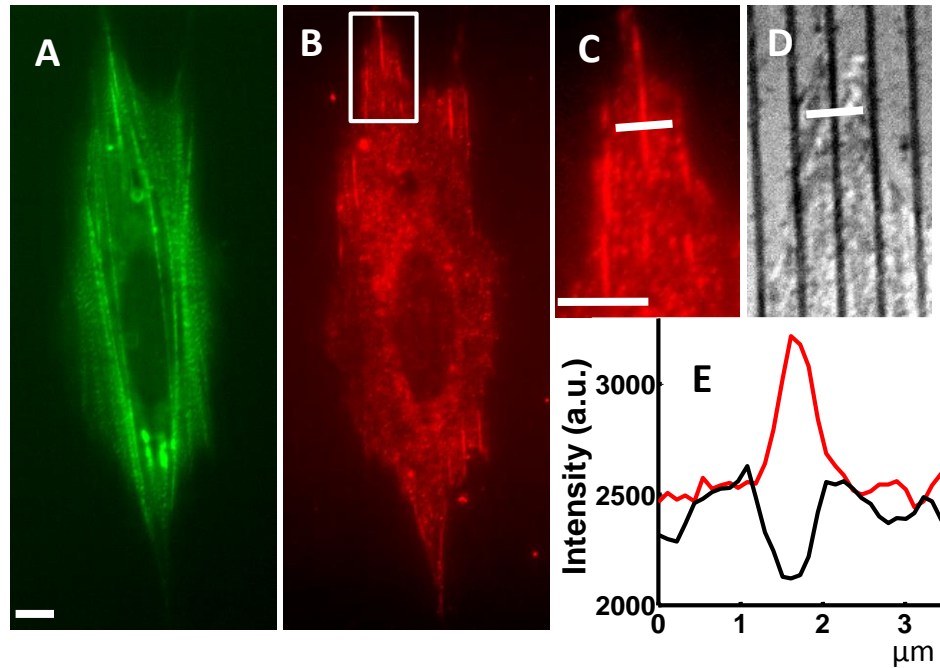
Figure 3-17 Localization of focal adhesions in the cell. (A) Widefield fluorescent image of EGFP-palladin on 3 µm substrate after 3 hours of spreading, fixing, and immunostaining of paxillin. Scale bar: 5 µm. (B) TIRF image of paxillin showing localizations of focal adhesions. (C) TIRF image of paxillin obtained from the white box in panel B. Scale bar: 5 µm. (D) IRM image of the region in panel C showing locations of ridges. (E)Intensity profile along the white line in panels C and D, which is perpendicular to the ridge. The red line profile corresponds to paxillin, and black line profile corresponds to the IRM image. The peak of the red line, which corresponds to focal adhesions, correlates with the trough of the black line which corresponds to the. These type of focal adhesions were considered to be on top of the ridges.
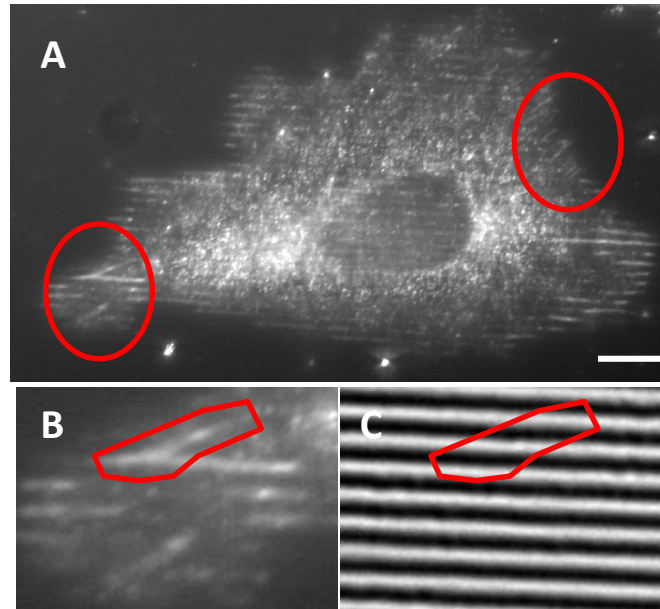
Figure 3-18 Examples of focal adhesions crossing the ridges.**(A)** TIRF image of paxillin showing localization of focal adhesions on a 1.5 µm substrate. Red circles highlight two regions with focal adhesions crossing the ridges. Scale bar: 10 µm. (B) TIRF image of paxillin obtained from the left red circles in (A) highlighting the focal adhesions crossing the ridges. **(C)** IRM image of areas in (B) showing location of ridges superimposed with the outline of focal adhesions in (B).

Comparing the angle distribution of focal adhesions with respect to the ridges, we see that for all patterned substrates these angles are quite small with median smaller than 10° for ridged surfaces. The angles show biphasic dependence with smallest angles for 1.0-1.75 µm pitch substrate (See Figure 3-19C)**.** Since focal adhesions do not favor crossing the ridges, and for smaller substrates grow mostly on top of the ridges, we do not see many focal adhesions with large angles on 1.0-1.75 µm pitch substrates. For larger ridge spacing, focal adhesions can grow between the ridges and hence the range of angles increases as we approach 10 µm surfaces.   Comparing the length of focal adhesions with each other we notice that for the majority of the patterns, focal adhesions growing on top of the ridges were longer compared to those at the bottom of the grooves, which

were similar in length to focal adhesions on flat surfaces (~ 3.5 µm) (See Figure 3-19D). This indicates that focal adhesions not only prefer to grow on top of ridges, but that the higher curvature of ridges facilitates focal adhesion growth as they can be almost twice as long (6.6 µm for 5µm pitch substrate). Among the ridges growing on top patterns from 1.5-5 µm showed the largest focal adhesions.
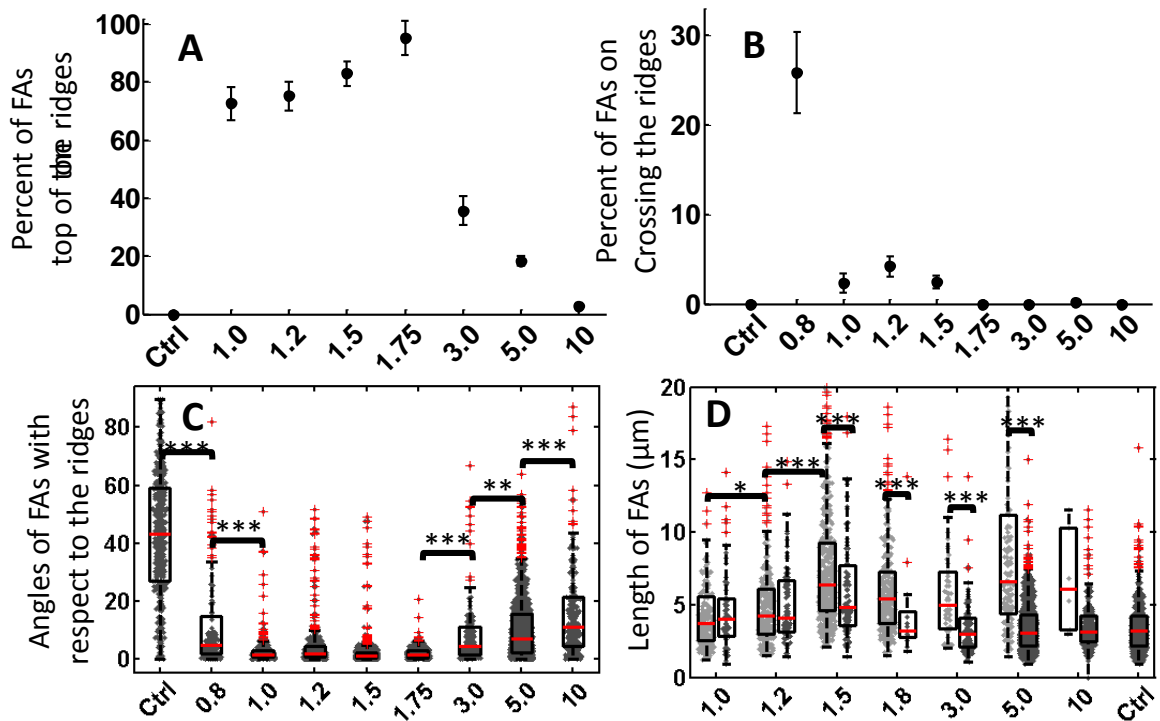
Figure 3-19 Characteristics of focal adhesions (**A**) Percent of FAs on top of the as a function of type of surface used. (**B**) Percent of FAs crossing the ridges as a function of surface used. Uncertainties for panels (A) and (B) were found as square root of number of counts. (**C**) Distribution of angles of focal adhesions with respect to type of surface used. All patterned surfaces were significantly different from flat surface. Statistical significance tests were performed using Wilcoxon test. (**D**) Distribution of length of focal adhesions with respect type of surface used. Each pattern size has two bar graphs corresponding to it. Left: light gray bar corresponds to the top of the ridges. Right: dark gray bar corresponds to the bottoms. Flat surface has only one bar. Statistical significance tests were performed using Wilcoxon test. For panels A-D, we used 10-20 cells totaling to 200-600 focal adhesions per surface used.

Our results confirm that focal adhesions can sense the topography of their environment, as the top surface of the ridges promoted focal adhesion maturation, since larger numbers of focal adhesions and longer focal adhesions were found on top of the ridges than in between. Ventral stress fibers originate in focal adhesions, and therefore are guided by direction of focal adhesions highlighting the importance of focal adhesion in topography sensing.

3.4.5 Dynamics of cell spreading on ridges.

While we do see that in well spread cells, actin cytoskeleton aligns, and moves along the ridges and FAs align themselves along the ridges, the sequence of events in the the early stages of spreading during the first minutes of cellular contact with ridges is not clear. Previously it has been suggested that microtubules were the first components of the cells to align as the alignment was seen 20 minutes after cell spreading [192]. Later Wojciak-Stothard et al. showed that actin condensates along the ridges within 5 minutes of spreading initiation suggesting that actin might be the primary component in the mechanosensing of surface topography [193].

As discussed in Chapter 2, during early spreading palladin appears diffusely throughout the cell, which is mostly quasi-circular during the first 30 minutes of spreading (See Figure 2-3). We wanted to further quantify the early events of cell spreading on the ridges by observing the dynamics of EGFP-palladin during the first few minutes of cell contact with the ridges. We obtained time-lapse images using total internal reflection fluorescence (TIRF) (See Figure 3-20). From the initial stages of spreading we can see that the cell interacts with ridges by sending out protrusion in the

grooves between the ridges. By drawing a kymograph in the direction perpendicular to the ridges, we can see that cell protrusions are stopped by ridges, which is indicated by straight vertical lines in the kymograph. This indicates that in the early stages of spreading, cell protrusions perpendicular to the ridges may be stalled and the cell edge could take a long time to overcome the ridges, while cell edge protrusions will preferentially occur parallel to the ridges. Thus, the cell might elongate and spread in the direction of the ridges showing some degree of alignment and topography sensing even before focal adhesions and stress fibers are formed.
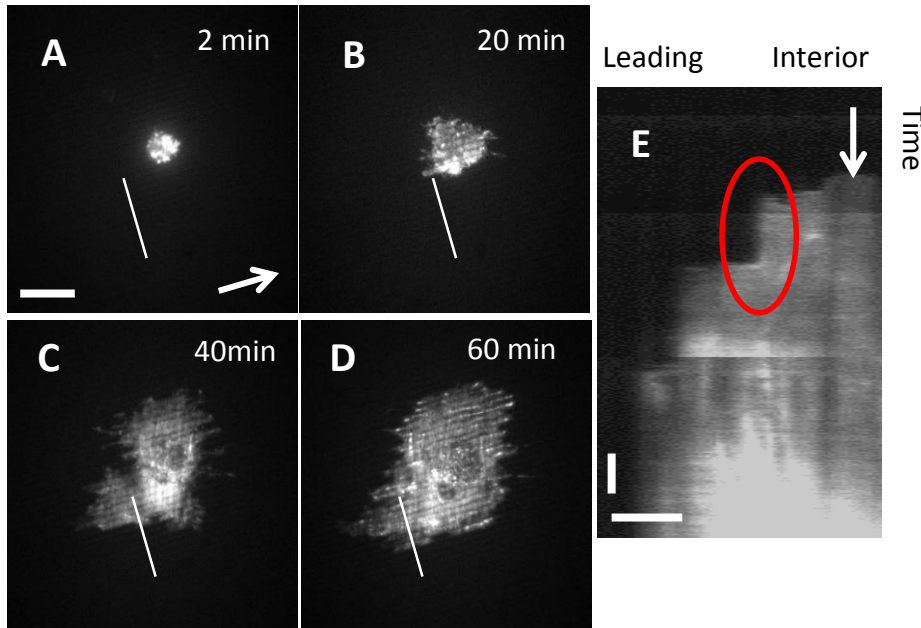
Figure 3-20 Topography sensing in the first minutes of spreading. (A,B,C,D) TIRF image of first 60 minutes of EGFP-Palladin cell spreading on 3μm substrate. Arrow in (A) indicates the direction of the ridges. Scale bar: 10 μm. (E) Kymograph along the line depicted in (A,B,C,D) perpendicular to the direction of the ridges showing protrusions stopped by ridges as indicated by straight vertical parts in kymograph. Scale bars: 5 μm horizontal,10 min. vertical.

3.5   Discussion

The goal of this study was to investigate the response of TAFs to surface topography and to elucidate the mechanism of topography sensing in cells. To achieve this, we examined both static images and time lapse movies of cells spread on surfaces with different topographical features. From static images we were able to obtain orientation and alignment of cells, stress fibers, and focal adhesions, while from the movies we were able to obtain the dynamical properties of the actin cytoskeleton.

Analysis of cell shape and stress fiber alignment indicated a strong biphasic relationship between the degree of alignment and the pitch of the substrates. While it has been shown that cells lose their mechanosensitivity on both extremes of the pattern pitch spectrum [104][106], we confirmed that the nature of the biphasic dependence was independent of the height of the ridges. Analysis of dynamics of palladin bands on actin stress fibers provides us a unique opportunity to quantify intracellular dynamics in a novel way, as tracking these bands gives us a measure of the intrinsic cytoskeletal dynamics without having to rely on externally introduced particles and their mode of attachment to the cytoskeleton. We observed that actin stress fibers underwent complex motion and exhibited regimes of subdiffusive and superdiffusive behavior. Analysis of instantaneous velocities showed that actin cytoskeleton is more active on patterned surfaces, as higher velocities were observed for all patterned surfaces compared with flat surface. Instantaneous velocities of palladin were higher for steps made in the direction of the ridges and exhibited a biphasic dependence on the pitch of the patterns with velocity magnitudes peaking for 3 μm pitch substrate. Analysis of MSD of moving particles provides a very effective tool for investigating the properties of diffusive motion. We analyzed MSD of moving palladin bands to obtain insight into the time-scale dependence

118

of their motion. The effective diffusion coefficient D, was higher for all patterned surfaces and peaked for the 3μm substrate. The power-law exponent β, was high for all patterns (1.65-1.81), indicating a strong superdiffusive motion , and also peaked for 3 μm substrate. Together both D, and β indicate a more dynamic actin cytoskeleton on all patterned surfaces at all time-scales.

It is interesting to note that cell migration has also been shown to be sensitive to substrate topography. Migration speed of NIH 3T3 fibroblasts was found to have a biphasic dependence on the pitch of ridges with the highest speeds for 5μm pitch substrates in the range of pitches from 1μm- 10 μm[104]. Furthermore, the study of *Dictyostelium* cells also shows a biphasic dependence with 1.5 μm substrates exhibiting the greatest contact guidance efficiency [176]. It is intriguing to see such similar results for different phenomena, and it provides some interesting insights into converting local response to overall cell behavior. Additionally TAFs have been shown to be more active on soft substrates (Chapter 2), further demonstrating the importance of mimicking in vivo environments of the cell.

In addition to the magnitude of the velocities, we analyzed the direction of the motion by looking at the angle of the motion with respect to the ridges, turning angles of the motion, as well as the power-law exponent of diffusive motion. All our results indicate that tracked particles are more likely to move along the direction of the ridges, and with increased velocity in that direction. Along with structural support actin cytoskeleton provides network for intracellular transportation. Faster motion of actin cytoskeleton suggests that the presence of ridges may create intracellular "highways" that allow for faster transport along the direction of the ridges. The various parameters to

quantify directionality also follow a biphasic relationship with respect to the pattern pitch.

Analysis of focal adhesions indicates the potential importance of these structures in mechanosensing of surface topography. Focal adhesions prefer to grow along the high curvature surfaces on the top of the ridges, mature to longer adhesions and are unlikely to cross the ridges. Since ventral stress fibers originate in focal adhesions, the direction of focal adhesions can guide the direction of ventral stress fibers, which can explain overall alignment of stress fibers, and henceforth the cell body along the patterns. Our results are consistent with theories suggesting that overall cell alignment is induced by alignment of focal adhesions [175], however focal adhesions alone do not explain the loss of mechanosensitivity for denser patterns. The orientation distribution of focal adhesions exhibited a different biphasic relationship, as compared to that of cell shape and stress fiber alignment, and was shifted towards smaller pitch substrates. Focal adhesions were aligned and grew on top of the ridges for 1 μm patterns. Furthermore, mechanosensing of topography cannot be explained only due acitn network organization as 10 μm pitch substrates exhibit velocities very similar to flat surfaces while showing strong alignment of stress fibers and cell shape. Together these results suggest that both focal adhesions and actin networks may work synergistically to facilitate cell alignment. Below, we present a qualitative model that could explain this phenomenon.

On flat surfaces the boundaries of the cell are usually defined either by stress fibers which span across the edge of the cell or focal adhesions, maturing in the "corners" of the cell (See Figure 3-21A-C). The dynamic analysis of palladin bands shows that actin prefers to move in the direction of the ridges and hence any misalignment of actin

stress fibers could provide additional strain to the actin network. As seen from Figure 3-21D-F small pattern sizes lead to high spatial density of focal adhesions. Regulating this density in order to have increased numbers of focal adhesions in places of higher stress fiber strain, may enable a cell to more easily maintain a shape and structures that are not aligned with the substrates. On substrates with large pattern pitch, longer focal adhesions are not capable of forming at such high density as the ridges are too far away from each other and the focal adhesions between the ridges are much smaller in size (See Figure 3-21G-I). In our model a group of long focal adhesions formed on several ridges in a row creates a stronghold necessary to anchor stress fibers that are not aligned with the substrate thus allowing for more orientation possibilities for the entire cell.
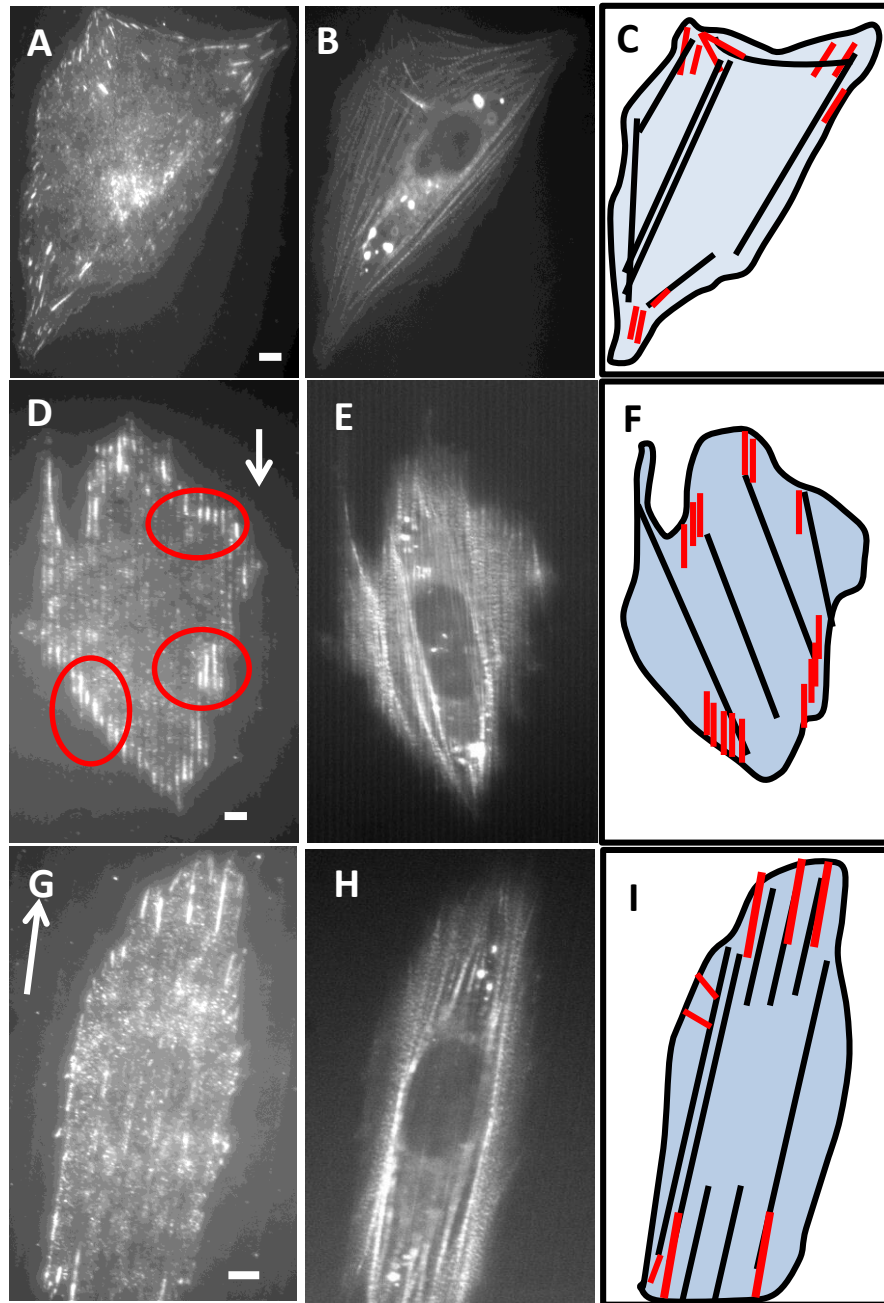
Figure 3-21 Schematic representation of the cells on nanopatterns. A) TIRF image of paxillin in TAF spread on flat surface. Scale bar: 5 µm. (B) Widefield fluorescence image of EGFP –palladin in TAF spread o the flat surface. (C) Schematic representation of the cell body in panels A,B. Light blue body represents the cell, black lines represent stress fibers, and red lines represent focal adhesions. Cell body is defined by either stress fibers spanning along the edge of the cell or focal adhesions located in the places of high curvature, "corners" of the cell. The cell in panels A-C has 3of those "corners". (D) TIRF image of paxillin in TAF spread on 1.2 µm pattern. The arrow shows the direction of the

ridges. Red circle point to concentration focal adhesions, where they are formed on top of every ridge, creating a high spatial density of focal adhesion. Scale bar: 5µm. (E) Widefield fluorescence image of EGFP-Palladin of the cell in panel D, showing stress fibers that are not as well aligned with the substrate. (F) Schematic of the cell in panels D and E showing how misaligned stress fibers can be reinforced by high density of focal adhesions. (G) TIRF image of paxillin in TAF spread on 5 µm pattern. The arrow shows the direction of the ridges. Most of the focal adhesions are either long focal adhesions formed on top of the ridges or small focal adhesions formed in between. Scale bar: 5 µm. (H) Widefield fluorescence image of EGFP-palladin showing actin stress fibers completely aligned with ridges. (I) Schematic of the cell in panels F, and G showing locations of focal adhesions and stress fibers. focal adhesions are not capable in forming long, high density structures that we see in panel H, thus allowing cell to stretch out in the direction of the ridges.

Analysis of the movement of palladin bands on stress fibers provides us with insight into the intrinsic dynamics of the actin cytoskeleton and its response to surface topography. Our data indicates both superdiffusive and subdiffusive motion of palladin bands on actin fibers. Superdiffusive motion can be explained by geometrical constraints of the actin cytoskeleton and the nature of stress fiber motion, since the motion is guided by retrograde flow of actin and is therefore directional towards the inside of the cell. It is somewhat puzzling to see subdiffusive behavior on smaller time scales. Several previously proposed models may be able to explain such behavior. "Stalling and hopping" motion of beads proposed by[194] argued that subdiffusive motion corresponds to stalling and superdiffusive motion with hopping of cytoskeletal bound beads. Our turning angle distributions highly resemble constrained motion of immobile particles on small time scales. Complex actin networks could potentially create such an environment for some parts of its network. Particle bound to actin cytoskeleton, experiences forces

from all surrounding filaments and under zero balance of forces can stay in the same location until further remodeling of actin cytoskeleton[195]. A previous study of the motion of cytoskeletal bound beads also observed a switch of the MSD from subdiffusive to superdiffusive motion[187]. In their theoretical paper, they proposed that force fluctuations, arising from activity of myosin motors within stress fibers could be the source of subdiffusive motion[196], since they observe the beads embedded in the gel under the cell exhibit similar dynamical properties as cytoskeletal bound beads. Although, their observed time scale of switching between subdiffusive and superdiffusive behavior , Δt_1, was different compared to ours, there are a few similarities between our results, including MSD fit coefficient distributions and turning angle distributions, suggesting that force fluctuations could lead to subdiffusive motion in our system as well.

Palladin is an actin-binding protein that helps maintain the structural integrity of stress fibers. By tracking palladin bands we involuntarily couple together the motion of stress fibers and the motion of palladin along stress fibers. In previous work with Brian Grooman [manuscript in preparation], we showed that parts of stress fibers constantly undergo myosin driven stress and relaxation periods during which the relative distance between two neighboring palladin bands increases and decreases. The distance between two palladin bands can change due to force fluctuations within the filaments and could explain subdiffusive motion on smaller time scales where fluctuation of stress fibers dominate the overall motion of palladin. Further, since stress fibers are connected to the ECM through focal adhesions, force fluctuations within stress fibers could translate into fluctuations of the surface on which the cell is attached. Therefore we believe, that one could decouple the motion OF stress fibers and the motion ON stress fibers by looking at

124

different time scale of overall motion defined by the time Δt_1, of switch between subdiffusive and super diffusive motion. Differences in Δt_1, can result from differences in overall stress within actin networks, as more stress on actin stress fibers could result in faster fluctuations of palladin bands and therefore modify the inherent timescales.

While testing any of these theories was out of the scope of this project, to really understand the underlying processes of subdiffusive motion, one would need to image cells for shorter time at shorter time scales, since the switch from subdiffusive to superdiffusvie motion seems to happen at around 1min time lag.

4   Summary and outlook

4.1   Thesis Summary

In this thesis, I have discussed different mechanisms that allow cells to respond to mechanical properties of their environment. By combining experimental work and quantitative analysis, we were able to better understand cellular mechanosensing at both cellular and subcellular levels.

In Chapter 2, we have shown that palladin is one of the actin binding proteins involved in mechanosensing of substrate elasticity. We show that palladin allows cells to sense higher stiffnesses and together with myosin works on proper traction force generation. We see that both palladin and α-actinin could potentially have similar roles in stress fiber assembly and traction force generation suggesting that cells could potentially regulate actin network contractility by varying the concentration of both cross-linkers.

In Chapter 3, we have shown that cells respond to an array of parallel ridges in a very robust biphasic manner independent of height of the structures. Furthermore analysis of dynamics of actin cytoskeleton shows that actin networks adjust not only their structure but dynamics, as the direction and magnitude of velocity depended strongly on the pitch of the patters exhibiting the same biphasic pattern. These results coupled with the results on focal adhesion localization provide a mechanism for topography sensing, in which both actin cytoskeleton and focal adhesion coordinate to adapt cell behavior.

It is interesting to point out some of the similarities between the results of the two different projects. In Chapter 2, while comparing the retrograde flow speeds between two cell types and gels of different elasticity, we see, that the velocities on stiff substrate (30-60 kPa) were almost twice less compared to the velocities on intermediate stiffness (10-30 kPa). Comparing them with glass we see that the differences in retrograde flow speeds between intermediate stiffness gel and glass are almost 5-fold. Similarly while measuring a different type of velocity in Chapter 3, we see a significant increase in velocities for all topographical substrates. Such differences in velocities reveal global differences in cell behavior on different substrates. These results highlight the need for scientists to mimic the real cellular environment in vitro, as by performing experiments on glass coverslips we drastically change the behavior of the cell.

4.2   Future Directions

Palladin is involved in formation of many cytoskeletal structures within the cell. Chapter 2 highlighted the role of palladin in focal adhesion assembly. To our knowledge, this is the first time palladin has been implicated in focal adhesion formation.

Furthermore we see an interesting dynamics between palladin and the focal adhesion protein, paxillin. We believe that further work needs to be done to understand the exact role of palladin in focal adhesion assembly as on glass, as on soft substrates.

Analysis of tracks of palladin bands showed that actin cytoskeleton undergoes a complex motion with both superdiffusive and subdiffusive components. Our data indicates that the source of subdiffusive motion is not the noise in our system, revealing two types of motion of stress fibers: (1) superdiffusive on long time scales, and (2) subdiffusive on short time scales. The motion of each palladin bands is "semi-caged", meaning that while the stress fibers is moving as a whole, palladin itself is stuck on the stress fiber. Therefore the only motion one would see from the movement of palladin along a stress fiber comes from expansion and contraction of stress fiber itself. We, therefore think that the detected subdiffusive motion corresponds to the movement of palladin bands along stress fibers. The parameters of the detected subdiffusive motion therefore would reveal the viscoelastic properties of the individual stress fiber. Further work is required to test this hypothesis, as one would need to image cells at a higher frame rate, with possibly better spacial resolution. Currently, there is a dearth of efficient experimental methods to measure the internal stress fluctuations within cells. Laser cutting of individual stress fibers can give an estimate of contractile tension [197]. Another possibility is a model based traction force microscopy, where locations of stress fibers and focal adhesions are analyzed together with traction force measurements to estimate the stress within stress fibers [198]. Once perfected, I believe palladin tracking could provide a unique way to measure the viscoelastic properties and force fluctuations of stress fibers without perturbing a cell.

[1]   F. H. C. Crick and A. F. W. Hughes, "The physical properties of cytoplasm," *Exp. Cell Res.*, vol. 1, no. 1, pp. 37–80, Jan. 1950.

[2]   H. P. Lodish, H; Berk, A; Kaiser, C;Krieger, M;Scott, M;Bretcher, A; Ploegh, *Molecular cell biology*. New York: W.H. Freeman and Company, 2008.

[3]   P. W. Bruce Alberts, Alexander Johnson, Julian Lewis, Martian Raff Keith Roberts, *Molecular Biology of The Cell*, vol. 40, no. 6. Garland Science Taylor & Francis Group, 2001.

[4]   D. Bray, *Cell Movent, From Molecules to Motility*, Second Edi. New York: Garland Publishing, 2001.

[5]   I. Fujiwara, S. Takahashi, H. Tadakuma, T. Funatsu, and S. Ishiwata, "Microscopic analysis of polymerization dynamics with individual actin filaments.," *Nat. Cell Biol.*, vol. 4, no. 9, pp. 666–73, Sep. 2002.

[6]   P. A. Kuhlman, "Dynamic changes in the length distribution of actin filaments during polymerization can be modulated by barbed end capping proteins," *Cell Motil. Cytoskeleton*, vol. 61, no. 1, pp. 1–8, May 2005.

[7]   E. S. Chhabra and H. N. Higgs, "The many faces of actin: matching assembly factors with cellular structures.," *Nat. Cell Biol.*, vol. 9, no. 10, pp. 1110–1121, 2007.

[8]   C. G. D. O. S. Remedios, D. Chhabra, M. Kekic, I. V Dedova, and M. Tsubakihara, "Actin Binding Proteins : Regulation of Cytoskeletal Microfilaments," pp. 433–473, 2003.

[9]   Y. Tseng, E. Fedorov, J. M. McCaffery, S. C. Almo, and D. Wirtz, "Micromechanics and ultrastructure of actin filament networks crosslinked by human fascin: a comparison with alpha-actinin.," *J. Mol. Biol.*, vol. 310, no. 2, pp. 351–66, Jul. 2001.

[10]   A. Mogilner and G. Oster, "Cell Motility Driven by Actin Polymerization," vol. 71, no. December, pp. 3030–3045, 1996.

[11]   M. Boukhelifa, M. M. Parast, J. E. Bear, F. B. Gertler, and C. A. Otey, "Palladin Is a Novel Binding Partner for Ena / VASP Family Members," vol. 29, no. September 2003, pp. 17–29, 2004.

[12]   O. Mykka, M. Gro, M. Ro, M. Lalowski, P. Salmikangas, H. Suila, and O. Carpe, "Characterization of Human Palladin , a Microfilament-," vol. 12, no. October, pp. 3060–3073, 2001.

[13]   M. Rönty, A. Taivainen, M. Moza, C. a. Otey, and O. Carpén, "Molecular analysis of the interaction between palladin and α-actinin," *FEBS Lett.*, vol. 566, pp. 30–34, 2004.

[14] S. Goicoechea, D. Arneman, A. Disanza, R. Garcia-Mata, G. Scita, and C. a Otey, "Palladin binds to Eps8 and enhances the formation of dorsal ruffles and podosomes in vascular smooth muscle cells.," *J. Cell Sci.*, vol. 119, pp. 3316–3324, 2006.

[15] A. S. Rachlin and C. a Otey, "Identification of palladin isoforms and characterization of an isoform-specific interaction between Lasp-1 and palladin.," *J. Cell Sci.*, vol. 119, pp. 995–1004, 2006.

[16] M. Boukhelifa, M. Moza, T. Johansson, A. Rachlin, M. Parast, S. Huttelmaier, P. Roy, B. M. Jockusch, O. Carpen, R. Karlsson, and C. a. Otey, "The proline-rich protein palladin is a binding partner for profilin," *FEBS J.*, vol. 273, pp. 26–33, 2006.

[17] M. M. Parast and C. a. Otey, "Characterization of palladin, a novel protein localized to stress fibers and cell adhesions," *J. Cell Biol.*, vol. 150, no. 3, pp. 643–655, 2000.

[18] M. Boukhelifa, M. M. Parast, J. G. Valtschanoff, a S. LaMantia, R. B. Meeker, and C. a Otey, "A role for the cytoskeleton-associated protein palladin in neurite outgrowth.," *Mol. Biol. Cell*, vol. 12, no. September, pp. 2721–2729, 2001.

[19] M. Boukhelifa, S. J. Hwang, J. G. Valtschanoff, R. B. Meeker, A. Rustioni, and C. a. Otey, "A critical role for palladin in astrocyte morphology and response to injury," *Mol. Cell. Neurosci.*, vol. 23, pp. 661–668, 2003.

[20] L. P. Cramer, M. Siebert, and T. J. Mitchison, "Identification of Novel Graded Polarity Actin Filament Bundles in Locomoting Heart Fibroblasts: Implications for the Generation of Motile Force," vol. 136, no. 6, pp. 1287–1305, 1997.

[21] K. Wang, J. F. Ash, and S. J. Singer, "Filamin, a new high-molecular-weight protein found in smooth muscle and non-muscle cells.," *Proc. Natl. Acad. Sci.*, vol. 72, no. 11, pp. 4483–4486, Nov. 1975.

[22] J. C. Adams, "Formation of stable microspikes containing actin and the 55 kDa actin bundling protein , fascin , is a consequence of cell adhesion to thrombospondin-1 : implications for the anti-adhesive activities of thrombospondin-1," vol. 1990, pp. 1977–1990, 1995.

[23] S. Pellegrin and H. Mellor, "Actin stress fibres.," *J. Cell Sci.*, vol. 120, no. Pt 20, pp. 3491–9, Oct. 2007.

[24] E. Lazarides, "TROPOMYOSIN ANTIBODY : THE SPECIFIC LOCALIZATION OF TROPOMYOSIN IN NONMUSCLE CELLS Cell Cultures Preparation of Tropomyosin Antibody Tropom yosin Purification," vol. 65, no. 13, 1975.

[25] A. Reymann, R. Boujemaa-paterski, J. Martiel, W. Cao, H. F. Chin, E. M. D. La Cruz, M. Théry, and L. Blanchoin, "Actin Network Architecture Can Determine Myosin Motor Activity," vol. 336, no. 6086, pp. 1310–1314, 2013.

[26] P. W. Oakes, Y. Beckham, J. Stricker, and M. L. Gardel, "Tension is required but not sufficient for focal adhesion maturation without a stress fiber template.," *J. Cell Biol.*, vol. 196, no. 3, pp. 363–74, Feb. 2012.

[27] G. Gateva, S. Tojkander, S. Koho, O. Carpen, and P. Lappalainen, "Palladin promotes assembly of non-contractile dorsal stress fibers through VASP recruitment.," *J. Cell Sci.*, vol. 127, no. Pt 9, pp. 1887–98, May 2014.

[28] B. Kovac, J. L. Teo, T. P. Mäkelä, and T. Vallenius, "Assembly of non-contractile dorsal stress fibers requires α-actinin-1 and Rac1 in migrating and spreading cells.," *J. Cell Sci.*, vol. 126, no. Pt 1, pp. 263–73, Jan. 2013.

[29] P. Hotulainen and P. Lappalainen, "Stress fibers are generated by two distinct actin assembly mechanisms in motile cells.," *J. Cell Biol.*, vol. 173, no. 3, pp. 383–94, May 2006.

[30] J. V. Small, K. Rottner, I. Kaverina, and K. I. Anderson, "Assembling an actin cytoskeleton for cell attachment and movement," *Biochim. Biophys. Acta - Mol. Cell Res.*, vol. 1404, no. 3, pp. 271–281, Sep. 1998.

[31] L. J. Peterson, Z. Rajfur, A. S. Maddox, C. D. Freel, Y. Chen, M. Edlund, C. Otey, and K. Burridge, "Fibers In Vivo," vol. 15, no. July, pp. 3497–3508, 2004.

[32] S. Kumar, I. Z. Maxwell, A. Heisterkamp, T. R. Polte, T. P. Lele, M. Salanga, E. Mazur, and D. E. Ingber, "Viscoelastic retraction of single living stress fibers and its impact on cell shape, cytoskeletal organization, and extracellular matrix mechanics.," *Biophys. J.*, vol. 90, no. 10, pp. 3762–73, May 2006.

[33] Y. Takada, X. Ye, and S. Simon, "The integrins.," *Genome Biol.*, vol. 8, no. 5, p. 215, Jan. 2007.

[34] R. Janoštiak, A. C. Pataki, J. Brábek, and D. Rösel, "Mechanosensors in integrin signaling: the emerging role of p130Cas.," *Eur. J. Cell Biol.*, vol. 93, no. 10–12, pp. 445–54, Oct. 2014.

[35] D. S. Harburger and D. A. Calderwood, "Integrin signalling at a glance.," *J. Cell Sci.*, vol. 122, no. Pt 2, pp. 159–63, Jan. 2009.

[36] R. O. Hynes, "Integrins: bidirectional, allosteric signaling machines.," *Cell*, vol. 110, no. 6, pp. 673–87, Sep. 2002.

[37] P. Kanchanawong, G. Shtengel, A. M. Pasapera, E. B. Ramko, W. Davidson, H. F. Hess, and C. M. Waterman, "Nanoscale architecture of integrin-based cell adhesions Pakorn," vol. 468, no. 7323, pp. 580–584, 2011.

[38] D. Riveline, E. Zamir, N. Q. Balaban, U. S. Schwarz, T. Ishizaki, S. Narumiya, Z. Kam, B. Geiger, and a. D. Bershadsky, "Focal Contacts as Mechanosensors: Externally Applied Local Mechanical Force Induces Growth of Focal Contacts by an Mdia1-Dependent and Rock-Independent Mechanism," *J. Cell Biol.*, vol. 153, no. 6, pp. 1175–1186, Jun. 2001.

[39]   C. K. Choi, M. Vicente-manzanares, J. Zareno, A. Leanna, A. Mogilner, A. R. Horwitz, and B. Engineering, "Actin and α-actinin orchestrate the assembly and maturation of nascent adhesions in a myosin II motor-independent manner Colin," *Nat Cell Biol.*, vol. 10, no. 9, pp. 1039–1050, 2008.

[40]   B. Hinz, "Masters and servants of the force: the role of matrix adhesions in myofibroblast force perception and transmission.," *Eur. J. Cell Biol.*, vol. 85, no. 3–4, pp. 175–81, Apr. 2006.

[41]   Y. Aratyn-Schaus and M. L. Gardel, "Transient frictional slip between integrin and the ECM in focal adhesions under myosin II tension.," *Curr. Biol.*, vol. 20, no. 13, pp. 1145–53, Jul. 2010.

[42]   J. Caetano-Lopes, H. Canhão, and J. E. Fonseca, "Osteoblasts and bone formation.," *Acta Reum. Port.*, vol. 32, no. 2, pp. 103–10, Jan. .

[43]   A. Lesman, J. Notbohm, D. A. Tirrell, and G. Ravichandran, "Contractile forces regulate cell division in three-dimensional environments.," *J. Cell Biol.*, vol. 205, no. 2, pp. 155–62, Apr. 2014.

[44]   A. Brugués, E. Anon, V. Conte, J. H. Veldhuis, M. Gupta, J. Colombelli, J. J. Muñoz, G. W. Brodland, B. Ladoux, and X. Trepat, "Forces driving epithelial wound healing," *Nat. Phys.*, vol. 10, no. 9, pp. 683–690, Aug. 2014.

[45]   B. Li and J. H.-C. Wang, "Fibroblasts and myofibroblasts in wound healing: force generation and measurement.," *J. Tissue Viability*, vol. 20, no. 4, pp. 108–20, Nov. 2011.

[46]   C.-P. Heisenberg and Y. Bellaïche, "Forces in tissue morphogenesis and patterning.," *Cell*, vol. 153, no. 5, pp. 948–62, May 2013.

[47]   S. Kumar and V. M. Weaver, "Mechanics, malignancy, and metastasis: the force journey of a tumor cell.," *Cancer Metastasis Rev.*, vol. 28, no. 1–2, pp. 113–27, Jun. 2009.

[48]   N. Hirokawa, Y. Noda, Y. Tanaka, and S. Niwa, "Kinesin superfamily motor proteins and intracellular transport.," *Nat. Rev. Mol. Cell Biol.*, vol. 10, no. 10, pp. 682–96, Oct. 2009.

[49]   A. J. Roberts, T. Kon, P. J. Knight, K. Sutoh, and S. A. Burgess, "Functions and mechanics of dynein motor proteins.," *Nat. Rev. Mol. Cell Biol.*, vol. 14, no. 11, pp. 713–26, Nov. 2013.

[50]   M. A. Hartman and J. A. Spudich, "The myosin superfamily at a glance.," *J. Cell Sci.*, vol. 125, no. Pt 7, pp. 1627–32, Apr. 2012.

[51]   J. T. Finer, R. M. Simmons, and J. A. Spudich, "Single myosin molecule mechanics: piconewton forces and nanometre steps.," *Nature*, vol. 368, no. 6467, pp. 113–9, Mar. 1994.

[52]   K. Burridge and M. Chrzanowska-Wodnicka, "Focal adhesions, contractility, and signaling.," *Annu. Rev. Cell Dev. Biol.*, vol. 12, pp. 463–518, Jan. 1996.

[53] Y. Cai, N. Biais, G. Giannone, M. Tanase, G. Jiang, J. M. Hofman, C. H. Wiggins, P. Silberzan, A. Buguin, B. Ladoux, and M. P. Sheetz, "Nonmuscle myosin IIA-dependent force inhibits cell spreading and drives F-actin flow.," *Biophys. J.*, vol. 91, no. 10, pp. 3907–20, Nov. 2006.

[54] S. R. Wylie and P. D. Chantler, "Separate but linked functions of conventional myosins modulate adhesion and neurite outgrowth.," *Nat. Cell Biol.*, vol. 3, no. 1, pp. 88–92, Jan. 2001.

[55] A. Mogilner and G. Oster, "Force Generation by Actin Polymerization II: The Elastic Ratchet and Tethered Filaments," *Biophys. J.*, vol. 84, no. 3, pp. 1591–1605, Mar. 2003.

[56] A. Upadhyaya, J. R. Chabot, A. Andreeva, A. Samadani, and A. van Oudenaarden, "Probing polymerization forces by using actin-propelled lipid vesicles.," *Proc. Natl. Acad. Sci. U. S. A.*, vol. 100, no. 8, pp. 4521–6, Apr. 2003.

[57] C. S. Peskin, G. M. Odell, and G. F. Oster, "Cellular motions and thermal fluctuations: the Brownian ratchet.," *Biophys. J.*, vol. 65, no. 1, pp. 316–24, Jul. 1993.

[58] M. Kaksonen, C. P. Toret, and D. G. Drubin, "Harnessing actin dynamics for clathrin-mediated endocytosis.," *Nat. Rev. Mol. Cell Biol.*, vol. 7, no. 6, pp. 404–14, Jun. 2006.

[59] M. J. Footer, J. W. Kerssemakers, J. A. Theriot, and M. Dogterom, "Direct measurement of force generation by actin filament polymerization using an optical trap," *Proc. Natl. Acad. Sci.*, vol. 104, no. 7, pp. 2181–2186, 2007.

[60] A. D. Bershadsky, N. Q. Balaban, and B. Geiger, "Adhesion-dependent cell mechanosensitivity.," *Annu. Rev. Cell Dev. Biol.*, vol. 19, pp. 677–95, Jan. 2003.

[61] A. Zemel, F. Rehfeldt, A. E. X. Brown, D. E. Discher, and S. A. Safran, "Optimal matrix rigidity for stress fiber polarization in stem cells.," *Nat. Phys.*, vol. 6, no. 6, pp. 468–473, Jun. 2010.

[62] P. A. Janmey and R. T. Miller, "Mechanisms of mechanical signaling in development and disease.," *J. Cell Sci.*, vol. 124, no. Pt 1, pp. 9–18, Jan. 2011.

[63] B. Geiger, J. P. Spatz, and A. D. Bershadsky, "Environmental sensing through focal adhesions.," *Nat. Rev. Mol. Cell Biol.*, vol. 10, no. 1, pp. 21–33, Jan. 2009.

[64] U. S. Schwarz, T. Erdmann, and I. B. Bischofs, "Focal adhesions as mechanosensors: the two-spring model.," *Biosystems.*, vol. 83, no. 2–3, pp. 225–32, Jan. .

[65] H. Wolfenson, Y. I. Henis, B. Geiger, and A. D. Bershadsky, "The heel and toe of the cell's foot: a multifaceted approach for understanding the structure and dynamics of focal adhesions.," *Cell Motil. Cytoskeleton*, vol. 66, no. 11, pp. 1017–29, Nov. 2009.

[66] J. T. Parsons, A. R. Horwitz, and M. A. Schwartz, "Cell adhesion: integrating cytoskeletal dynamics and cellular tension.," *Nat. Rev. Mol. Cell Biol.*, vol. 11, no. 9, pp. 633–43, Sep. 2010.

[67] P. Roca-Cusachs, A. del Rio, E. Puklin-Faucher, N. C. Gauthier, N. Biais, and M. P. Sheetz, "Integrin-dependent force transmission to the extracellular matrix by α-actinin triggers adhesion maturation.," *Proc. Natl. Acad. Sci. U. S. A.*, vol. 110, no. 15, pp. E1361–70, Apr. 2013.

[68] A. I. Bachir, J. Zareno, K. Moissoglu, E. F. Plow, E. Gratton, and A. R. Horwitz, "Integrin-associated complexes form hierarchically with variable stoichiometry in nascent adhesions.," *Curr. Biol.*, vol. 24, no. 16, pp. 1845–53, Aug. 2014.

[69] S. L. Gupton and C. M. Waterman-Storer, "Spatiotemporal Feedback between Actomyosin and Focal-Adhesion Systems Optimizes Rapid Cell Migration," *Cell*, vol. 125, no. 7, pp. 1361–1374, Jun. 2006.

[70] C. P. Johnson, H.-Y. Tang, C. Carag, D. W. Speicher, and D. E. Discher, "Forced unfolding of proteins within cells.," *Science*, vol. 317, no. 5838, pp. 663–6, Aug. 2007.

[71] A. del Rio, R. Perez-Jimenez, R. Liu, P. Roca-Cusachs, J. M. Fernandez, and M. P. Sheetz, "Stretching single talin rod molecules activates vinculin binding.," *Science*, vol. 323, no. 5914, pp. 638–41, Jan. 2009.

[72] C. Grashoff, B. D. Hoffman, M. D. Brenner, R. Zhou, M. Parsons, M. T. Yang, M. A. McLean, S. G. Sligar, C. S. Chen, T. Ha, and M. A. Schwartz, "Measuring mechanical tension across vinculin reveals regulation of focal adhesion dynamics.," *Nature*, vol. 466, no. 7303, pp. 263–6, Jul. 2010.

[73] M. Glogauer, P. Arora, G. Yao, I. Sokholov, J. Ferrier, and C. A. McCulloch, "Calcium ions and tyrosine phosphorylation interact coordinately with actin to regulate cytoprotective responses to stretching.," *J. Cell Sci.*, vol. 110 (Pt 1, pp. 11–21, Jan. 1997.

[74] T. Kobayashi and M. Sokabe, "Sensing substrate rigidity by mechanosensitive ion channels with stress fibers and focal adhesions.," *Curr. Opin. Cell Biol.*, vol. 22, no. 5, pp. 669–76, Oct. 2010.

[75] A. J. Engler, S. Sen, H. L. Sweeney, and D. E. Discher, "Matrix elasticity directs stem cell lineage specification.," *Cell*, vol. 126, no. 4, pp. 677–89, Aug. 2006.

[76] N. D. Evans, C. Minelli, E. Gentleman, V. LaPointe, S. N. Patankar, M. Kallivretaki, X. Chen, C. J. Roberts, and M. M. Stevens, "Substrate stiffness affects early differentiation events in embryonic stem cells.," *Eur. Cell. Mater.*, vol. 18, pp. 1–13; discussion 13–4, Jan. 2009.

[77] N. Eroshenko, R. Ramachandran, V. K. Yadavalli, and R. R. Rao, "Effect of substrate stiffness on early human embryonic stem cell differentiation.," *J. Biol. Eng.*, vol. 7, no. 1, p. 7, Jan. 2013.

[78] J. S. Park, J. S. Chu, A. D. Tsou, R. Diop, Z. Tang, A. Wang, and S. Li, "The effect of matrix stiffness on the differentiation of mesenchymal stem cells in response to TGF-β.," *Biomaterials*, vol. 32, no. 16, pp. 3921–30, Jun. 2011.

[79]   J. H. Wen, L. G. Vincent, A. Fuhrmann, Y. S. Choi, K. C. Hribar, H. Taylor-Weiner, S. Chen, and A. J. Engler, "Interplay of matrix stiffness and protein tethering in stem cell differentiation.," *Nat. Mater.*, vol. 13, no. 10, pp. 979–87, Oct. 2014.

[80]   S. Dupont, L. Morsut, M. Aragona, E. Enzo, S. Giulitti, M. Cordenonsi, F. Zanconato, J. Le Digabel, M. Forcato, S. Bicciato, N. Elvassore, and S. Piccolo, "Role of YAP/TAZ in mechanotransduction.," *Nature*, vol. 474, no. 7350, pp. 179–83, Jun. 2011.

[81]   L. Trichet, J. Le Digabel, R. J. Hawkins, S. R. K. Vedula, M. Gupta, C. Ribrault, P. Hersen, R. Voituriez, and B. Ladoux, "Evidence of a large-scale mechanosensing mechanism for cellular adaptation to substrate stiffness.," *Proc. Natl. Acad. Sci. U. S. A.*, vol. 109, no. 18, pp. 6933–8, May 2012.

[82]   A. L. H. P. W. D. Stopak, "Silicone Rubber Substrata: A New Wrinkle in the Study of Cell Locomotion," *Sci. New Ser.*, vol. 208, no. 4440, pp. 177–179, 1980.

[83]   B. Sabass, M. L. Gardel, C. M. Waterman, and U. S. Schwarz, "High resolution traction force microscopy based on experimental and computational advances.," *Biophys. J.*, vol. 94, no. 1, pp. 207–20, Jan. 2008.

[84]   J. C. Del Alamo, R. Meili, B. Alonso-Latorre, J. Rodríguez-Rodríguez, A. Aliseda, R. A. Firtel, and J. C. Lasheras, "Spatio-temporal analysis of eukaryotic cell motility by improved force cytometry.," *Proc. Natl. Acad. Sci. U. S. A.*, vol. 104, no. 33, pp. 13343–8, Aug. 2007.

[85]   K. A. Beningo and Y.-L. Wang, "Flexible substrata for the detection of cellular traction forces.," *Trends Cell Biol.*, vol. 12, no. 2, pp. 79–84, Feb. 2002.

[86]   J. Lee, M. Leonard, T. Oliver, A. Ishihara, and K. Jacobson, "Traction forces generated by locomoting keratocytes.," *J. Cell Biol.*, vol. 127, no. 6 Pt 2, pp. 1957–64, Dec. 1994.

[87]   J. P. Butler, I. M. Tolić-Nørrelykke, B. Fabry, and J. J. Fredberg, "Traction fields, moments, and strain energy that cells exert on their surroundings.," *Am. J. Physiol. Cell Physiol.*, vol. 282, no. 3, pp. C595–605, Mar. 2002.

[88]   B. Ladoux and A. Nicolas, "Physically based principles of cell adhesion mechanosensitivity in tissues.," *Rep. Prog. Phys.*, vol. 75, no. 11, p. 116601, Nov. 2012.

[89]   M. Dembo and Y. L. Wang, "Stresses at the cell-to-substrate interface during locomotion of fibroblasts.," *Biophys. J.*, vol. 76, no. 4, pp. 2307–16, Apr. 1999.

[90]   S. V Plotnikov, B. Sabass, U. S. Schwarz, and C. M. Waterman, *High-resolution traction force microscopy.*, 1st ed., vol. 123. Elsevier Inc., 2014.

[91]   T. Betz, D. Koch, Y.-B. Lu, K. Franze, and J. a Käs, "Growth cones as soft and weak force generators.," *Proc. Natl. Acad. Sci. U. S. A.*, vol. 108, no. 33, pp. 13420–5, Aug. 2011.

[92] K. L. Hui, L. Balagopalan, L. E. Samelson, and A. Upadhyaya, "Cytoskeletal forces during signaling activation in Jurkat T-cells.," *Mol. Biol. Cell*, vol. 26, no. 4, pp. 685–95, Feb. 2015.

[93] A. Saez, A. Buguin, P. Silberzan, and B. Ladoux, "Is the mechanical activity of epithelial cells controlled by deformations or forces?," *Biophys. J.*, vol. 89, no. 6, pp. L52–4, Dec. 2005.

[94] S.-Y. Tee, J. Fu, C. S. Chen, and P. a Janmey, "Cell shape and substrate rigidity both regulate cell stiffness.," *Biophys. J.*, vol. 100, no. 5, pp. L25–7, Mar. 2011.

[95] M. Ghibaudo, A. Saez, L. Trichet, A. Xayaphoummine, J. Browaeys, P. Silberzan, A. Buguin, and B. Ladoux, "Traction forces and rigidity sensing regulate cell functions," *Soft Matter*, vol. 4, no. 9, p. 1836, 2008.

[96] J. Solon, I. Levental, K. Sengupta, P. C. Georges, and P. a Janmey, "Fibroblast adaptation and stiffness matching to soft elastic substrates.," *Biophys. J.*, vol. 93, no. 12, pp. 4453–61, Dec. 2007.

[97] Y. Aratyn-Schaus, P. W. Oakes, and M. L. Gardel, "Dynamic and structural signatures of lamellar actomyosin force generation.," *Mol. Biol. Cell*, vol. 22, no. 8, pp. 1330–9, Apr. 2011.

[98] L. Bozec, G. van der Heijden, and M. Horton, "Collagen fibrils: nanoscale ropes.," *Biophys. J.*, vol. 92, no. 1, pp. 70–5, Jan. 2007.

[99] G. A. Abrams, S. L. Goodman, P. F. Nealey, M. Franco, and C. J. Murphy, "Nanoscale topography of the basement membrane underlying the corneal epithelium of the rhesus macaque.," *Cell Tissue Res.*, vol. 299, no. 1, pp. 39–46, Jan. 2000.

[100] S. L. Goodman, P. A. Sims, and R. M. Albrecht, "Three-dimensional extracellular matrix textured biomaterials.," *Biomaterials*, vol. 17, no. 21, pp. 2087–95, Nov. 1996.

[101] J. le Digabel, M. Ghibaudo, L. Trichet, A. Richert, and B. Ladoux, "Microfabricated substrates as a tool to study cell mechanotransduction.," *Med. Biol. Eng. Comput.*, vol. 48, no. 10, pp. 965–76, Oct. 2010.

[102] C. C. Berry, G. Campbell, A. Spadiccino, M. Robertson, and A. S. G. Curtis, "The influence of microscale topography on fibroblast attachment and motility.," *Biomaterials*, vol. 25, no. 26, pp. 5781–8, Nov. 2004.

[103] S. a Biela, Y. Su, J. P. Spatz, and R. Kemkemer, "Different sensitivity of human endothelial cells, smooth muscle cells and fibroblasts to topography in the nano-micro range.," *Acta Biomater.*, vol. 5, no. 7, pp. 2460–6, Sep. 2009.

[104] D.-H. Kim, K. Han, K. Gupta, K. W. Kwon, K.-Y. Suh, and A. Levchenko, "Mechanosensitivity of fibroblast cell shape and movement to anisotropic substratum topography gradients.," *Biomaterials*, vol. 30, no. 29, pp. 5433–44, Oct. 2009.

[105] E. Lamers, R. van Horssen, J. te Riet, F. C. van Delft, R. Luttge, X. F. Walboomers, and J. a Jansen, "The influence of nanoscale topographical cues on initial osteoblast morphology and migration.," *Eur. Cell. Mater.*, vol. 20, pp. 329–43, Jan. 2010.

[106] E. Lamers, X. F. Walboomers, M. Domanski, J. te Riet, F. C. M. J. M. van Delft, R. Luttge, L. a J. a Winnubst, H. J. G. E. Gardeniers, and J. a Jansen, "The influence of nanoscale grooved substrates on osteoblast behavior and extracellular matrix deposition.," *Biomaterials*, vol. 31, no. 12, pp. 3307–16, Apr. 2010.

[107] V. Ottani, M. Raspanti, and a Ruggeri, "Collagen structure and functional implications," *Micron*, vol. 32, no. 3, pp. 251–260, Apr. 2001.

[108] A. J. Dulgar-Tulloch, R. Bizios, and R. W. Siegel, "Human mesenchymal stem cell adhesion and proliferation in response to ceramic chemistry and nanoscale topography.," *J. Biomed. Mater. Res. A*, vol. 90, no. 2, pp. 586–94, Aug. 2009.

[109] C. J. Bettinger, Z. Zhang, S. Gerecht, J. T. Borenstein, and R. Langer, "Enhancement of In Vitro Capillary Tube Formation by Substrate Nanotopography.," *Adv. Mater.*, vol. 20, no. 1, pp. 99–103, Jan. 2008.

[110] S. J. Liliensiek, S. Campbell, P. F. Nealey, and C. J. Murphy, "The scale of substratum topographic features modulates proliferation of corneal epithelial cells and corneal fibroblasts.," *J. Biomed. Mater. Res. A*, vol. 79, no. 1, pp. 185–92, Oct. 2006.

[111] E. YIM, R. REANO, S. PANG, A. YEE, C. CHEN, and K. LEONG, "Nanopattern-induced changes in morphology and motility of smooth muscle cells," *Biomaterials*, vol. 26, no. 26, pp. 5405–5413, Sep. 2005.

[112] J. Y. Lim, J. C. Hansen, C. A. Siedlecki, J. Runt, and H. J. Donahue, "Human foetal osteoblastic cell response to polymer-demixed nanotopographic interfaces.," *J. R. Soc. Interface*, vol. 2, no. 2, pp. 97–108, Mar. 2005.

[113] K. R. Milner and C. A. Siedlecki, "Fibroblast response is enhanced by poly(L-lactic acid) nanotopography edge density and proximity.," *Int. J. Nanomedicine*, vol. 2, no. 2, pp. 201–11, Jan. 2007.

[114] M. J. Dalby, N. Gadegaard, R. Tare, A. Andar, M. O. Riehle, P. Herzyk, C. D. W. Wilkinson, and R. O. C. Oreffo, "The control of human mesenchymal cell differentiation using nanoscale symmetry and disorder.," *Nat. Mater.*, vol. 6, no. 12, pp. 997–1003, Dec. 2007.

[115] S. Oh, K. S. Brammer, Y. S. J. Li, D. Teng, A. J. Engler, S. Chien, and S. Jin, "Stem cell fate dictated solely by altered nanotube dimension.," *Proc. Natl. Acad. Sci. U. S. A.*, vol. 106, no. 7, pp. 2130–5, Feb. 2009.

[116] M.-H. You, M. K. Kwak, D.-H. Kim, K. Kim, A. Levchenko, D.-Y. Kim, and K.-Y. Suh, "Synergistically enhanced osteogenic differentiation of human mesenchymal stem cells by culture on nanostructured surfaces with induction media.," *Biomacromolecules*, vol. 11, no. 7, pp. 1856–62, Jul. 2010.

[117] T. Sjöström, M. J. Dalby, A. Hart, R. Tare, R. O. C. Oreffo, and B. Su, "Fabrication of pillar-like titania nanostructures on titanium and their interactions with human skeletal stem cells," *Acta Biomater.*, vol. 5, no. 5, pp. 1433–1441, Jun. 2009.

[118] I. Nagata, A. Kawana, and N. Nakatsuji, "Perpendicular contact guidance of CNS neuroblasts on artificial microstructures," vol. 408, pp. 401–408, 1993.

[119] I. Nagata and N. Nakatsuji, "Rodent CNS neuroblasts exhibit both perpendicular and parallel contact guidance on the aligned parallel neurite bundle," vol. 590, pp. 581–590, 1991.

[120] A. I. Teixeira, G. a Abrams, P. J. Bertics, C. J. Murphy, and P. F. Nealey, "Epithelial contact guidance on well-defined micro- and nanostructured substrates.," *J. Cell Sci.*, vol. 116, no. Pt 10, pp. 1881–92, May 2003.

[121] A. I. Teixeira, G. a McKie, J. D. Foley, P. J. Bertics, P. F. Nealey, and C. J. Murphy, "The effect of environmental factors on the response of human corneal epithelial cells to nanoscale substrate topography.," *Biomaterials*, vol. 27, no. 21, pp. 3945–54, Jul. 2006.

[122] N. Q. Balaban, U. S. Schwarz, D. Riveline, P. Goichberg, G. Tzur, I. Sabanay, D. Mahalu, S. Safran, A. Bershadsky, L. Addadi, and B. Geiger, "Force and focal adhesion assembly: a close relationship studied using elastic micropatterned substrates.," *Nat. Cell Biol.*, vol. 3, no. 5, pp. 466–72, May 2001.

[123] J. Stricker, Y. Aratyn-Schaus, P. W. Oakes, and M. L. Gardel, "Spatiotemporal constraints on the force-dependent growth of focal adhesions.," *Biophys. J.*, vol. 100, no. 12, pp. 2883–93, Jun. 2011.

[124] K. A. Beningo, M. Dembo, I. Kaverina, J. V Small, and Y. L. Wang, "Nascent focal adhesions are responsible for the generation of strong propulsive forces in migrating fibroblasts.," *J. Cell Biol.*, vol. 153, no. 4, pp. 881–8, May 2001.

[125] A. Nicolas, B. Geiger, and S. A. Safran, "Cell mechanosensitivity controls the anisotropy of focal adhesions.," *Proc. Natl. Acad. Sci. U. S. A.*, vol. 101, no. 34, pp. 12520–5, Aug. 2004.

[126] P. Marcq, N. Yoshinaga, and J. Prost, "Rigidity sensing explained by active matter theory.," *Biophys. J.*, vol. 101, no. 6, pp. L33–5, Sep. 2011.

[127] B. Ladoux, E. Anon, M. Lambert, A. Rabodzey, P. Hersen, A. Buguin, P. Silberzan, and R.-M. Mège, "Strength dependence of cadherin-mediated adhesions.," *Biophys. J.*, vol. 98, no. 4, pp. 534–42, Feb. 2010.

[128] P. W. Oakes, S. Banerjee, M. C. Marchetti, and M. L. Gardel, "Geometry Regulates Traction Stresses in Adherent Cells," *Biophys. J.*, vol. 107, no. 4, pp. 825–833, Aug. 2014.

[129] T. Iskratsch, H. Wolfenson, and M. P. Sheetz, "Appreciating force and shape — the rise of mechanotransduction in cell biology," *Nat. Rev. Mol. Cell Biol.*, vol. 15, no. 12, pp. 825–33, Oct. 2014.

[130] V. Vogel and M. Sheetz, "Local force and geometry sensing regulate cell functions.," *Nat. Rev. Mol. Cell Biol.*, vol. 7, no. 4, pp. 265–75, Apr. 2006.

[131] C. M. Lo, H. B. Wang, M. Dembo, and Y. L. Wang, "Cell movement is guided by the rigidity of the substrate.," *Biophys. J.*, vol. 79, no. 1, pp. 144–52, Jul. 2000.

[132] D. Wirtz, K. Konstantopoulos, and P. C. Searson, "The physics of cancer: the role of physical interactions and mechanical forces in metastasis.," *Nat. Rev. Cancer*, vol. 11, no. 7, pp. 512–22, Jul. 2011.

[133] M. J. Paszek, N. Zahir, K. R. Johnson, J. N. Lakins, G. I. Rozenberg, A. Gefen, C. A. Reinhart-King, S. S. Margulies, M. Dembo, D. Boettiger, D. A. Hammer, and V. M. Weaver, "Tensional homeostasis and the malignant phenotype.," *Cancer Cell*, vol. 8, no. 3, pp. 241–54, Sep. 2005.

[134] C. G. Galbraith, K. M. Yamada, and M. P. Sheetz, "The relationship between force and focal complex development.," *J. Cell Biol.*, vol. 159, no. 4, pp. 695–705, Nov. 2002.

[135] M. Yoshigi, "Mechanical force mobilizes zyxin from focal adhesions to actin filaments and regulates cytoskeletal reinforcement," *J. Cell Biol.*, vol. 171, no. 2, pp. 209–215, Oct. 2005.

[136] M. A. Smith, E. Blankman, M. L. Gardel, L. Luettjohann, C. M. Waterman, and M. C. Beckerle, "A zyxin-mediated mechanism for actin stress fiber maintenance and repair.," *Dev. Cell*, vol. 19, no. 3, pp. 365–76, Sep. 2010.

[137] R. D. S. Dixon, D. K. Arneman, A. S. Rachlin, N. R. Sundaresan, M. J. Costello, S. L. Campbell, and C. a Otey, "Palladin is an actin cross-linking protein that uses immunoglobulin-like domains to bind filamentous actin.," *J. Biol. Chem.*, vol. 283, no. 10, pp. 6222–31, Mar. 2008.

[138] M. R. Beck, C. A. Otey, and S. L. Campbell, "Structural characterization of the interactions between palladin and α-actinin.," *J. Mol. Biol.*, vol. 413, no. 3, pp. 712–25, Oct. 2011.

[139] M. Rönty, A. Taivainen, M. Moza, C. A. Otey, and O. Carpén, "Molecular analysis of the interaction between palladin and alpha-actinin.," *FEBS Lett.*, vol. 566, no. 1–3, pp. 30–4, May 2004.

[140] B. Grooman, I. Fujiwara, C. Otey, and A. Upadhyaya, "Morphology and viscoelasticity of actin networks formed with the mutually interacting crosslinkers: palladin and alpha-actinin.," *PLoS One*, vol. 7, no. 8, p. e42773, Jan. 2012.

[141] N. A. Bhowmick, E. G. Neilson, and H. L. Moses, "Stromal fibroblasts in cancer initiation and progression.," *Nature*, vol. 432, no. 7015, pp. 332–7, Nov. 2004.

[142] R. Kalluri and M. Zeisberg, "Fibroblasts in cancer.," *Nat. Rev. Cancer*, vol. 6, no. 5, pp. 392–401, May 2006.

[143] Y. R. Chin and A. Toker, "The Actin-Bundling Protein Palladin Is an Akt1-Specific Substrate that Regulates Breast Cancer Cell Migration," *Mol. Cell*, vol. 38, no. 3, pp. 333–344, May 2010.

[144] T. A. Brentnall, L. A. Lai, J. Coleman, M. P. Bronner, S. Pan, and R. Chen, "Arousal of cancer-associated stroma: overexpression of palladin activates fibroblasts to promote tumor invasion.," *PLoS One*, vol. 7, no. 1, p. e30219, Jan. 2012.

[145] G. S. Karagiannis, T. Poutahidis, S. E. Erdman, R. Kirsch, R. H. Riddell, and E. P. Diamandis, "Cancer-associated fibroblasts drive the progression of metastasis through both paracrine and mechanical pressure on cancer tissue.," *Mol. Cancer Res.*, vol. 10, no. 11, pp. 1403–18, Nov. 2012.

[146] G. Kharaishvili, D. Simkova, K. Bouchalova, M. Gachechiladze, N. Narsia, and J. Bouchal, "The role of cancer-associated fibroblasts, solid stress and other microenvironmental factors in tumor progression and therapy resistance.," *Cancer Cell Int.*, vol. 14, p. 41, Jan. 2014.

[147] D. T. Butcher, T. Alliston, and V. M. Weaver, "A tense situation: forcing tumour progression.," *Nat. Rev. Cancer*, vol. 9, no. 2, pp. 108–22, Feb. 2009.

[148] M. V Apte, P. S. Haber, T. L. Applegate, I. D. Norton, G. W. McCaughan, M. a Korsten, R. C. Pirola, and J. S. Wilson, "Periacinar stellate shaped cells in rat pancreas: identification, isolation, and culture," *Gut*, vol. 43, no. 1, pp. 128–133, Jul. 1998.

[149] M. Y. Watari N, Hotta Y, "Morphological studies on a vitamin A-storing cell and its complex with macrophage observed in mouse pancreatic tissues following excess vitamin A administration," *Okajimas Folia Anat Jpn*, 1982.

[150] M. A. X. G. Bachem, E. Schneider, H. Groß, H. Weidenbach, R. M. Schmid, G. Adler, A. Menke, M. Siech, H. Beger, and A. Gru, "Identification, Culture, and Characterization of Pancreatic Stellate Cells in Rats and Humans," pp. 421–432, 1998.

[151] I. N, "The vitamin A-storing cells in the human and rat pancreas," *Kurume Med J*, vol. 37, no. 2, pp. 67–81, 1990.

[152] B. Hinz, S. H. Phan, V. J. Thannickal, A. Galli, M.-L. Bochaton-Piallat, and G. Gabbiani, "The myofibroblast: one function, multiple origins.," *Am. J. Pathol.*, vol. 170, no. 6, pp. 1807–16, Jun. 2007.

[153] B. Hinz, "The myofibroblast: paradigm for a mechanically active cell.," *J. Biomech.*, vol. 43, no. 1, pp. 146–55, Jan. 2010.

[154] J. Köninger, T. Giese, F. F. di Mola, M. N. Wente, I. Esposito, M. G. Bachem, N. a Giese, M. W. Büchler, and H. Friess, "Pancreatic tumor cells influence the composition of the extracellular matrix.," *Biochem. Biophys. Res. Commun.*, vol. 322, no. 3, pp. 943–9, Sep. 2004.

[155] M. G. Bachem, M. Schünemann, M. Ramadani, M. Siech, H. Beger, A. Buck, S. Zhou, A. Schmid-Kotsas, and G. Adler, "Pancreatic carcinoma cells induce fibrosis by stimulating proliferation and matrix synthesis of stellate cells," *Gastroenterology*, vol. 128, no. 4, pp. 907–921, Apr. 2005.

[156] S. Yoshida, T. Yokota, M. Ujiki, X.-Z. Ding, C. Pelham, T. E. Adrian, M. S. Talamonti, R. H. Bell, and W. Denham, "Pancreatic cancer stimulates pancreatic stellate cell proliferation and TIMP-1 production through the MAP kinase pathway.," *Biochem. Biophys. Res. Commun.*, vol. 323, no. 4, pp. 1241–5, Oct. 2004.

[157] K. L. Pogue-Geile, R. Chen, M. P. Bronner, T. Crnogorac-Jurcevic, K. W. Moyes, S. Dowen, C. a Otey, D. a Crispin, R. D. George, D. C. Whitcomb, and T. a Brentnall, "Palladin mutation causes familial pancreatic cancer and suggests a new cancer mechanism.," *PLoS Med.*, vol. 3, no. 12, p. e516, Dec. 2006.

[158] S. M. Goicoechea, R. García-Mata, J. Staub, a Valdivia, L. Sharek, C. G. McCulloch, R. F. Hwang, R. Urrutia, J. J. Yeh, H. J. Kim, and C. a Otey, "Palladin promotes invasion of pancreatic cancer cells by enhancing invadopodia formation in cancer-associated fibroblasts.," *Oncogene*, no. January, pp. 1–9, Mar. 2013.

[159] O. C. Otey, Carol a, "Alpha-Actinin Revisited: A Fresh Look at an Old Player," *Cell Motil. Cytoskeleton*, vol. 58, pp. 104–111, 2004.

[160] and O. C. Mikko Rönty, Anu Taivainen, Leena Heiska, Carol Otey, Elisabeth Ehler, Woo Keun Song, "Palladin interacts with SH3 domains of SPIN90 and Src and is required for Src-induced cytoskeletal remodeling," vol. 313, no. 12, pp. 2575–2585, 2008.

[161] S. Swift, J. Lorens, P. Achacoso, and G. P. Nolan, "Rapid production of retroviruses for efficient gene delivery to mammalian cells using 293T cell-based systems.," *Curr. Protoc. Immunol.*, vol. Chapter 10, p. Unit 10.17C, May 2001.

[162] Y. Aratyn-Schaus, P. W. Oakes, J. Stricker, S. P. Winter, and M. L. Gardel, "Preparation of complaint matrices for quantifying cellular contraction.," *J. Vis. Exp.*, no. 46, Jan. 2010.

[163] S. M. Goicoechea, D. Arneman, and C. a Otey, "The role of palladin in actin organization and cell motility Silvia," *Cell*, vol. 87, pp. 517–525, 2009.

[164] S. V Plotnikov, A. M. Pasapera, B. Sabass, and C. M. Waterman, "Force fluctuations within focal adhesions mediate ECM-rigidity sensing to guide directed cell migration.," *Cell*, vol. 151, no. 7, pp. 1513–27, Dec. 2012.

[165] J. Colombelli, a. Besser, H. Kress, E. G. Reynaud, P. Girard, E. Caussinus, U. Haselmann, J. V. Small, U. S. Schwarz, and E. H. K. Stelzer, "Mechanosensing in actin stress fibers revealed by a close correlation between force and protein localization," *J. Cell Sci.*, vol. 122, no. 11, pp. 1928–1928, May 2009.

[166] K. Lam Hui, C. Wang, B. Grooman, J. Wayt, and A. Upadhyaya, "Membrane dynamics correlate with formation of signaling clusters during cell spreading.," *Biophys. J.*, vol. 102, no. 7, pp. 1524–33, Apr. 2012.

[167] M. L. Gardel, B. Sabass, L. Ji, G. Danuser, U. S. Schwarz, and C. M. Waterman, "Traction stress in focal adhesions correlates biphasically with actin retrograde flow speed.," *J. Cell Biol.*, vol. 183, no. 6, pp. 999–1005, Dec. 2008.

[168] C. H. Lin, E. M. Espreafico, M. S. Mooseker, and P. Forscher, "Myosin drives retrograde F-actin flow in neuronal growth cones.," *Biol. Bull.*, vol. 192, no. 1, pp. 183–5, Feb. 1997.

[169] P. Hotulainen and P. Lappalainen, "Stress fibers are generated by two distinct actin assembly mechanisms in motile cells.," *J. Cell Biol.*, vol. 173, no. 3, pp. 383–94, May 2006.

[170] N. Endlich, C. A. Otey, W. Kriz, and K. Endlich, "Movement of stress fibers away from focal adhesions identifies focal adhesions as sites of stress fiber assembly in stationary cells," *Cell Motil. Cytoskeleton*, vol. 64, no. 12, pp. 966–976, Dec. 2007.

[171] L. J. Peterson, Z. Rajfur, A. S. Maddox, C. D. Freel, Y. Chen, M. Edlund, C. Otey, and K. Burridge, "Simultaneous stretching and contraction of stress fibers in vivo.," *Mol. Biol. Cell*, vol. 15, no. 7, pp. 3497–508, Jul. 2004.

[172] L. W. Janson, J. R. Sellers, and D. L. Taylor, "Actin-binding proteins regulate the work performed by myosin II motors on single actin filaments," *Cell Motil. Cytoskeleton*, vol. 22, no. 4, pp. 274–280, Jan. 1992.

[173] A. Curtis and C. Wilkinson, "FUWlEW Topographical control of cells," vol. 18, no. 24, pp. 1573–1583, 1998.

[174] D.-H. Kim, P. P. Provenzano, C. L. Smith, and A. Levchenko, "Matrix nanotopography as a regulator of cell function.," *J. Cell Biol.*, vol. 197, no. 3, pp. 351–60, Apr. 2012.

[175] C. J. Bettinger, R. Langer, and J. T. Borenstein, "Engineering substrate topography at the micro- and nanoscale to control cell function.," *Angew. Chem. Int. Ed. Engl.*, vol. 48, no. 30, pp. 5406–15, Jan. 2009.

[176] M. K. Driscoll, X. Sun, C. Guven, J. T. Fourkas, and W. Losert, "Cellular contact guidance through dynamic sensing of nanotopography," *ACS Nano*, vol. 8, no. 4, pp. 3546–3555, 2014.

[177] K. A. Diehl, J. D. Foley, P. F. Nealey, and C. J. Murphy, "Nanoscale topography modulates corneal epithelial cell migration," *J. Biomed. Mater. Res. Part A*, vol. 75A, no. 3, pp. 603–611, Dec. 2005.

[178] C. S. Ranucci and P. V. Moghe, "Substrate microtopography can enhance cell adhesive and migratory responsiveness to matrix ligand density," *J. Biomed. Mater. Res.*, vol. 54, pp. 149–161, 2001.

[179] A. P. Mello, Y. Volkov, D. Kelleher, and P. J. Prendergast, "Comparative locomotory behavior of T lymphocytes versus T lymphoma cells on flat and grooved surfaces.," *Ann. Biomed. Eng.*, vol. 31, no. 9, pp. 1106–13, Oct. 2003.

[180] K. S. Brammer, S. Oh, J. O. Gallagher, and S. Jin, "Enhanced cellular mobility guided by TiO2 nanotube surfaces," *Nano Lett.*, vol. 8, no. 150628, pp. 786–793, 2008.

[181] P. P. Provenzano, D. R. Inman, K. W. Eliceiri, S. M. Trier, and P. J. Keely, "Contact guidance mediated three-dimensional cell migration is regulated by Rho/ROCK-dependent matrix reorganization.," *Biophys. J.*, vol. 95, no. 11, pp. 5374–84, Dec. 2008.

[182] P. P. Provenzano, K. W. Eliceiri, J. M. Campbell, D. R. Inman, J. G. White, and P. J. Keely, "Collagen reorganization at the tumor-stromal interface facilitates local invasion.," *BMC Med.*, vol. 4, no. 1, p. 38, Jan. 2006.

[183] Brian James Grooman, "The Role of the actin crosslinker palladin: from reconstituted networks t live cells," University of Maryland College Park, 2013.

[184] F. Aguet, C. Antonescu, M. Mettlen, S. Schmid, and G. Danuser, "Advances in analysis of low signal-to-noise images link dynamin and AP2 to the functions of an endocytic checkpoint," *Dev. Cell*, vol. 26, pp. 279–291, 2013.

[185] C. P. Brangwynne, G. H. Koenderink, F. C. Mackintosh, and D. A. Weitz, "Nonequilibrium microtubule fluctuations in a model cytoskeleton.," *Phys. Rev. Lett.*, vol. 100, no. 11, p. 118104, Mar. 2008.

[186] D. Mizuno, C. Tardin, C. F. Schmidt, and F. C. Mackintosh, "Nonequilibrium mechanics of active cytoskeletal networks.," *Science*, vol. 315, no. 5810, pp. 370–3, Jan. 2007.

[187] C. Raupach, D. Zitterbart, C. Mierke, C. Metzner, F. Müller, and B. Fabry, "Stress fluctuations and motion of cytoskeletal-bound markers," *Phys. Rev. E*, vol. 76, no. 1, p. 011918, Jul. 2007.

[188] N. Fakhri, A. D. Wessel, C. Willms, M. Pasquali, D. R. Klopfenstein, F. C. MacKintosh, and C. F. Schmidt, "High-resolution mapping of intracellular fluctuations using carbon nanotubes.," *Science*, vol. 344, no. 6187, pp. 1031–5, 2014.

[189] M. Guo, A. J. Ehrlicher, M. H. Jensen, M. Renz, J. R. Moore, R. D. Goldman, J. Lippincott-Schwartz, F. C. Mackintosh, and D. a Weitz, "Probing the stochastic, motor-driven properties of the cytoplasm using force spectrum microscopy.," *Cell*, vol. 158, no. 4, pp. 822–32, 2014.

[190] H. C. BERG and D. A. BROWN, "Chemotaxis in Escherichia coli analysed by Three-dimensional Tracking," *Nature*, vol. 239, no. 5374, pp. 500–504, Oct. 1972.

[191] X. F. Walboomers, H. J. Croes, L. A. Ginsel, and J. A. Jansen, "Growth behavior of fibroblasts on microgrooved polystyrene.," *Biomaterials*, vol. 19, no. 20, pp. 1861–8, Oct. 1998.

[192] C. Oakley and D. M. Brunette, "The sequence of alignment of microtubules, focal contacts and actin filaments in fibroblasts spreading on smooth and grooved titanium substrata.," *J. Cell Sci.*, vol. 106 (Pt 1, pp. 343–54, Sep. 1993.

[193] B. Wójciak-Stothard, A. S. Curtis, W. Monaghan, M. McGrath, I. Sommer, and C. D. Wilkinson, "Role of the cytoskeleton in the reaction of fibroblasts to multiple grooved substrata.," *Cell Motil. Cytoskeleton*, vol. 31, no. 2, pp. 147–58, Jan. 1995.

[194] P. Bursac, G. Lenormand, B. Fabry, M. Oliver, D. A. Weitz, V. Viasnoff, J. P. Butler, and J. J. Fredberg, "Cytoskeletal remodelling and slow dynamics in the living cell.," *Nat. Mater.*, vol. 4, no. 7, pp. 557–61, Jul. 2005.

[195] I. Y. Wong, M. L. Gardel, D. R. Reichman, E. R. Weeks, M. T. Valentine, A. R. Bausch, and D. A. Weitz, "Anomalous diffusion probes microstructure dynamics of entangled F-actin networks.," *Phys. Rev. Lett.*, vol. 92, no. 17, p. 178101, Apr. 2004.

[196] C. Metzner, C. Raupach, D. Paranhos Zitterbart, and B. Fabry, "Simple model of cytoskeletal fluctuations," *Phys. Rev. E*, vol. 76, no. 2, p. 021925, Aug. 2007.

[197] K. Tanner, A. Boudreau, M. J. Bissell, and S. Kumar, "Dissecting regional variations in stress fiber mechanics in living cells with laser nanosurgery.," *Biophys. J.*, vol. 99, no. 9, pp. 2775–83, Nov. 2010.

[198] J. R. D. Soiné, C. A. Brand, J. Stricker, P. W. Oakes, M. L. Gardel, and U. S. Schwarz, "Model-based Traction Force Microscopy Reveals Differential Tension in Cellular Actin Bundles.," *PLoS Comput. Biol.*, vol. 11, no. 3, p. e1004076, Mar. 2015.